

Study of QCD-like theories at nonzero temperatures and densities

Dissertation
zur Erlangung des Doktorgrades
der Naturwissenschaften

vorgelegt beim Fachbereich Physik
der Johann Wolfgang Goethe-Universität
in Frankfurt am Main

von
Tian Zhang
aus der Volksrepublik China

Frankfurt am Main, 2012
(D 30)

vom Fachbereich Physik der Johann Wolfgang Goethe-Universität in
Frankfurt am Main als Dissertation angenommen.

Dekan: Prof. Dr. Michael Huth

Gutachter: Prof. Dr. Dirk H. Rischke, P.D. Dr. Aleksi Vuorinen

Datum der Disputation: 27.04.2012

Abstract

In this thesis I use effective models to investigate the properties of QCD-like theories at nonzero temperature and baryon chemical potential.

First I construct a PNJL model using a lattice spin model with nearest-neighbor interactions for the gauge sector and four-fermion interactions for the quarks in (pseudo)real representations of the gauge group. Calculating the phase diagram in the plane of temperature and quark chemical potential in QCD with adjoint quarks, it is qualitatively confirmed that the critical temperature of the chiral phase transition is much higher than the deconfinement transition temperature. At a chemical potential equal to half of the diquark mass in the vacuum, a diquark Bose–Einstein condensation (BEC) phase transition occurs. In the two-color case, a Ginzburg–Landau expansion is used to study the tetracritical behavior around the intersection point of the deconfinement and BEC transition lines which are both of second order. A compact expression for the expectation value of the Polyakov loop in an arbitrary representation of the gauge group is obtained for any number of colors, which allows us to study Casimir scaling at both nonzero temperature and chemical potential.

Subsequently I study the thermodynamics of two-color QCD (QC_2D) at high temperature and/or density using ZQCD, a dimensionally reduced superrenormalizable effective theory, formulated in terms of a coarse grained Wilson line. In the absence of quarks, the theory is required to respect the Z_2 center symmetry, while the effects of quarks of arbitrary masses and chemical potentials are introduced via soft Z_2 breaking operators. Perturbative matching of the effective theory parameters to the full theory is carried out explicitly, and it is argued how the new theory can be used to explore the phase diagram of two-color QCD.

Zusammenfassung

Seit mehr als der Hälfte des Jahrhunderts ist die QCD wegen ihrer vielen interessanten Eigenschaften attraktiv. Anders als Photonen in der QED tragen die Gluonen in der QCD, welche eine Nicht-Abelsche Eichtheorie ist, nichtverschwindene Eichladungen. Deswegen können die Gluonen unter sich wechselwirken. Dies führt zu eigenartigen Eigenschaften, wie z.B. asymptotischer Freiheit und Farbeinschluß.

Während viele störungstheoretische Berechnungen für schwache Kopplung durchgeführt werden, sind sie bei den niedrigen Energieskalen nicht anwendbar. Das Verhalten der QCD bei starken Kopplungen ist noch nicht voll verstanden.

Weitere Inspirationen können möglicherweise aus der QCD bei endlicher Temperatur und Dichte bekommen werden. Mit steigender Temperatur und Dichte werden neue Phasen in QCD-Materie auftreten. Die Stärke der QCD-Kopplung und die Vakuumstruktur werden durch Viel-Körper-Effekte verändert. In den neuen Phasen sind die Farbladungen nicht mehr eingeschlossen. Das Vakuum wird durch die Restaurierung der chiralen Symmetrie geändert. Phasenübergänge können daher auftreten. Es gibt Experimente, die diese Voraussage verfolgen, wie z.B. bei RHIC, LHC und FAIR. Die QCD bei endlicher Temperatur kann auch numerisch auf dem Gitter simuliert werden. Obwohl Experimente keine eindeutige Information über mögliche Phasenübergänge geliefert haben, wird diese Idee von den Ergebnissen der Gitter-QCD unterstützt. Die Schwierigkeit der Gitter-QCD liegt wegen des Vorzeichenproblems daran, dass die gängigen Monte-Carlo bei Technikendlicher Dichte nicht mehr benutzt werden können.

QCD-ähnliche Theorien können uns beim Verstehen der QCD helfen. Obwohl sie nicht die wahren Theorien sind, die unser Universum beschreiben, kann durch diese einfachen Modelle ein tiefer Einblick in die ungelösten Probleme gewonnen werden. Außerdem können diese Theorien auf dem Gitter simuliert werden. Die numerischen Ergebnisse der Gitter-

Rechnungen können dann zur Bestätigung der Schlussfolgerungen aus den theoretischen Herleitungen benutzt werden. In dieser Arbeit werden QCD-ähnliche Theorien bei endlicher Temperatur und Dichte untersucht. Besondere Schwerpunkte sind der Phasenübergang des Farb-Deconfinement und die Restaurierung der chiralen Symmetrie.

In dieser Arbeit untersuche ich QCD-ähnliche Theorien vom Typ I und II, nämlich mit Quarks in der realen und pseudorealen Darstellung der Eichgruppe. Sie haben sehr verschiedene Phasendiagramme im Vergleich zu QCD. Hier nehme ich Zweifarben-QCD (QC_2D) und Dreifarben-Adjoint-QCD (aQCD) als Beispiele und untersuche ihre Phasendiagramme und das Casimir-Skalierungsverhalten.

Um den Eichsektor zu gestalten, wird ein einfaches Gitter-Spin-Modell mit den Wechselwirkungen zwischen Nächsten-Nachbarn angewendet, inspiriert vom Starken Kopplungs-Limes. Dies ist dann an Kontinuum-Quarks gekoppelt, in einer Art ähnlich wie dem Polyakov-loop NJL (PNJL) Modell. Die Wirkung des Eichsektors ist gegeben durch

$$\mathcal{S}_g[L] = -N_c^2 e^{-a/T} \sum_{\mathbf{x}, \mathbf{y}} \ell_F(\mathbf{x}) \ell_F^*(\mathbf{x} + \mathbf{y}),$$

wobei \mathbf{x} die Gitterlänge und \mathbf{y} der Abstand zwischen den Nachbarn sind. $\ell_F(\mathbf{x}) \equiv \frac{1}{N_c} \text{Tr} L_F(\mathbf{x})$ ist die Spur der Polyakov-Schleife in der fundamentalen Darstellung.

Der Quarksektor ist mit Vier-Fermionen-Wechselwirkungen konstruiert. Im Nambu-Formalismus ist die Lagrange-Dichte

$$\mathcal{L}_{\text{QCD-like}} = \bar{\Psi} i \not{D} \Psi - \left[\frac{1}{2} m_0 \bar{\Psi}^C \begin{pmatrix} 0 & \mathbb{1} \\ \pm \mathbb{1} & 0 \end{pmatrix} \Psi + \text{H.c.} \right].$$

Diese Wechselwirkung bezieht sich auf die Flavoursymmetrie in QCD-ähnlichen Theorien, die sogenannte $SU(2N_f)$. Das Quarkfeld ist dann an den Eichsektor durch die kovariante Ableitung, $\mathcal{D}_\mu \psi = (\partial_\mu - ig T_a A_\mu^a) \psi$, gekoppelt.

Die Parameter im PNJL-Modell können getrennt für den Eich- und Quarksektor bestimmt werden. Danach kann das Phasendiagramm in Mittlererfeld-Näherung berechnet werden. Abbildung 0.1 zeigt das Phasendiagramm von aQCD_{2D} mit einer Quarksorte, in der Darstellung Temperatur gegen chemisches Potential der Quarks. Der Deconfinement-Übergang, verbunden mit der Brechung der zentralen Z_2 , ist durch die schwarze durchgezogene Linie gekennzeichnet, während die rote gestrichelte Linie den BEC Übergang andeutet, bei dem die Baryonzahl $U(1)_B$ gebrochen ist. Außer diesen zwei scharfen Phasenübergängen gibt es einen Crossover, der mit der Auflösung des chiralen Kondensats verbunden ist. Dies tritt bei einer Temperatur auf, die viel höher als die des Deconfinement-Übergangs ist.

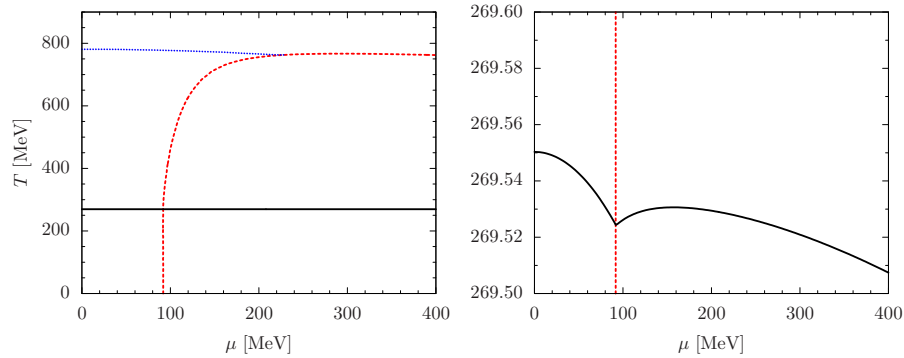


Abbildung 0.1: Phasendiagramm der Zweifarb-QCD mit einer Sorte von Adjoint-Quarks.

Die Temperatur des Deconfinement-Übergangs hängt extrem schwach vom chemischen Potential ab. Der Grund liegt offensichtlich daran, dass die Adjoint-Quarks neutral bezüglich der zentralen Symmetrie sind. Das Verhalten der Übergangslinien in der Nähe ihrer Kreuzungen wird in dieser Arbeit detailliert analysiert. Zum Schluss tritt der Null-Temperatur BEC-Übergang bei $\mu = 92$ MeV auf, welches mit der Tatsache übereinstimmt, dass, unter unserer Parametrisierung, die Masse des Pion/Diquark-Multiplets im Vakuum gleich $m_\pi = 184$ MeV ist.

Das Phasendiagramm von aQCD wird im Rahmen unseres PNJL-Modells auch in dieser Arbeit berechnet. Während das Phasendiagramm auf großen Skalen wie das von aQC_{2D} aussieht, gibt es einen beträchtlichen Unterschied in der Topologie, wenn eine Vergrößerung in der Nähe der Kreuzung von Deconfinement- und BEC-Übergangslinien vorgenommen wird. Weil

der Deconfinement-Übergang jetzt von erster Ordnung ist, ist die kritische Linie für BEC gebrochen und trifft die Deconfinement-Linie an zwei dreifachen kritischen Punkten. Deswegen existiert ein schmaler Bereich in den chemischen Potentialen, wo das Diquark-Kondensat in einem Phasenübergang erster Ordnung ungewöhnlich verschwindet, wenn die Temperatur steigt.

Die Casimir-Skalierungshypothese behauptet, dass das Farb-Singlet-Potential zwischen statischem Quark und Antiquark in einem mittleren Abstand proportional zur quadratischen Casimir Invariante, $C_2(\mathcal{R})$, ist, wobei \mathcal{R} die Darstellung der Quarks bedeutet. Das kann eine Gelegenheit zum Verstehen des nichtperturbativen Verhaltens der QCD-ähnlichen Theorien schaffen, und sollte solche ein notwendiger Bestandteil jedes Modells sein soll, das versucht, die QCD-(Thermo)Dynamik nachzuahmen.

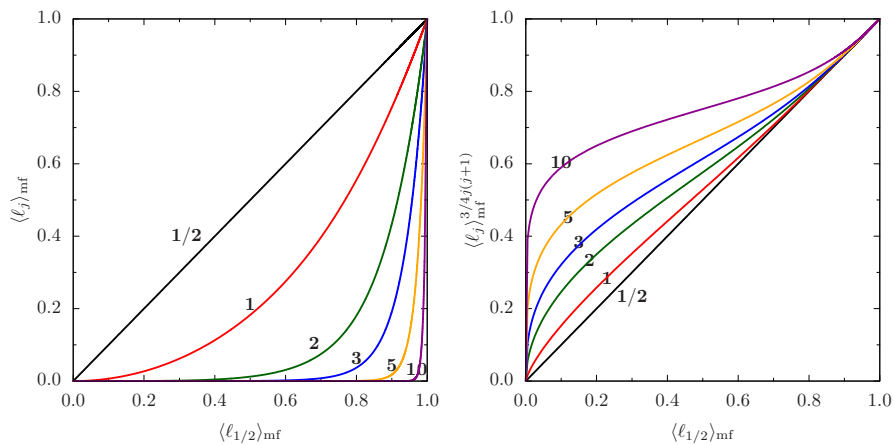


Abbildung 0.2: Erwartungswerte der Polyakov-Schleifen.

Abbildung 0.2 zeigt die Erwartungswerte der Polyakov-Schleife in den gewählten Darstellungen gegen die in der fundamentalen Darstellung. Durch Vergleich zwischen dem linken und dem rechten Bild, die die nichtskalierten und skalierten Polyakov-Schleifen zeigen, sieht man, dass die Casimir-Skalierung sehr gut reproduziert ist, wenn sich der Wert der fundamentalen Schleife gegen Eins nähert, welches hohen Temperaturen entspricht. Es wird schlechter bei niedrigen Temperaturen, wo das Modell der Wechselwirkungen zwischen den nächsten Nachbarn zu einfach ist.

EQCD, eine dimensional reduzierte effektive Theorie für QCD, kann die Dynamik der QCD für großen Abständen und bei sehr hohen Temperaturen

gut reproduzieren. Aber es gibt Zeichen dafür, dass EQCD nicht in der Lage ist, die korrekten Resultate bis zu Temperaturen von wenigen T_c zu produzieren, wobei T_c die kritische Temperatur des Deconfinement-Übergangs ist. EQCD zu modifizieren und eine neue effektive Theorie zu entwickeln, die sich auf die zentrale Symmetrie bezieht, ist ein möglicher Weg, um das Problem zu überwinden. Die neue Theorie, ZQCD genannt, soll in der Lage sein, die Ergebnisse von QCD oder EQCD bei asymptotisch hohen Temperaturen zu reproduzieren und sich auch auf die zentrale Symmetrie zu beziehen, damit sie bis zu Temperaturen um T_c gültig bleibt.

Die Lagrange-Dichte von ZQCD ist gegeben durch

$$\mathcal{L} = \frac{1}{g_3^2} \left[\frac{1}{2} \text{Tr} F_{ij}^2 + \text{Tr} (D_i \mathcal{Z}^\dagger D_i \mathcal{Z}) + V(\mathcal{Z}) \right],$$

wobei g_3 die Eichkopplung der effektiven Theorie ist, $D_i \equiv \partial_i - i[A_i, \cdot]$, $F_{ij} \equiv \partial_i A_j - \partial_j A_i - i[A_i, A_j]$ und das Potential $V(\mathcal{Z})$ ist

$$V(\mathcal{Z}) = h_1 \text{Tr}(\mathcal{Z}^\dagger \mathcal{Z}) + h_2 (\text{Tr} \mathcal{Z}^\dagger \mathcal{Z})^2 + \\ + g_3^2 \left[\frac{s_1}{2} \vec{\Pi}^2 + \frac{s_2}{4} (\vec{\Pi}^2)^2 + s_3 \Sigma^4 + \frac{s_4}{2} \Sigma^3 + \frac{s_5}{2} \Sigma \vec{\Pi}^2 \right].$$

\mathcal{Z} ist hier das Matrixfeld und kann wie folgt parametrisiert werden:

$$\mathcal{Z} = \frac{1}{2} (\Sigma \mathbb{1} + i \vec{\Pi} \cdot \vec{\sigma}),$$

wobei $\vec{\Pi}$ als die Nullmode der elektrischen Gluonen identifiziert wird. Wegen des Fermion-Effekts brechen die letzten zwei Terme des oben erwähnten effektiven Potentials die zentrale Symmetrie Z_2 leicht. Wenn $s_{4,5}$ zu Null geht, wird die Situation auf den Yang-Mills-Fall reduziert, in dem die zentrale Symmetrie eine exakte Symmetrie ist.

Das Σ -Feld wird ein nichtverschwindendes Kondensat bei $\langle \Sigma \rangle = v_0 = 2T$ haben, welches zur spontanen Brechung der $SU(2) \otimes SU(2)$ Symmetrie in der Lagrange-Dichte führt. Das Higgs-Feld bekommt eine harte Masse und entkoppelt von der weichen Energieskala. Das Feld kann ausintegriert werden, nachdem die Entwicklung des effektiven Potentials um das Minimum vorgenommen wird. Das resultierende Potential stimmt dann mit dem von

EQCD über und die Parameter können auf diesem Wege bestimmt werden. Die Bestimmung der Parameter in der führenden Ordnung ergibt

$$\begin{aligned} s_1 - 4s_3v_0^2 - \frac{3}{2}s_4v_0 + s_5v_0 &= \frac{2T}{3} - \frac{T\kappa_0^-}{\pi^2}, \\ 2s_2 + 8s_3 + \frac{3s_4}{2v_0} - \frac{2s_5}{v_0} &= \frac{2}{3\pi^2T} + \frac{\kappa_2^-}{12\pi^2T}, \end{aligned}$$

wobei die Konstante κ_ℓ^\pm mit den Effekten der Quarks verbunden sind.

Die Parameter $s_{4,5}$ können nicht durch Vergleich zwischen ZQCD und EQCD bestimmt werden, weil sie die globale Information von der Brechung der zentralen Symmetrie tragen. Sie werden durch Vergleich der Energie- und Masseaufspaltung bei den Minima der ZQCD zu denen in QCD bestimmt. Die Details findet man in dieser Arbeit.

Nachdem die Parameter zur führenden Ordnung bestimmt sind, können die Profile der freien Ergie als eine Anwendung der ZQCD berechnet werden. Es ist die Domänenwand in der Yang-Mills-Theorie und die Domänenblase mit dynamischen Quarks. Die Domänenwand ohne Quarks wird zu $\sigma = 0.91\sigma_{\text{YM}}$ vorhergesagt. Man erhält auch den Radius einer statischen Domänenblase, $R = 2g\sigma/(\delta T^3)$.

Acknowledgements

First of all, I would like to express my deep gratitude to my supervisor Dirk H. Rischke. His inspiration shows the direction in physics as a lighthouse on the ocean, and leads to my fruitful research.

I am deeply grateful to Tomáš Brauner for his patient and elegant instruction throughout my study. From the numerous discussions with him, I learned a lot, not only about the knowledge itself, but also on the ways of thinking and learning. My Ph.D. project would never proceed so smoothly without his help. My appreciation also goes to Aleksi Vuorinen for his hospitality when I visited Bielefeld in December, 2010 and February, 2011.

I also gratefully thank the support from Pengfei Zhuang who was my supervisor of master degree in Beijing. I thank the discussion and help from my colleagues: Weitian Deng, Francesco Giacosa, Elena Gubankova, Lianyi He, Xuguang Huang, Aleksi Kurkela, Yunpeng Liu, Nan Su, Harmen Warringa, Zhe Xu, and many other colleagues and friends not listed here. The financial supports from DAAD and HGS-HIRE are also heartily acknowledged.

I reserve the last and special place to my family for their lasting support and love, including my parents and my fiancée, Chao Yang.

To my family

Contents

1. Introduction	3
2. QCD and effective models	7
2.1. QCD and its symmetries	7
2.1.1. Color symmetry	7
2.1.2. Center symmetry	8
2.1.3. Color confinement	10
2.1.4. Chiral symmetry	12
2.2. QCD phase diagram	14
2.3. QCD-like theories	15
2.4. Effective theories	17
2.4.1. General philosophy of EFT	17
2.4.2. NJL model	21
2.4.3. PNJL model	22
2.4.4. Dimensional reduction and EQCD	23
3. QCD-like theories at nonzero T and μ: a PNJL model study	27
3.1. Model setup	28
3.1.1. Gauge sector	28
3.1.2. Quark sector	31
3.1.3. Mean-field approximation	33
3.1.4. Parameter fixing in the quark sector	35
3.2. Two colors	36
3.2.1. Phase diagram	37
3.2.2. Tetracritical point	41
3.2.3. Casimir scaling	43
3.3. Three colors	45
3.3.1. Phase diagram	47

3.3.2. Casimir scaling	49
4. Dimensional reduction for two-color QCD	51
4.1. Model setup of ZQCD	52
4.2. Identification of the fields	54
4.3. Matching of the soft parameters	56
4.3.1. Perturbative matching of the Lagrangians	56
4.3.2. The Z_2 breaking parameters	58
4.4. Extended field configurations	59
5. Conclusions	63
A. Haar measure of unitary groups	67
B. Fierz transformation of the current–current interaction	75
C. Gauge group averaging with continuum quarks	77
D. Group integration for $SU(N)$	81
E. EQCD parameters in the presence of massive fermions	85
F. Center symmetry for the $SU(2)$ gauge group	89
G. One-loop effective potential of ZQCD	91
Bibliography	97
List of figures	105
List of tables	107

*“The most incomprehensible thing about
the world is that it is comprehensible.”*

— Albert Einstein

Chapter 1.

Introduction

The exploration of the building blocks of our universe has never stopped since the electron was first discovered in 1897. More and more elementary particles were discovered successively, including three generations of quarks and leptons, and gauge bosons which act as carriers of the fundamental forces.¹ Besides the elementary ones, many composite particles have also been found in experiments, including a large number of hadron species. In order to explain all the experimental results, theorists dedicated tens of years of effort to build theoretical frameworks for the interactions between particles. The endeavor finally led to the unification of electromagnetic and weak interactions in 1960s and the establishment of quantum chromodynamics (QCD) by early 1970s. These theories are already standard material in textbooks of quantum field theory for many years.

For more than half a century, QCD keeps attracting a lot of attention due to its various and interesting properties. It consists only of quarks in a localized color gauge group and gluons as the mediator. However, the world of QCD is far more complicate than its basic ingredients may appear. Unlike the abelian gauge theory quantum electrodynamics (QED) where photons have no electric charge, the gluons in QCD, which is a *non-abelian* gauge theory, carry nonzero color charges. Therefore, gluons can interact between themselves, leading to distinctive consequences. For example, the color interaction between quarks becomes not stronger but weaker at smaller distance, which is known as *asymptotic freedom*. This is a consequence of the non-abelian nature of gluon dynamics, with or without quarks. This “running” behavior

¹There may be another species, an elementary boson, the Higgs boson, which is a hypothetical massive elementary particle introduced in the Standard Model to explain why other particles have mass. As of the writing of this thesis (December of 2011) there have been searches for the Standard Model Higgs boson with the ATLAS and CMS experiments, and candidate events are observed around 125 GeV. However, a definitive statement on the existence or non-existence of the Higgs cannot be made before more data is collected, most likely not before the end of 2012.

of the QCD coupling strength is measured in experiments, as shown in Figure 1.1: α_s becomes smaller when measured at higher energy scales.

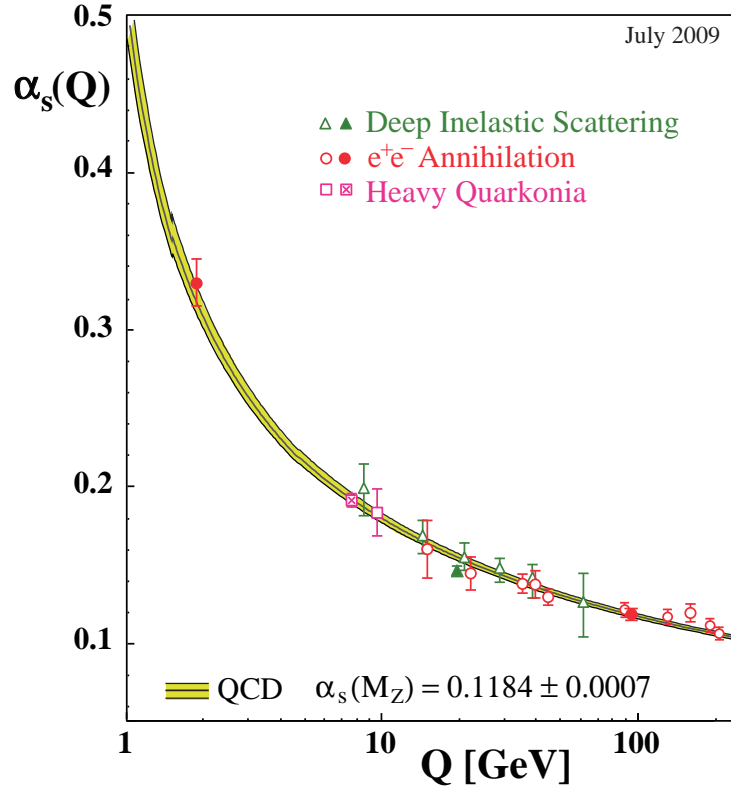


Figure 1.1.: The measurements of α_s as a function of the energy scale Q . The curves are QCD predictions given the value of $\alpha_s(M_{Z^0})$ as shown in the figure. The empty, full and crossed symbols are extracted values from experiments and lattice calculations. Plot is taken from Ref. [1].

While a perturbative treatment is applicable in the weak-coupling regime, it fails to be practical at low energy scales, where the coupling is no longer small as seen in Figure 1.1. It is exactly at such scales where a large amount of hadrons emerges and their properties need to be explained. The behavior of QCD at strong coupling is not fully understood yet. Amazing puzzles are left unsolved, including the structure of hadrons, the phenomenon of color confinement, and the structure of the QCD vacuum. It is believed that the solutions are closely related to the non-abelian properties of Yang-Mills theories which are the simplest non-abelian theories with only gluons.²

More inspiration may be obtained from QCD at nonzero temperature and density. With increasing temperature and density, new phases will emerge in QCD matter under extreme

²The understanding of Yang-Mills theories is selected as one of the seven Millennium Prize Problems.

conditions, where the strength of the QCD coupling and its vacuum structure will be changed by many-body effects. In the new phases the color charges are no more confined, the vacuum is changed due to the restoration of chiral symmetry, and thus phase transitions can be expected. There are experiments pursuing this goal, such as at the Relativistic Heavy-Ion Collider (RHIC) at Brookhaven National Laboratory (BNL), the Large Hadron Collider (LHC) at the European Organization for Nuclear Research (CERN), and the Facility for Antiproton and Ion Research (FAIR) under construction at GSI Helmholtzzentrum für Schwerionenforschung (GSI). QCD at nonzero temperature can also be numerically simulated on discrete spacetime lattices, which is known as lattice QCD. Although the experiments have not given definite information about phase transitions, this idea is supported by the results from lattice QCD. The problem of lattice QCD is that, due to the sign problem, standard Monte-Carlo techniques based on importance sampling cannot be used at nonzero density.

QCD-like theories³ can shed light on our understanding of QCD. They are not theories that describe our universe, but can be simpler models to get deeper insight into our unsolved problems. Furthermore, some of them can be simulated on lattice, the results from which can be used to confirm the conclusion from a theoretical derivation. In this thesis I will study QCD-like theories at nonzero temperature and density, especially focusing on the deconfinement phase transition and the restoration of chiral symmetry.

The thesis is organized as follows. In Chapter 2 I will present the concepts of QCD, its symmetries and the phase diagram. The philosophy of effective theories will also be discussed. At the end of Chapter 2 I will introduce QCD-like theories for use in the following chapters. Then in Chapter 3 I will exploit the Polyakov-loop Nambu–Jona-Lasinio (PNJL) model to study the phase transitions of QCD-like theories at low temperature and density, where the gauge coupling is large and perturbative methods cannot be used. After that in Chapter 4 I will turn to the other direction, *i.e.*, approaching the phase transition region from high temperatures. There a three-dimensional effective theory will be built to describe the physics from high temperatures down to the critical temperature. Unlike the case of low temperature and density, perturbation theory can be applied at high temperature and is expected to work also near the critical temperature. Finally, Chapter 5 gives the conclusions. Some technical details are delegated to the appendices.

³There are several different kinds of QCD-like theories, such as QCD with an imaginary chemical potential, at nonzero isospin density, and QCD with quarks in a different representation of the color group other than the fundamental one. In this thesis, the term “QCD-like” refers to the last case.

Throughout the thesis, I use natural units in which Planck's and Boltzmann's constants as well as the speed of light are equal to one, *i.e.*, $\hbar = k_B = c = 1$. The metric tensor in the Minkowski space is $g_{\mu\nu} = g^{\mu\nu} = \text{diag}(1, -1, -1, -1)$.

Chapter 2.

QCD and effective models

This chapter is for pedagogical purpose. I will first present the symmetries in QCD, including the center symmetry and chiral symmetry, and the putative phase diagram of QCD. Then I introduce QCD-like theories and discuss some of their properties. After that the notion of effective theories is explained, followed by the PNJL model and EQCD which will be used in later chapters.

2.1. QCD and its symmetries

2.1.1. Color symmetry

The Lagrangian of QCD in Minkowski spacetime is given by

$$\mathcal{L} = -\frac{1}{4}F_{\mu\nu}^a F^{a\mu\nu} + \bar{\psi}(i\not{D} - m)\psi, \quad (2.1)$$

where $F_{\mu\nu}^a = \partial_\mu A_\nu^a - \partial_\nu A_\mu^a + g f^{abc} A_\mu^b A_\nu^c$ is the gluon field strength tensor with the QCD coupling constant g and the structure constants f^{abc} of the color SU(3) group, $D_\mu = \partial_\mu - igA_\mu^a t^a$ is the gauge covariant derivative with the color generators t^a , and m is the mass matrix of the quark field ψ . The first term in Eq.(2.1) is the Lagrangian of SU(3) Yang-Mills theory. The generators t^a in \not{D} should be in the same representation of SU(3) as the quarks ψ , which, in QCD, is the fundamental representation.

Under a color SU(3) transformation, $V(x) = e^{ia^a(x)t^a}$, the fields transform as

$$\begin{aligned}\psi(x) &\rightarrow \psi'(x) = V(x)\psi(x), \\ A_\mu^a(x)t^a &\rightarrow A'_\mu^a(x)t^a = V(x)\left(A_\mu^a(x)t^a + ig^{-1}\partial_\mu\right)V^\dagger(x).\end{aligned}\tag{2.2}$$

The QCD Lagrangian (2.1) is invariant under this local gauge transformation.

Since I will study QCD matter in equilibrium statistical mechanics using the imaginary-time formalism, the fields depends on spacetime coordinates (\mathbf{x}, τ) , where the imaginary time τ corresponds to it in Minkowski spacetime. At nonzero temperature T , the range of τ is $[0, \beta]$, where $\beta = T^{-1}$, and the fields obey the boundary conditions

$$\begin{aligned}\varphi(\mathbf{x}, \tau = \beta) &= \varphi(\mathbf{x}, \tau = 0) && \text{periodic for boson fields,} \\ \psi(\mathbf{x}, \tau = \beta) &= -\psi(\mathbf{x}, \tau = 0) && \text{anti-periodic for fermion fields.}\end{aligned}\tag{2.3}$$

Thus there exist such constrains for the local gauge transformation that the boundary conditions (2.3) should be preserved. A trivial choice is the strictly periodic transformation as

$$V(\mathbf{x}, \tau = \beta) = V(\mathbf{x}, \tau = 0).\tag{2.4}$$

It is easy to see that the transformed fields ψ' and A' in Eq.(2.2) are still (anti)periodic under the transformation (2.4), provided that the conditions (2.3) hold before such a transformation.

Is there any nontrivial transformation other than the strictly periodic one (2.4) which also preserves the boundary condition (2.3)? The answer is yes for pure gluo-dynamics without quarks, *i.e.*, Yang-Mills theory. If there exist quarks in the system, the answer depends on the color representation of the quarks. The following subsection is dedicated to this question.

2.1.2. Center symmetry

The nontrivial transformations proposed above, which preserve the periodic boundary condition (2.3), are found to be¹

$$V_{\tau=\beta} = e^{i\theta} \cdot V_{\tau=0}, \quad \theta \in \left\{0, \frac{2\pi}{3}, \frac{4\pi}{3}\right\},\tag{2.5}$$

¹Since there is no confusion in this subsection, \mathbf{x} is not written explicitly.

i.e., the group element for $\tau = \beta$ is the same as that for $\tau = 0$ up to a overall factor. It is obvious that the strictly periodic transformation (2.4) is one of the three pieces in Eq.(2.5).

Given the periodic gluon field $A_\mu^a(\tau = \beta) = A_\mu^a(\tau = 0)$, the A' in Eq.(2.2) transformed under Eq.(2.5) obeys $A_\mu^{\prime a}(\tau = \beta) = A_\mu^{\prime a}(\tau = 0)$ because the phase angle $e^{i\theta}$ commutes with the generators and thus cancels. However, such a cancellation does not mean that the angle θ can be any real number. Because $V_{\tau=0}$ and $V_{\tau=\beta}$ are both SU(3) elements, the phase $e^{i\theta}$ should also be an SU(3) element. From group theory we know that every group \mathcal{G} has a normal subgroup $\mathcal{Z}(\mathcal{G})$, all elements of which commute with any element of \mathcal{G} . This subgroup $\mathcal{Z}(\mathcal{G})$ is called the *center* of \mathcal{G} . Thus $\mathcal{Z}(\mathcal{G})$ is an abelian group and its elements are always proportional to the unit matrix in any irreducible representation of \mathcal{G} . The center of the SU(N) group in a faithful representation is $\{e^{i2k\pi/N} | k = 0, \dots, N - 1\}$. The three factors in Eq.(2.5) constitute exactly the center of SU(3) in the fundamental representation.

Since both the Lagrangian of Yang-Mills theory and the periodic boundary conditions (2.3) are invariant under the twisted transformation (2.5), we say that Yang-Mills theory has a *center symmetry* Z_3 , and gluons carry no center charge. It is required that the twisted local color transformation $V(\mathbf{x}, \tau)$ is still continuous in spacetime. Thus the phase θ must be the same for all spatial coordinates \mathbf{x} , *i.e.*, the center symmetry is a global one.

Now what happens to quarks is different. Since the quark field transforms as $\psi' = V\psi$, the anti-periodic condition (2.3) before the transformation (2.5) implies that $\psi'(\tau = \beta) = e^{i\theta}\psi'(\tau = 0)$, *i.e.*, the breaking of the anti-periodic condition. This is a consequence of the fact that in QCD quarks are in the fundamental representation, which is a faithful representation of SU(3) resulting in a nontrivial center group. Although the Lagrangian (2.1) is still invariant under the twisted local color transformation (2.5), we say that the presence of fundamental quark breaks the center symmetry because the boundary condition is broken, and that quarks carry nonzero center charge. We will see something different in QCD-like theories in Section 2.3, namely that not all quarks break the center symmetry.

It turns out that the center symmetry is closely related to the phenomenon of color confinement. In the following subsection I will study this phenomenon and its relation to the center symmetry.

2.1.3. Color confinement

Color confinement is an experimental fact: color-charged particles are not observed in isolations in the final states of experiments; color charges are always confined inside hadrons. This is equivalent to requiring that all hadrons which can be directly observed should be singlets of the color SU(3) group, *i.e.*, invariant under color transformations. Such requirement is consistent with the fact that among the many low-lying configurations of quarks only $q\bar{q}$, qqq , and $\bar{q}\bar{q}\bar{q}$ states, which generate singlets of color SU(3), are verified as final hadrons.

Although the dynamical mechanism of color confinement is still not completely clear, it is widely accepted that the color charges will be liberated at sufficiently high temperatures and that there exists a deconfined phase[2, 3, 4]. The existence of such a transition is also suggested by lattice-QCD calculations: as the temperature increases, thermodynamic quantities, such as pressure, energy density, and entropy density, rapidly rise at a certain critical temperature, indicating that many degrees of freedom which are confined at low temperatures are released when heated. This phenomenon appears both in Yang-Mills theory [5] and with quarks [6], therefore it may be related to the fact that the coupling constant becomes small at high temperatures.

Considering the free energy is helpful for our understanding. It is shown that the difference in free energy when we put a static quark at \mathbf{r}_1 and a static antiquark at \mathbf{r}_2 into the system can be expressed as

$$e^{-\beta F_{\mathcal{R},\bar{\mathcal{R}}}} = \langle \ell_{\mathcal{R}}(\mathbf{x}_1) \ell_{\bar{\mathcal{R}}}^{\dagger}(\mathbf{x}_2) \rangle, \quad (2.6)$$

where $\beta = T^{-1}$ is the inverse temperature, $F_{\mathcal{R},\bar{\mathcal{R}}}$ is the free energy above the vacuum with a quark in the color representation \mathcal{R} and an antiquark in $\bar{\mathcal{R}}$, sitting at \mathbf{x}_1 and \mathbf{x}_2 , respectively. Here $\langle \dots \rangle$ means the ensemble average, and the traced Polyakov loop in the quark's representation is defined as

$$\ell_{\mathcal{R}}(\mathbf{x}) = \frac{1}{\dim\mathcal{R}} \text{Tr} L_{\mathcal{R}}(\mathbf{x}) = \frac{1}{\dim\mathcal{R}} \text{Tr} \mathcal{P} \exp \left(ig \int_0^{\beta} d\tau A_0^a(\mathbf{x}, \tau) t_{\mathcal{R}}^a \right), \quad (2.7)$$

where the trace is in color space and the path-ordered integral is along the imaginary time line for a given spatial point \mathbf{x} . Here the Polyakov loop $L_{\mathcal{R}}(\mathbf{x})$ is a matrix in the representation \mathcal{R} of the SU(3) color group. The behavior of the free energy at large distance is further constrained

by the cluster property as

$$\langle \ell_{\mathcal{R}}(\mathbf{x}_1) \ell_{\mathcal{R}}^\dagger(\mathbf{x}_2) \rangle \xrightarrow{|\mathbf{x}_1 - \mathbf{x}_2| \rightarrow \infty} \langle \ell_{\mathcal{R}}(\mathbf{x}_1) \rangle \langle \ell_{\mathcal{R}}^\dagger(\mathbf{x}_2) \rangle = |\langle \ell_{\mathcal{R}}(0) \rangle|^2, \quad (2.8)$$

which means

$$F_{\mathcal{R}, \overline{\mathcal{R}}}(\mathbf{x}_1 - \mathbf{x}_2) \xrightarrow{|\mathbf{x}_1 - \mathbf{x}_2| \rightarrow \infty} 2F_{\mathcal{R}}. \quad (2.9)$$

If $F_{\mathcal{R}}$ diverges, then it requires infinite energy to separate a quark-antiquark pair, which means the color charge is confined in such a case. This corresponds to $\langle \ell_{\mathcal{R}} \rangle = 0$. Thus the vanishing average value of Polyakov loop is a test of confinement.

The relation to the center symmetry can be seen when we consider the transformation of the Polyakov loop under the center symmetry. Here we consider the Polyakov loop in a faithful representation \mathcal{R} , for example, the fundamental one. For an arbitrary local color transformation $V(x)$, the Polyakov loop changes as

$$L_{\mathcal{R}}(\mathbf{x}) \rightarrow V_{\tau=\beta} L_{\mathcal{R}}(\mathbf{x}) V_{\tau=0}^\dagger. \quad (2.10)$$

Under the center symmetry (2.5), the traced loop changes as

$$\ell_{\mathcal{R}}(\mathbf{x}) \rightarrow e^{i\theta} \ell_{\mathcal{R}}(\mathbf{x}), \quad (2.11)$$

and its average value transforms in the same way

$$\langle \ell_{\mathcal{R}} \rangle \rightarrow e^{i\theta} \langle \ell_{\mathcal{R}} \rangle. \quad (2.12)$$

When the vacuum is an eigenstate of the center transformation, $\langle \ell_{\mathcal{R}} \rangle$ should also be invariant, thus the only possibility is a vanishing average value of the traced Polyakov loop, which in turn corresponds to an infinite energy $F_{\mathcal{R}}$ and the color confined phase. Oppositely, if a nonzero value of $\langle \ell_{\mathcal{R}} \rangle$ is found, then the vacuum is no longer an eigenstate of the center transformation, *i.e.*, the center symmetry is spontaneously broken, corresponding to a finite $F_{\mathcal{R}}$ and a color deconfined phase. Therefore, the deconfining of the color charges is indeed related to the breaking of the center symmetry.

The center symmetry is well-defined when there are only gluons in the system.² If we couple fundamental quarks with finite mass to gluons, the center symmetry is explicitly broken. The center symmetry is an approximate symmetry in this case and the order parameter is not necessarily zero even in the confined phase. This can smoothen the sharp phase transition and leads to a crossover from the confined phase to the deconfined phase. The presence of quarks also introduces another complexity, *i.e.*, the chiral symmetry.

2.1.4. Chiral symmetry

The QCD Lagrangian (2.1) has global symmetries for massless quark fields in flavor space. Taking two flavors of quarks as an example, the transformations are defined as

$$\begin{array}{lll}
 \text{isospin} & \psi \rightarrow e^{-i\omega \cdot \frac{\tau}{2}} \psi & J_\mu^k = \bar{\psi} \gamma_\mu \tau^k \psi \\
 \text{chiral} & \psi \rightarrow e^{-i\gamma_5 \theta \cdot \frac{\tau}{2}} \psi & J_{5\mu}^k = \bar{\psi} \gamma_\mu \gamma_5 \tau^k \psi \\
 \text{baryonic} & \psi \rightarrow e^{-i\alpha} \psi & J_\mu = \bar{\psi} \gamma_\mu \psi \\
 \text{axial} & \psi \rightarrow e^{-i\gamma_5 \beta} \psi & J_{5\mu} = \bar{\psi} \gamma_\mu \gamma_5 \psi
 \end{array} \tag{2.13}$$

where τ^k ($k = 1, 2, 3$) are Pauli matrices in flavor space. According to Noether's theorem, conserved charges can be defined from continuous symmetries. Here J are the Noether currents of the corresponding symmetries, and conserved charges can be defined as $Q = \int d^3x J_0$.

The baryon charge is strictly conserved in QCD. The isospin symmetry is well-defined as long as the mass parameters for two flavors, conventionally u - and d -quark, are the same. It is also conserved in QCD. Unlike the isospin which transforms the left- and right-quark exactly the same way in flavor space, the chiral symmetry transforms them in an opposite direction. It is spontaneously broken in the ground state, *i.e.*, the physical vacuum is not an eigenstate under the chiral transformation, resulting in several Nambu–Goldstone bosons. The axial symmetry is in fact absent in QCD because it is broken on the quantum level due to the instanton effects.³ Therefore, generalizing to an arbitrary N_f , the flavor symmetry of QCD is in fact a global $SU(N_f)_L \times SU(N_f)_R \times U(1)_B$ group.

²Static quarks are not dynamic particles. They can be understood as fermions which are first coupled to the Yang-Mills theory and mass are then sent to ∞ . In such a way we can study the effects of static quarks in any color representation, such as the free energy and the potential between them.

³This is called $U(1)_A$ anomaly. It is related to the topological configurations of the gluon fields. In fact the chiral symmetry is also broken by an anomaly due to electroweak interaction but we do not consider this in QCD. For details see Chapter 19 of Ref. [7].

The light mesons, such as pion and kaon, observed in experiments are identified as the Nambu–Goldstone bosons coming from the spontaneous breaking of chiral symmetry. They are massive because in QCD quarks have small masses, thus the chiral symmetry is an approximate one and these mesons obtain light masses, which are still far less than the typical mass of hadrons (~ 1 GeV). Since in the low-energy region quarks and gluons are confined in hadrons, the lightest degrees of freedom are these Goldstone bosons, therefore physics on this energy scale is dominated by the spontaneous breaking of chiral symmetry and its Goldstone bosons.

The mechanism of the spontaneous breaking of chiral symmetry can be understood as follows. Since quarks have small masses and strong attractive interactions, it does not cost much energy to create an extra quark-antiquark pair. Thus the QCD vacuum has a structure containing a condensate of quark-antiquark pairs. These fermion pairs must have zero total momentum and angular momentum, which implies that left-handed quarks and the antiparticles of right-handed quarks condense in the pairing process. It is the condensate in the vacuum that breaks the chiral symmetry. The vacuum with a quark pair condensate can be expressed as

$$\langle \bar{\psi}\psi \rangle = \langle \bar{\psi}_L\psi_R + \bar{\psi}_R\psi_L \rangle, \quad (2.14)$$

which is not invariant under a chiral transformation. Actually it is the same operator as in the quark mass term. When this condensate is nonzero, the chiral symmetry is broken, which mixes the two quark helicities and gives quarks an effective mass even though the quarks may appear massless on the Lagrangian level.

It is expected that at high temperature and density, the spontaneous breaking of chiral symmetry will be reduced and finally disappear due to the thermal fluctuations and diminishing coupling strength. Such restoration of chiral symmetry may be seen in experiments from the signal that the masses of mesons which are connected by the chiral transformation become degenerate. To detect chiral symmetry restoration is one of the major goals of ultrarelativistic heavy-ion experiments. The interplay between chiral symmetry restoration and deconfinement is still not clear.

2.2. QCD phase diagram

The $T - \mu$ phase diagram of QCD matter is summarized in Figure 2.1. I will describe it from left to right, *i.e.*, from the lower to the higher density region.

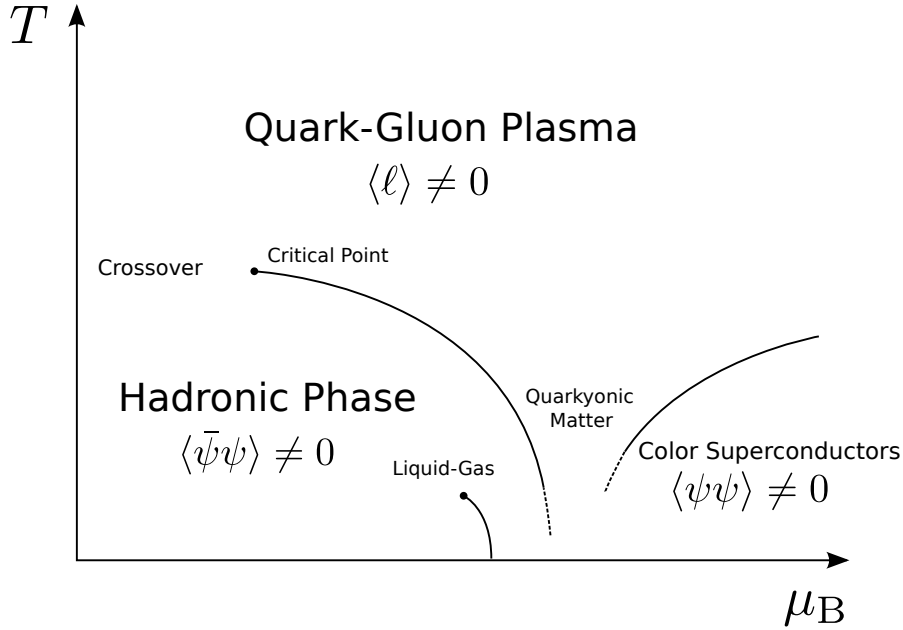


Figure 2.1.: The $T - \mu_B$ phase diagram of QCD.

At very low baryon chemical potential $\mu \ll T$, the system is in the hadronic phase at low temperatures and is a quark-gluon plasma at high temperatures. There is a crossover region above which the chiral symmetry is restored and color charges are deconfined, around 150 MeV – 200 MeV. If it were SU(3) Yang-Mills theory without quarks, the well-defined center symmetry will break around 270 MeV, according to results of lattice QCD. The presence of quarks spoils the sharp transition of center symmetry breaking, and lowers its transition temperature.

In the region with larger μ , there is no reliable information from first-principle lattice QCD calculations. Nevertheless, most of the chiral models suggest that there is a QCD critical point located at the end of a first-order phase transition line. Searching for this critical point is of great experimental interest.

At low temperature $T \simeq 0$, a non-vanishing baryon density of nuclear matter⁴ arises at $\mu_N \simeq 924$ MeV. At the threshold $\mu = \mu_N$ the density jumps from zero to normal nuclear density 0.17fm^{-3} . Above it the nuclear matter is a nuclear superfluid. This first-order phase transition is called the liquid-gas transition of nuclear matter. It weakens as temperature grows and finally ends in a second-order critical point at $T \simeq 15$ MeV – 20 MeV.

If μ is asymptotically large, *i.e.*, $\mu \gg \Lambda_{\text{QCD}}$, the ground state of QCD matter can be analyzed with weak-coupling methods. It turns out that at low T quarks will form Cooper pairs and condense in the vacuum state. This phenomenon is called color superconductivity.

I will study the phase diagram of QCD-like theories in Chapter 3, which is very different from that of QCD. In the following section I will give a brief introduction to QCD-like theories and the motivation to study them.

2.3. QCD-like theories

Studying QCD-like theories may provide us with clues about how to solve the problems in QCD. In QCD, the color group is $SU(3)$ and the quarks are in its fundamental representation. QCD-like theories can be created by changing the color group and/or the quarks' representation. In this thesis I focus on two types of QCD-like theories:

Type I: quarks in a *strictly real* representation of the gauge group,

Type II: quarks in a *pseudoreal* representation of the gauge group.⁵

The typical examples of type-I theories include QCD with adjoint quarks of two (aQC₂D) or three (aQCD) colors. Type-II theories include two-color QCD with fundamental quarks (QC₂D).

The first advantage of type-I and type-II QCD-like theories is that they are free of the fermion sign problem [8, 9, 10, 11, 12, 13, 14]. The sign problem [15] is an obstacle for numerical simulations of QCD with nonzero baryon chemical potential μ . In lattice QCD the

⁴The nucleon mass is about 939 MeV. The binding energy in isospin-symmetric nuclear matter is around 16 MeV.

⁵Consider a compact Lie group. A *real* representation \mathcal{R} is equivalent to its conjugate representation $\bar{\mathcal{R}}$. The similarity transformation matrix, U , is a unitary matrix. U can be either symmetric or antisymmetric. If U is symmetric, \mathcal{R} is called *strictly real*, otherwise it is *pseudoreal*.

partition function of QCD in Euclidean spacetime is written as

$$\mathcal{Z} = \int \mathcal{D}[A, \bar{\psi}, \psi] e^{-\int d^4x (\mathcal{L}_{\text{gl}}(A) + \bar{\psi} M(A) \psi)} = \int \mathcal{D}[A] \det M(A) e^{-S_{\text{gl}}[A]}, \quad (2.15)$$

where quantities with subscript “gl” are for the pure gluon sector. Without the baryon chemical potential μ , we always have $\det M(A) \geq 0$ for any configuration of the gluon field A . Thus, this determinant can be used for importance sampling in Monte-Carlo calculations. When $\mu > 0$, $\det_{\mu} M(A)$ is generally complex and its real part can be negative, thus it cannot be interpreted as a probability distribution. Even after rewriting $\det_{\mu} M(A) = |\det_{\mu} M(A)| e^{i\theta}$, the averaging of the phase θ still causes problems. However, it can be shown that with nonzero μ , this determinant in type-I theories is always non-negative and in type-II is at least real. Thus these theories can be simulated numerically on the lattice including density effects.⁶

The second motivation to study QCD-like theories is that the flavor symmetry of quarks is very different to that in QCD. With N_f massless quark flavors, the global flavor symmetry is $SU(2N_f)$ rather than the usual chiral group $SU(N_f)_L \times SU(N_f)_R \times U(1)_B$. The reason is that the charge-conjugated⁷ quark field $(\psi_R)^C$ which is a left-handed spinor transforms in the same way as the left-handed quark ψ_L under both color and Lorentz transformations, so it is allowed to transform them into each other while keeping the color symmetry intact. This means that the multiplets of states in the spectrum will contain modes of different baryon number. In particular, apart from the pions the Nambu–Goldstone (NG) bosons of the spontaneously broken flavor symmetry will also include diquarks. These light diquarks are colorless bosons carrying baryon charge, and hence at low temperature and sufficiently high chemical potential, they will undergo Bose–Einstein condensation (BEC). This feature is very different from QCD, leading to a different topology of the phase diagram, as will be shown in Chapter 3.

Besides the advantages mentioned above, in type-I theories the Z_{N_c} center symmetry remains intact in the presence of dynamical quarks. This leads to a well-defined deconfinement phase transition, accompanied by spontaneous center symmetry breaking, instead of a crossover as in QCD [16]. The associated order parameter is the expectation value of the Polyakov loop. For the two- and three-color cases investigated in this thesis, the deconfinement transition is of second and of first order, respectively.

In Chapter 3 I will study the phase diagrams of aQC₂D and aQCD, both belonging to type I, using the Polyakov-loop Nambu–Jona-Lasinio (PNJL) model and in Chapter 4 I study

⁶In type-II theories, we need an even number of flavors for the lattice simulations to be feasible.

⁷The charge-conjugated quark field is defined as $\psi^C = C\bar{\psi}^T$ with the charge conjugation matrix C .

QC₂D, belonging to type II, using dimensionally reduced effective theory. Now it is time to introduce these effective theories for use in the following chapters.

2.4. Effective theories

2.4.1. General philosophy of EFT

Because the coupling constant of QCD becomes larger when the energy scale decreases, perturbative methods become more and more imprecise for physics around and below the scale of Λ_{QCD} . Finally they fail to be applicable for calculations at these energy scales. In such a situation, effective field theories (EFT) are not only convenient but also necessary to overcome this problem.

An effective field theory⁸ includes appropriate degrees of freedom to describe the phenomena occurring below a certain energy scale, Λ , called the *cutoff*. The high-energy Hilbert states in the underlying fundamental theory do not appear directly in the low-energy phenomena, but they still influence the low-energy physics as a background of virtual fluctuations excited and annihilated in the vacuum. The beauty of effective theories is that these effects on the low-energy physics can be reproduced to any desired precision using a finite number of interactions and tuning their parameters.

An effective field theory can be intuitively constructed by explicitly integrating out the heavy modes above Λ in the underlying theory. This is known as the Wilsonian approach. If we denote the light modes as ϕ_L , the heavy ones as ϕ_H , the actions of the underlying and effective theory as $\mathcal{S}[\phi_L, \phi_H]$ and $\mathcal{S}_{\text{EFT}}[\phi_L]$ respectively, then in terms of a path integral it can be expressed as

$$\mathcal{Z} = \int \mathcal{D}[\phi_L, \phi_H] e^{-\mathcal{S}[\phi_L, \phi_H]} = \int \mathcal{D}[\phi_L] e^{-\mathcal{S}_{\text{EFT}}[\phi_L]}. \quad (2.16)$$

After integrating out the high-energy states ϕ_H , the Lagrangian of the effective theory, \mathcal{L}_{EFT} , contains all possible interactions that are allowed by the symmetry of the theory and the regu-

⁸This topic can be found in many textbooks and the literature, e.g. Refs. [7, 17, 18, 19, 20, 21].

larization. It can be expressed as

$$\mathcal{L}_{\text{EFT}} = \sum_i \lambda_i \mathcal{O}_i$$

which is an infinite sum over local operators⁹, \mathcal{O}_i , composed of fields and their derivatives.¹⁰ The derivative in a term simply means that this type of interaction depends on external momenta. The coupling constants, λ_i , are called Wilson coefficients.

A specific effective theory should include a method to organize the terms and a systematic scheme of power counting to assess the importance of Feynman diagrams generated by the interaction terms. Generally speaking, the terms can be ordered by the mass dimension of the operators, $d_i \equiv [\mathcal{O}_i]$, which is possible because there are only a finite number of interactions with the same dimension d_i . This order is equivalent to the order of their importance to the low-energy physics. The reason will be shown below.

Because there are infinitely many terms in \mathcal{L}_{EFT} , it is impossible to calculate all of them. In fact this is also not necessary, thanks to the nontrivial information provided by a dimensional analysis. Every term $\lambda_i \mathcal{O}_i$ in the Lagrangian must have the same energy dimension d as space-time, which implies that the coupling, λ_i , must have $[\lambda_i] = d - d_i$. Because the operators come from integrating out the heavy states, the most natural energy scales on which the Wilson coefficients depend are the heavy masses, M_{heavy} . Since their values are controlled beyond the cutoff, Λ , we can express the contribution from the high energy sector as

$$\lambda_i \mathcal{O}_i = \frac{g_i(\Lambda)}{\Lambda^{d_i-d}} \mathcal{O}_i,$$

where $g_i(\Lambda)$ are dimensionless coefficients.^{11,12} At a given energy scale E much lower than Λ , the contribution of $\lambda_i \mathcal{O}_i$ is suppressed by $\left(\frac{E}{\Lambda}\right)^{d_i-d}$. This behavior ensures that up to a desired precision, only a finite number of interactions are required to calculate observables provided

⁹The *nonlocal* operators obtained from the functional integration can be expanded into a series of *local* operators as long as $E \ll \Lambda$.

¹⁰The operators, \mathcal{O}_i , also contain the quark mass matrix in chiral perturbation theory, because it is treated as a small expansion parameter in the scheme of power counting for the low-energy regime.

¹¹The coefficients g_i can contain factors from group theory, combinatorial factors, and phase-space factors. If the size of g_i is unnaturally large or small, an explanation is required. For example a small g_i may come from a weak breaking of some symmetry, otherwise g_i would vanish without this breaking.

¹²The coefficients $g_i(\Lambda)$ are functions of the cutoff Λ because renormalization group theory tells us that the lower the energy scales we integrate out, the more states will contribute to the coupling constants. However the low-energy physics is unaffected because the change of the coefficients compensates the change in the cutoff.

the energy E is fixed. The higher the desired precision, the more higher-dimensional operators are required.

It is a convention to classify the operators according to their dimension, or equivalently by their importance. The contribution from terms with $d_i < d$ are the most important and are called *relevant* interactions. The terms with $d_i = d$, which are called *marginal* interactions, give contributions of order one. The interactions with $d_i > d$ are called *irrelevant* and their contribution is suppressed by the powers of $\left(\frac{E}{\Lambda}\right)$. The irrelevant operators are also the non-renormalizable ones, but they cause no trouble here because the effective theory is not supposed to be applicable at arbitrarily high energy scales but only at scales below Λ .

Although the Wilson coefficients can in principle be calculated perturbatively using the Wilsonian approach to integrate out all heavy modes above Λ , this procedure is cumbersome beyond the leading order. There is a more practical and systematic method to construct an effective model from the underlying theory. To implement this method several steps should be followed. First, the low-energy degrees of freedom should be identified for the effective theory, which should include at least the physical particles observed in experiments. Then one constructs the most general low-energy Lagrangian consistent with the symmetries of the underlying theory and the regularization, starting with the relevant interactions and adding the ones with higher dimension order by order. After that, in order to determine the coefficients, one matches the low-energy results of the effective theory to the results of the full theory which are expanded around the low-energy limit. Finally, the solution to the renormalization group equations can be used to improve the coefficients, which is equivalent to resumming logarithmic contributions. In Chapter 4 I will follow this procedure to match coefficients of ZQCD, a dimensionally reduced effective theory of QCD with Z_2 symmetry, at the leading order.

The cutoff Λ is the energy scale below which the physics can be well described by the effective theory. When the underlying theory is already known, the cutoff Λ is easy to define. For example we can set it equal to the mass of a heavy particle. What about when we do not know the fundamental theory? In such a case we can use effective theory to predict at which energy new physics will emerge, *i.e.*, we can extract Λ from experimental data. In order to see this, let us imagine that experiments are carried out at an energy scale E . Here E may be the energy in the center-of-mass frame. A field theory which has $\Lambda = \infty$ and contains only renormalizable interactions is built to explain the data. The parameters are fitted by computing several observables to sufficient order of the perturbative expansion in some small expansion parameters and matching the results to the data. If the data not used in the

fit can be explained by the theory, we accept the theory as a candidate for describing nature. Now we keep E unchanged and improve the precision of the experiment. Then we repeat the process of fitting parameters and explaining unused data, until we arrive at a new level of precision where some calculation cannot explain the data even if the perturbative calculation is made to high enough order in the small expansion parameters. At this point the only way out is adding new interactions of first order in the $\left(\frac{E}{\Lambda}\right)$ expansion, which are also the possible non-renormalizable terms with the lowest dimension. Since their contributions can be used to explain the discrepancy in the latest experiment, the order $\left(\frac{E}{\Lambda}\right)^{d_i-d}$ of the new interactions should be the same as the precision of the data. Hence we can estimate the order of Λ for the new physics. By adding a finite number of new terms and tuning the existing and newly added coefficients, the new data can be explained to the new precision.¹³ On the other hand, if we increase the energy E instead of keeping it unchanged, the contribution of order $\left(\frac{E}{\Lambda}\right)^{d_i-d}$ becomes larger such that a low precision experiment can find new physics. However, more interaction terms may be necessary in order to achieve the same precision as at a lower E , again because the $\left(\frac{E}{\Lambda}\right)$ expansion converges less well. When E approaches Λ , the effective theory turns out to be useless because the $\left(\frac{E}{\Lambda}\right)$ expansion no longer converges. In such a case the energies are so high that the hidden heavy degrees of freedom are about to be excited, which should also be contained in the effective theory.

In fact it is the nature of effective theories that makes our physics research possible. The universe has a vast hierarchy of scales, from the cosmic distance to the tiniest particles. It will be impossible to do anything if all levels of scales are taken into account. In fact we always start with ignoring the short-range structure and focusing on the relevant scale of a particular problem, as the “leading order” of the effective theory. Then with more precise experiments we include the effects of short-range structures as higher-order corrections. At the same time more fundamental theories are proposed to reproduce the coefficients and used to derive the interactions in the effective theory. Finally most of these theories are ruled out by new experimental data and only one survives, which is in the position of an effective theory for the next scale. Then history repeats itself with the newer physics.

¹³Because a number of non-renormalizable interactions are added, the calculation should be regulated by the value of Λ estimated for the *new* physics.

2.4.2. NJL model

The Nambu–Jona-Lasinio (NJL) model was first used to study the interaction between nucleons before quarks were known [22]. Now it is widely used as an effective model for QCD below the energy scale of Λ_{QCD} [23, 24, 25]. The biggest advantage of the NJL model is that it inherits all the symmetries of QCD, as a result it is successful in describing the physics related to the flavor symmetries, such as the spontaneous breaking of chiral symmetry, its restoration at nonzero temperature and density, and the properties of Goldstone bosons. Again taking $N_f = 2$ as an example, the Lagrangian of the NJL model, which preserves the flavor $SU(N_f)_L \times SU(N_f)_R \times U(1)_B$ symmetry, reads

$$\mathcal{L}_{\text{NJL}} = \bar{\psi}(i\cancel{\partial} - m)\psi + G \left[(\bar{\psi}\psi)^2 + (\bar{\psi}i\gamma_5\tau\psi)^2 \right]. \quad (2.17)$$

The interaction between quarks in the NJL model is a four-fermion interaction which can be understood as integrating out gluons as shown in Figure 2.2.

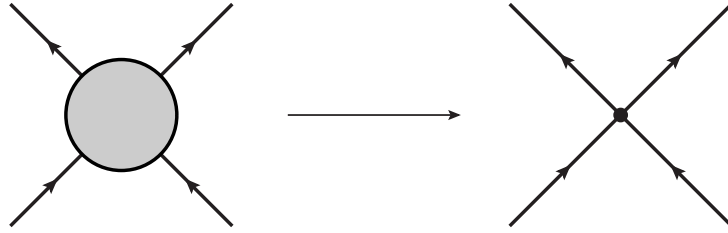


Figure 2.2.: Four-fermion interaction in the NJL model.

The parameters in the NJL model include the mass parameters of quarks m , the coupling constant G , and the regularization parameters, for example the cutoff Λ in momentum loop integrals. They are usually fixed by calculating physical quantities at $T = \mu = 0$, such as the mass of pion m_π , the pion-decay constant f_π , and the quark condensate density $\langle \bar{\psi}\psi \rangle$. After fixing the parameters, the NJL model can be used to calculate the spontaneous breaking of chiral symmetry. In mean-field approximation (MFA), the bilinear operator $\bar{\psi}\psi$ can be written as

$$\bar{\psi}\psi = \langle \bar{\psi}\psi \rangle + \hat{\delta}, \quad (2.18)$$

where $\hat{\delta} = \bar{\psi}\psi - \langle\bar{\psi}\psi\rangle$. Substituting this approximation back into the Lagrangian and ignoring the $\hat{\delta}^2$ term, the approximation becomes

$$(\bar{\psi}\psi)^2 \simeq 2\langle\bar{\psi}\psi\rangle\bar{\psi}\psi - \langle\bar{\psi}\psi\rangle^2. \quad (2.19)$$

Thus the Lagrangian again becomes a free theory for quasi-fermions with effective mass

$$m^* = m - 2G\langle\bar{\psi}\psi\rangle, \quad (2.20)$$

where m is the mass parameter in the NJL Lagrangian. The condensate $\langle\bar{\psi}\psi\rangle$ can in turn be expressed as a loop integral of a quasi-fermion with effective mass m^* . Then finally Eq. (2.20) becomes a self-consistency equation for m^* , which is called the *gap equation*. It can be expressed using Feynman diagrams as shown in Figure 2.3.

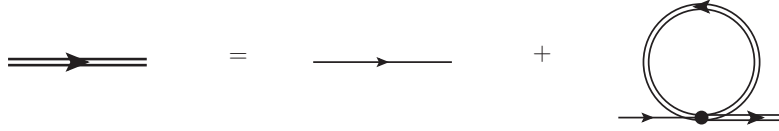


Figure 2.3.: The Feynman diagrams for the gap equation using the MFA in the NJL model. A single line is the propagator of a free quark and a double line is that of a quasi-fermion with effective mass m^* .

The solution of the gap equation in the NJL model verifies the belief that the condensate $\bar{\psi}\psi$ becomes small, *i.e.*, chiral symmetry is restored, at high temperature and high baryon chemical potential. Because gluons are absent in the NJL model, however, it cannot correctly describe the color confinement on its accessible energy scales.

2.4.3. PNJL model

In order to include the missing gluon sector and the confinement feature in NJL the model, the Polyakov-loop Nambu–Jona-Lasinio (PNJL) model was proposed [26, 27, 28, 29, 30]. In the PNJL model an effective potential for the Polyakov loop is added to the thermodynamic potential of the NJL model, and the Polyakov loop is coupled to quarks by a constant temporal background gluon field in the covariant derivative. It is expressed as

$$\mathcal{L}_{\text{PNJL}} = \bar{\psi}(i\not{D} - m)\psi + G\left[(\bar{\psi}\psi)^2 + (\bar{\psi}i\gamma_5\tau\psi)^2\right] - \mathcal{U}(\ell, \bar{\ell}, T). \quad (2.21)$$

where $D_\mu = \partial_\mu - iA_\mu$ and the gauge coupling is absorbed into the A_μ field, \mathcal{U} is the effective potential of traced Polyakov loops, T is the temperature.

The parameters in the PNJL model include the old ones of the NJL model and new ones in the gauge sector. The old ones are still fixed by the same method as in the NJL model, because at $T = 0$ the contribution from the gauge sector vanishes, thus the PNJL reduces to the NJL model. To fix the new parameters in the gauge sector, imagine we send the quark mass to infinity to decouple quarks from our model. Then the thermodynamic quantities of the pure gauge sector can be calculated to match known results from lattice calculation of the corresponding Yang-Mills theory, for example the temperature of the center symmetry transition, the pressure, entropy density, and energy density.

After fixing the old and new parameters separately, predictions can be made and compared to results of lattice QCD. The successful qualitative reproduction of the coincidence of the deconfinement and the chiral restoration temperatures, T_d and T_χ , in QCD is one of the great virtues of the PNJL model. However, as I will show in Chapter 3, QCD-like theories with adjoint quarks are very different with respect to this feature. First, $T_d \ll T_\chi$, resulting in a broad range of temperatures exhibiting deconfined, but still chirally broken matter [31, 32, 33]. Second, T_d does not change much compared to the pure gauge theory when quarks are coupled in, because adjoint quarks carry zero center charge.

2.4.4. Dimensional reduction and EQCD

In the imaginary time formalism the fields in the partition function \mathcal{Z} fulfill periodic boundary conditions (here ϕ is used for both the gluon field A_a^μ and the quark field ψ)

$$\phi(\mathbf{x}, \tau = 0) = \pm \phi(\mathbf{x}, \tau = \beta). \quad (2.22)$$

They can be decomposed into Fourier modes in τ , i.e.,

$$\phi(\mathbf{x}, \tau) = \sqrt{T} \sum_n e^{i\omega_n \tau} \varphi_n(\mathbf{x}), \quad (2.23)$$

with Matsubara frequencies $\omega_n = 2n\pi T$ for bosons and $\nu_n = (2n + 1)\pi T$ for fermions. The Matsubara frequencies act as a mass for the n -th component $\varphi_n(\mathbf{x})$, which can be seen from

the bosonic propagator

$$\mathcal{D}_0(\omega_n, \mathbf{p}) = \frac{1}{\mathbf{p}^2 + (\omega_n^2 + m^2)}$$

and the fermionic one

$$\mathcal{S}_0(\omega_n, \mathbf{p}) = \frac{\not{p} + m}{\mathbf{p}^2 + (v_n^2 + m^2)}.$$

Now let us consider a theory in which the bosons have vanishing mass terms. It is easy to see that the zeroth component $\varphi_0(\mathbf{x})$ of the boson fields remains almost massless and all other components obtain masses of at least $2\pi T$. The fermions always have nonzero masses larger than or equal to πT for all the Fourier components, no matter whether the fermionic mass term vanishes or not.

In such a case, the lightest low-energy excitation in the theory is the zeroth component of the boson field. This provides an opportunity to integrate out all heavy modes above T , *i.e.*, all nonzero bosonic modes and all fermionic modes, to build an effective theory containing only the bosonic zero mode $\varphi_0(\mathbf{x})$. This effective theory lives in three-dimensional space and can be used to reproduce the static correlation functions at long distances $R \gg 1/T$ because the contribution from the exchange of any massive mode with frequency ω_n is exponentially suppressed¹⁴ at large R , with the exception of the zero mode. This process is called *dimensional reduction* [34].

Before we start to construct the effective theory for the bosonic zero mode, it is necessary to have a closer look at the existing energy scales. The fact that the only dimensional quantity in the theory is the temperature T does not imply that the only energy scale in the system is of the typical kinetic energy of the particles, $\sim T$. In fact, the screening effect in the heat bath generates a nonzero mass for the boson fields, which is much lower than T . This scale corresponds to the screening of the long-range force at a much longer distance than T^{-1} . For example in massless $\lambda\phi^4$ theory this scale is of order $\sqrt{\lambda}T$, in QED it is of order eT , and in QCD it is of order gT . Moreover, in nonabelian gauge theories exists another much lower scale [35]. In QCD it is of order g^2T due to the screening of the chromomagnetic force at a

¹⁴This behavior can be intuitively seen from the bosonic propagator

$$\langle \varphi_n(\mathbf{x}) \varphi_{-n}(\mathbf{0}) \rangle = \int \frac{d^3 p}{(2\pi)^3} \frac{e^{i\mathbf{p}\cdot\mathbf{x}}}{\mathbf{p}^2 + \omega_n^2} = \frac{e^{-|\omega_n|R}}{4\pi R},$$

where $R \equiv |\mathbf{x}|$.

distance $(g^2T)^{-1}$, in addition to the scale gT due to the screening of the chromoelectric force at distance $(gT)^{-1}$. Thus we can construct an effective theory in three space dimensions for the scale gT for QCD, which is called electrostatic QCD (EQCD) [36]. It is still possible to build another effective theory for the lower scale g^2T , based on EQCD, which is called magnetostatic QCD (MQCD). In this thesis I only discuss the scale gT , *i.e.*, EQCD.

In EQCD the degrees of freedom are the electrostatic gluon $A_0^a(\mathbf{x})$ and the magnetostatic gluon $A_i^a(\mathbf{x})$ with the space index $i = 1, 2, 3$ and the color index $a = 1, \dots, 8$. They are the zero modes of the gluon field $A_\mu^a(\mathbf{x}, \tau)$. The magnetostatic gluon now inherits the color gauge symmetry while the electrostatic gluon is in the adjoint representation of this residual symmetry. Thus it is not hard to write down the relevant and marginal operators for EQCD,

$$\mathcal{L}_{\text{EQCD}} = \frac{1}{4}G_{ij}^a G_{ij}^a + \frac{1}{2}(D_i A_0)^a (D_i A_0)^a + \frac{1}{2}m_E^2 A_0^a A_0^a + \frac{1}{8}\lambda_E (A_0^a A_0^a)^2 + \delta\mathcal{L}_{\text{EQCD}}, \quad (2.24)$$

where $G_{ij}^a = \partial_i A_j^a - \partial_j A_i^a + g_E f^{abc} A_i^b A_j^c$ is the magnetostatic field strength with coupling constant g_E . The term $\delta\mathcal{L}_{\text{EQCD}}$ contains all other local gauge-invariant operators of dimension 3 and higher. The parameters g_E , m_E , λ_E , and the parameters in $\delta\mathcal{L}_{\text{EQCD}}$ are functions of the QCD coupling g , the temperature T , and the ultraviolet regulator Λ_E of EQCD. The scale Λ_E plays the role to separate the scale T from the scale gT . Another parameter f_E , which is the coefficient of the unit operator omitted in Eq.(2.24), is needed to reproduce the free energy density of thermal QCD. It can be defined using the partition function of QCD as

$$\mathcal{Z}_{\text{QCD}} = \int \mathcal{D}[A_\mu^a, \psi, \bar{\psi}] e^{-S_{\text{QCD}}} = e^{-V \cdot f_E} \int \mathcal{D}[A_0^a(\mathbf{x}), A_i^a(\mathbf{x})] e^{-\int d^3x \mathcal{L}_{\text{EQCD}}}. \quad (2.25)$$

This f_E can be understood as the contribution to free energy from the nonzero modes above T . It also depends on g , T , and Λ_E . The static correlation functions and the free energy of QCD can be reproduced by tuning the parameters of $\mathcal{L}_{\text{EQCD}}$, including g_E , m_E , λ_E , and f_E . The dependence of Λ_E in these EQCD parameters will finally be cancelled by the loop integrals and cutoff-independent observables can be reproduced.

Chapter 3.

QCD-like theories at nonzero T and μ : a PNJL model study

In this chapter I will focus on type-I and type-II QCD-like theories, namely, those with quarks in a *strictly real* and *pseudoreal* representation of the gauge group, respectively. As discussed in Section 2.3, they have very different phase diagrams compared to QCD. Here I will take two-color (QC₂D) and three-color adjoint QCD (aQCD) for examples and study their phase diagrams and the behavior of Casimir scaling.

To model the gauge sector, I will use a simple lattice spin model with nearest-neighbor interaction, inspired by the strong-coupling expansion [14, 26, 37, 38, 39, 40]. This is then coupled to continuum quarks in a fashion similar to the Polyakov-loop NJL (PNJL) model [26, 27, 28, 29, 30]. The successful qualitative reproduction of the coincidence of the deconfinement and chiral restoration temperatures, T_d and T_χ , in QCD is then one of the great virtues of the PNJL model. On the other hand, aQCD is very different. First, $T_d \ll T_\chi$, resulting in a broad range of temperatures exhibiting deconfined, but still chirally broken matter [31, 32, 33] (see also Refs. [41, 42] for related theories with periodic boundary conditions for quarks). Second, T_d does not change much compared to the pure gauge theory when quarks are coupled in, because adjoint quarks carry zero center charge. I will confirm these features.

This chapter is organized as follows. In Sec. 3.1 I will introduce the model, working out separately the actions in the gauge and quark sectors. The gauge part is well known from literature, and I therefore just elaborate on the Weiss mean-field approximation. In the quark part I deal with the task to construct an interaction Lagrangian with $SU(2N_f)$ flavor symmetry. While this was previously achieved for QC₂D and actually applies equally well to all type-II theories, here I construct analogously a model Lagrangian for type-I theories. Section 3.2 is

devoted to two-color QCD. I study the phase diagram of aQC₂D and derive the Ginzburg–Landau (GL) theory that governs the behavior of the system near the tetracritical point. I will show a simple *closed* analytic expression for the expectation values of the Polyakov loop in all representations, valid in pure gauge theory as well as with dynamical quarks in an arbitrary representation. In Sec. 3.3 I will show analogous results for aQCD.¹

3.1. Model setup

In this section I discuss the model that I later on use for numerical computations. In the gauge sector I employ a simple lattice-inspired model, which can in principle be used for any number of colors. The quark NJL Lagrangian derived afterwards is applicable to all QCD-like theories with quarks in a real representation. This is natural: the Lagrangian is based almost exclusively on the flavor symmetry and is therefore valid for an arbitrary number of colors. The numerical values of the parameters in the model will be fixed in the following sections when I come to the discussion of concrete results.

3.1.1. Gauge sector

The starting point for the pure gauge sector is an effective theory for the Polyakov loop inspired by the lattice strong-coupling expansion. I closely follow the notation and line of argument of Ref. [26]. The action of the model is given by

$$\mathcal{S}_g[L] = -N_c^2 e^{-a/T} \sum_{\mathbf{x}, \mathbf{y}} \ell_{\mathbb{F}}(\mathbf{x}) \ell_{\mathbb{F}}^*(\mathbf{x} + \mathbf{y}), \quad (3.1)$$

where \mathbf{x} are the lattice sites and \mathbf{y} are the neighboring sites. (Boldface is used to indicate spatial vectors.) The only adjustable parameter a is related to the string tension and can be extracted from numerical simulations of the full (pure) gauge theory. Furthermore, $\ell_{\mathbb{F}}(\mathbf{x}) \equiv \frac{1}{N_c} \text{Tr} L_{\mathbb{F}}(\mathbf{x})$ is the traced Polyakov loop in the fundamental representation; in the full gauge theory, the Polyakov loop in a given representation \mathcal{R} is defined as

$$L_{\mathcal{R}}(\mathbf{x}) \equiv \mathcal{P} \exp \left[i \int_0^{1/T} d\tau A_4^a(\mathbf{x}, \tau) T_{a\mathcal{R}} \right], \quad (3.2)$$

¹This chapter is based on the publication Ref. [43].

where $T_{a\mathcal{R}}$ are the gauge generators in this representation.

In the so-called Polyakov gauge where temporal gluon fields have constant values, this simplifies to

$$L_{\mathcal{R}}(\mathbf{x}) = \exp [iA_4^a(\mathbf{x})T_{a\mathcal{R}}/T]. \quad (3.3)$$

Moreover, only the components of A_4^a corresponding to generators that form the Cartan subalgebra of the gauge group are nonzero. Let these components be $\theta_i T$. (There are $N_c - 1$ independent ones; the conventional factor T makes the variables θ_i dimensionless.) Each representation of the gauge group is characterized by a set of weights, $w_{i\alpha}$, that represent the eigenvalues of the generators of the Cartan subalgebra in this representation; the index α labels the different eigenvectors of the Cartan subalgebra. The traced Polyakov loop in representation \mathcal{R} then reads

$$\ell_{\mathcal{R}}(\mathbf{x}) = \frac{1}{\dim \mathcal{R}} \sum_{\alpha} e^{i\theta_i(\mathbf{x})w_{i\alpha}}. \quad (3.4)$$

In the fundamental representation, the Polyakov loop (in the Polyakov gauge) is usually represented as $\text{diag}(e^{i\theta_1}, \dots, e^{i\theta_{N_c-1}}, e^{-i(\theta_1 + \dots + \theta_{N_c-1})})$. This corresponds to the choice of the N_c weights of the fundamental representation as $w_{i\alpha} = \delta_{i\alpha}$ for $\alpha = 1, \dots, N_c - 1$, and $w_{iN_c} = -1$ for all i . Equivalently, it can be written by defining $\theta_{N_c} = -(\theta_1 + \dots + \theta_{N_c-1})$ up to an integer multiple of 2π .

In the Weiss mean-field approximation, the nearest-neighbor interaction is linearized and the action (3.1) is replaced with the action $\mathcal{S}_{\text{mf}}(\alpha, \beta)$, depending on two mean fields α, β ,²

$$\mathcal{S}_{\text{mf}}(\alpha, \beta) = -N_c \sum_{\mathbf{x}} [\alpha \text{Re } \ell_{\text{F}}(\mathbf{x}) + i\beta \text{Im } \ell_{\text{F}}(\mathbf{x})]. \quad (3.5)$$

The dynamical variables of the model (3.1) are the (untraced) Polyakov loops $L(\mathbf{x})$ and its partition function is therefore obtained as $\mathcal{Z}_g \equiv \exp(-\Omega_g/T) = \int \prod_{\mathbf{x}} dL(\mathbf{x}) \exp(-\mathcal{S}_g[L])$, where dL is the group-invariant (Haar) measure of the $\text{SU}(N_c)$ gauge group. For the sake of future reference, let us add that in terms of the phases θ_i , the Haar measure can be written as

$$dL = \prod_{i=1}^{N_c-1} d\theta_i \prod_{i<j}^{N_c} |e^{i\theta_i} - e^{i\theta_j}|^2, \quad (3.6)$$

²Here, I adhere to the notation introduced in Ref. [26]. The symbol β is not to be confused with the inverse temperature.

The integration over the variables θ_i is performed over the range $[0, 2\pi]$. More details of the Haar measure can be found in Appendix A.

The thermodynamic potential can now be rewritten by subtracting and adding the mean-field action, resulting in the expression

$$\frac{\Omega_g}{T} = -\log\langle e^{-(S_g - S_{\text{mf}})} \rangle_{\text{mf}} - \log \int \prod_{\mathbf{x}} dL(\mathbf{x}) e^{-S_{\text{mf}}}. \quad (3.7)$$

Here and in the following, $\langle \cdot \rangle_{\text{mf}}$ is the average with respect to the distribution defined by the mean-field action. For a given (not necessarily local) function $O[L]$ of the Polyakov loop, it reads

$$\langle O \rangle_{\text{mf}} = \frac{\int \prod_{\mathbf{x}} dL(\mathbf{x}) O[L] e^{-S_{\text{mf}}}}{\int \prod_{\mathbf{x}} dL(\mathbf{x}) e^{-S_{\text{mf}}}}. \quad (3.8)$$

Note that when the function O is local and does not depend explicitly on the coordinate, the product over lattice sites can be dropped.

Equation (3.7) is still exact; no approximation has been made so far. By the same token, the thermodynamic potential Ω_g is independent of the arbitrary variables α, β . In the Weiss mean-field approximation, one replaces $\langle e^{-(S_g - S_{\text{mf}})} \rangle_{\text{mf}}$ with $e^{-\langle S_g - S_{\text{mf}} \rangle_{\text{mf}}}$ [26]. The mean fields are then determined selfconsistently from the stationarity condition. In fact, as long as $\beta = 0$ so that the averaging is done with a real mean-field action, one can use Jensen's inequality³ to show that this approximation provides a strict upper bound for the exact free energy. Its optimum estimate is then obtained by minimizing with respect to α .

The final formula for the Weiss mean-field gauge thermodynamic potential reads

$$\begin{aligned} \frac{\Omega_g^{\text{W}} a_s^3}{TV} = & -2(d-1)N_c^2 e^{-a/T} \langle \ell_{\text{F}} \rangle_{\text{mf}} \langle \ell_{\text{F}}^* \rangle_{\text{mf}} + \frac{N_c}{2} [(\alpha + \beta) \langle \ell_{\text{F}} \rangle_{\text{mf}} + (\alpha - \beta) \langle \ell_{\text{F}}^* \rangle_{\text{mf}}] - \\ & - \log \int dL e^{N_c(\alpha \text{Re } \ell_{\text{F}} + i\beta \text{Im } \ell_{\text{F}})}. \end{aligned} \quad (3.9)$$

³Jensen's inequality states rather generally that for any real convex function f , $f(\langle x \rangle) \leq \langle f(x) \rangle$, where the averaging involves either a (weighted) arithmetic mean in the discrete version of the inequality, or an integral average over a given probability distribution in the continuous version.

Here a_s denotes the lattice spacing and the factor a_s^3/V is just the inverse of the number of lattice sites; d stands for the dimensionality of spacetime so that $2(d - 1)$ is the number of nearest neighbors on a cubic lattice.

3.1.2. Quark sector

The Lagrangian of the quark sector cannot be derived from the underlying gauge theory directly. However, it is strongly constrained by the requirement that it inherits all the symmetries of the QCD-like theory. As already stressed above, in theories with N_f massless quark flavors in a (pseudo)real representation of the gauge group, the usual chiral symmetry is promoted to $SU(2N_f)$. In order to see how this comes about, let us start from the Lagrangian of the quark sector, including a common mass m_0 for all quark flavors,

$$\mathcal{L}_{\text{QCD-like}} = \bar{\psi} i \mathcal{D} \psi - m_0 \bar{\psi} \psi, \quad (3.10)$$

where $\mathcal{D}_\mu \psi = (\partial_\mu - ig T_a A_\mu^a) \psi$ is the gauge-covariant derivative. Indices are suppressed so that this formula holds for quarks in any representation of the gauge group.

The fact that the quark representation is (pseudo)real means that there is a unitary matrix \mathcal{P} in color space such that $\mathcal{P} \psi^C$ has the same transformation properties under the gauge group as ψ .⁴ It is then advantageous to trade the Dirac spinor, consisting of the left- and right-handed components, for the purely left-handed Nambu spinor,

$$\Psi = \begin{pmatrix} \psi_L \\ \mathcal{P} \psi_R^C \end{pmatrix}. \quad (3.11)$$

A crucial fact known from the theory of Lie algebras is that \mathcal{P} is either symmetric or anti-symmetric according to whether the quark representation is real or pseudoreal [44]. Writing collectively $\mathcal{P}^T = \pm \mathcal{P}$ and using $(\mathcal{P} \psi_R^C)^C = \mathcal{P}^* \psi_R$, we can introduce the charge-conjugated Nambu spinor,

$$\Psi^C = \mathcal{P} \begin{pmatrix} \psi_L^C \\ (\mathcal{P} \psi_R^C)^C \end{pmatrix} = \begin{pmatrix} \mathcal{P} \psi_L^C \\ \pm \psi_R \end{pmatrix}. \quad (3.12)$$

⁴Since \mathcal{P} is a matrix in color space, it commutes with the charge conjugation matrix C which is a matrix in the Dirac space. In QC_2D , \mathcal{P} can be set to τ_2 , *i.e.*, the second Pauli matrix in color space. In aQCD , \mathcal{P} can be set to $\mathbb{1}$.

The Dirac conjugate of both Ψ and Ψ^C is defined naturally by conjugating the individual components. The Lagrangian (3.10) then becomes, in the Nambu formalism,

$$\mathcal{L}_{\text{QCD-like}} = \bar{\Psi} i \not{D} \Psi - \left[\frac{1}{2} m_0 \bar{\Psi}^C \begin{pmatrix} 0 & \mathbb{1} \\ \pm \mathbb{1} & 0 \end{pmatrix} \Psi + \text{H.c.} \right]. \quad (3.13)$$

First of all, we can see that in the chiral limit, the Lagrangian of a QCD-like theory indeed has an $SU(2N_f)$ symmetry. Note that baryon number is already incorporated in this simple group, for it is represented by the block matrix $\frac{1}{2} \text{diag}(\mathbb{1}, -\mathbb{1})$ in Nambu space. The change of the overall phase of the Nambu spinor corresponds to the axial $U(1)_A$ symmetry which is broken at the quantum level by instanton effects. Since the mass term has the same structure as the chiral condensate, we can also immediately infer that for type-I (type-II) theories the order parameter for flavor symmetry breaking transforms as a(n) (anti)symmetric rank-two tensor of $SU(2N_f)$. Therefore, the two classes of theories have different symmetry-breaking patterns and subsequently also different low-energy spectra. The symmetry-breaking patterns in the vacuum are $SU(2N_f) \rightarrow SO(2N_f)$ and $SU(2N_f) \rightarrow Sp(2N_f)$ for type I and type II, respectively [11].

The task to construct an NJL-type interaction compatible with the $SU(2N_f)$ symmetry is most easily accomplished using the Nambu notation (3.11). It is useful to stress right at the outset that as long as only color-singlet channels are considered, each of the Lagrangians to be constructed below applies to the whole class of QCD-like theories (type-I or type-II), regardless of the detailed structure of the gauge group or the quark representation. In fact, NJL Lagrangians for type-II theories with two quark flavors were already constructed in Ref. [45]. Here I follow the same line of argument with the necessary modifications for the type-I case.

One property that further distinguishes type-I and type-II theories is the severity of the sign problem. While I remarked before that all QCD-like theories considered here are free from the sign problem, one should be a bit careful with type-II theories. There, the determinant of the Dirac operator is in general real, but needs not be positive. In order that there be no sign problem, one therefore has to consider an even number of flavors. On the other hand, type-I theories have no sign problem for any number of flavors [8]. As a warm-up exercise, we thus start with the simplest case of one flavor.

In the following, the Pauli matrices $\sigma_{0,1,2,3} = \{\mathbb{1}, \sigma_1, \sigma_2, \sigma_3\}$ are used to denote the block matrices in Nambu space, and $\tau_{0,1,2,3} = \{\mathbb{1}, \tau_1, \tau_2, \tau_3\}$ are used to denote the flavor generators for $N_f = 2$. The symmetric rank-two tensor representation of the flavor $SU(2) \simeq SO(3)$ group

is real and three-dimensional. Using the basis of symmetric unimodular unitary matrices as $\vec{\Sigma} = \{\mathbb{1}, i\sigma_1, i\sigma_3\}$, two four-fermion interaction terms can be immediately constructed,

$$\begin{aligned}\mathcal{L}_{1f,U(2)} &= G|\overline{\Psi^C}\vec{\Sigma}\Psi|^2 = G[(\bar{\psi}\psi)^2 + (\bar{\psi}i\gamma_5\psi)^2 + |\overline{\psi^C}\gamma_5\psi|^2 + |\overline{\psi^C}\psi|^2], \\ \mathcal{L}_{1f,SU(2)} &= \frac{G}{2}[(\overline{\Psi^C}\vec{\Sigma}\Psi)^2 + \text{H.c.}] = -G[(\bar{\psi}\psi)^2 - (\bar{\psi}i\gamma_5\psi)^2 + |\overline{\psi^C}\gamma_5\psi|^2 - |\overline{\psi^C}\psi|^2].\end{aligned}\quad (3.14)$$

While the former preserves the axial $U(1)_A$, the latter breaks it explicitly. It is easy to verify that $\mathcal{L}_{1f,SU(2)}$ is the 't Hooft determinant term, i.e.

$$\mathcal{L}_{1f,SU(2)} = 2G(\det \overline{\Psi_i^C}\Psi_j + \text{H.c.}). \quad (3.15)$$

For two flavors, the ten basis matrices of the symmetric rank-two tensor representation of the flavor $SU(4)$ group are chosen as the symmetric Kronecker products of σ and τ , i.e.

$$\vec{\Sigma} = \{\sigma_{\text{sym}} \otimes \tau_{\text{sym}}, \sigma_{\text{antisym}} \otimes \tau_{\text{antisym}}\}. \quad (3.16)$$

Since the 10-dimensional representation of $SU(4)$ is complex, only one of the above two possibilities to construct an invariant interaction term remains,

$$\begin{aligned}\mathcal{L}_{2f,U(4)} &= G|\overline{\Psi^C}\vec{\Sigma}\Psi|^2 \\ &= G[(\bar{\psi}\psi)^2 + (\bar{\psi}i\gamma_5\vec{\tau}\psi)^2 + (\bar{\psi}i\gamma_5\psi)^2 + (\bar{\psi}\vec{\tau}\psi)^2 + \sum_S |\overline{\psi^C}\tau_S\psi|^2 + \sum_S |\overline{\psi^C}\gamma_5\tau_S\psi|^2],\end{aligned}\quad (3.17)$$

which preserves $U(1)_A$ automatically. (Here τ_S denotes the set of symmetric Pauli matrices, $\tau_S = \{\mathbb{1}, \tau_1, \tau_3\}$.) A $U(1)_A$ breaking interaction can again be introduced by the 't Hooft determinant term, but such a term will be an eight-fermion contact interaction which is not considered here in the model.

3.1.3. Mean-field approximation

I will employ the usual mean-field approximation, introducing the collective bosonic fields via the Hubbard–Stratonovich transformation and subsequently replacing them with their vacuum expectation values. To that end, however, one first needs to guess which condensates (order parameters) will appear in the phase diagram. The case of type-II theories with two quark flavors was worked out in Ref. [45]: as long as just the baryon chemical potential is considered,

one only needs the chiral condensate, $\sigma = -2G\langle\bar{\psi}\psi\rangle$, and the scalar diquark condensate, $\Delta = 2iG\langle\psi^T C\gamma_5\mathcal{P}\tau_2\psi\rangle$. Since the diquark wave function is antisymmetric in color as well as spin indices, it must, by means of the Pauli principle, also be antisymmetric with respect to flavor. The (spin-zero) diquark in type-II theories therefore mixes quarks of different flavors. Consequently, in the presence of an isospin chemical potential the diquark pairing feels stress and eventually diminishes via a first-order phase transition, with a narrow window of chemical potentials featuring inhomogeneous pairing [45, 46].

In type-I theories the scalar order parameters are symmetric in color and antisymmetric in spin indices, hence they must be symmetric in flavor. This is in accordance with the fact that for two flavors, there are altogether nine NG bosons of the SU(4)/SO(4) coset, the isospin triplet of pions and the isospin triplet of (complex) diquarks. At zero isospin chemical potential, the isospin multiplets are strictly degenerate. In particular all uu , dd , and $ud + du$ diquarks can condense when the baryon chemical potential exceeds their common mass. Moreover, for arbitrarily small isospin chemical potential, the diquarks formed from quarks of the same flavor will be favored. Such single-flavor condensates do not feel stress at nonzero chemical potential, and the phase diagram of type-I theories will therefore not contain inhomogeneous phases, as observed in Ref. [47].

With the above argument in mind, we can restrict the attention to single-flavor condensates. The fact that the two-flavor four-fermion interaction (3.17) automatically preserves $U(1)_A$ means that the condensates differing just by opposite parity will be degenerate. However, we know from the Vafa–Witten theorem that in the vacuum parity is not spontaneously broken [48]. The degeneracy will be eventually lifted by instanton effects, manifested in the eight-quark ‘t Hooft interaction term. Within the present model, I will simply ignore the negative-parity channels.

As long as we only deal with one-flavor condensates, we can write down the contribution to the thermodynamic potential from a single quark flavor. This equals the thermodynamic potential of free fermionic quasiparticles. In presence of a pairing gap Δ , their dispersion relation reads $E_k^e = \sqrt{(\xi_k^e)^2 + \Delta^2}$, where $\xi_k^e = \epsilon_k + e\mu$, $e = \pm$, and $\epsilon_k = \sqrt{k^2 + M^2}$; $M = m_0 + \sigma$ is the constituent quark mass and μ the quark chemical potential. The gauge and quark sectors are coupled in the PNJL spirit [27]. In the Polyakov gauge the temporal component of the gauge field is constant. The individual quark color states in a given representation will then have, in the presence of the background gauge field, effective chemical potentials $iT \sum_i \theta_i w_{i\alpha}$. Since the quasiparticle spectrum discussed above is the same for all color states in the representation (this is because all condensates are color singlets!), the thermodynamic

potential of one quark flavor will simply be

$$\begin{aligned} \frac{\Omega_q}{VN_f} = & \frac{\sigma^2 + \Delta^2}{4G} - \sum_e \int \frac{d^3\mathbf{k}}{(2\pi)^3} \times \\ & \times \left\{ E_{\mathbf{k}}^e \dim \mathcal{R} + 2T \log \left\langle \prod_{\alpha} \left[1 + 2 \cos(\theta_i w_{i\alpha}) e^{-E_{\mathbf{k}}^e/T} + e^{-2E_{\mathbf{k}}^e/T} \right]^{1/2} \right\rangle_{\text{mf}} \right\}. \end{aligned} \quad (3.18)$$

The power of 1/2 in the second line compensates the doubling of the number of degrees of freedom in the Nambu formalism.

The group average must be performed once the quarks are coupled to the Polyakov loop. Note that I do not average the full quark thermodynamic potential, but only the argument of the logarithm. This replacement was introduced in Eq. (13) of Ref. [26] as a convenient approximation to $\langle \Omega_q \rangle_{\text{mf}}$. However, in Appendix C I present a heuristic argument showing that the prescription (3.18) is actually superior to the full average $\langle \Omega_q \rangle_{\text{mf}}$. While with fundamental quarks considered in Ref. [26] the numerical difference between the two ways of evaluating the quark sector thermodynamic potential is negligible, it is pointed out that with adjoint quarks, taking the average $\langle \Omega_q \rangle_{\text{mf}}$ would lead to unphysical artifacts which are not present in Eq. (3.18).

3.1.4. Parameter fixing in the quark sector

The NJL part of the model has three adjustable parameters: the coupling G , the current quark mass m_0 , and the ultraviolet cutoff that regulates divergent integrals. (Here I use the three-momentum regularization scheme.) These need to be fixed by fitting to three selected observables. A conventional, and convenient, choice are the chiral condensate, pion mass, and pion decay constant in the vacuum. While the pion mass is more or less a free parameter that can be easily modified in lattice simulations by tuning the quark mass, the remaining two parameters depend on the single physical scale of the underlying theory, and cannot therefore be adjusted at will.

In three-color QCD with fundamental quarks, one can directly use experimental observables. In QC₂D, the input parameters were determined in Ref. [49] from their three-color counterparts by N_c -rescaling. Unfortunately, we are not aware of suitable lattice data that would allow us to fix the parameters directly in the case of aQCD and aQC₂D. We therefore use the following indirect argument. Suppose that there is a theory with both fundamental and adjoint quarks. Gauge invariance can then only be maintained when the coupling of quarks to

gluons is the same in both representations. Since the effective meson-channel Lagrangians of the NJL type can be derived from a one-gluon-exchange-inspired interaction, this allows us to fix the ratio of the effective couplings in the fundamental and adjoint quarks sectors.

Concretely, assume the current–current interaction

$$\mathcal{L}_{\text{int}} = -g(\bar{\psi}\gamma^\mu T_{aR}\psi)^2. \quad (3.19)$$

The coupling g can be directly related to the microscopic QCD coupling and the screening mass of the gluon in the one-gluon-exchange approximation. We can therefore assume that it is the same for fundamental and adjoint quarks. Performing the Fierz transformation to the meson channel yields the effective NJL coupling $G_{\text{F}} = g(N_c^2 - 1)/(2N_c^2 N_f)$ for fundamental quarks [25]. For adjoint quarks we analogously obtain $G_{\text{A}} = gN_c/[(N_c^2 - 1)N_f]$. This results in the ratio

$$\frac{G_{\text{A}}}{G_{\text{F}}} = \frac{2N_c^3}{(N_c^2 - 1)^2}. \quad (3.20)$$

The derivation of this relation is sketched in Appendix B. In the following sections, I will use it to infer the value of the coupling for adjoint quarks from that for the fundamental ones and will not refer to the original current–current interaction anymore.

Equation (3.20) would at first glance suggest that the coupling for adjoint quarks is weaker than for the fundamental ones (with the exception $N_c = 2$). One may then wonder why the chiral restoration temperature is much higher for adjoint quarks. The reason for this is that in the gap equation, the coupling is multiplied by the number of quark degrees of freedom coming from the quark loop. The effective coupling ratio for adjoint versus fundamental quarks therefore is $2N_c^2/(N_c^2 - 1)$ which is always larger than two.

3.2. Two colors

For two colors, the group integration is easily done and it is possible to find closed analytic expressions for all general formulas derived above. First, there is just one independent phase θ , associated with the only diagonal generator of the SU(2) gauge group. The $(2j + 1)$ -dimensional spin- j representation then has weights $-2j\theta, \dots, +2j\theta$, and one immediately ob-

tains

$$\ell_j = \frac{1}{2j+1} \frac{\sin[(2j+1)\theta]}{\sin\theta}. \quad (3.21)$$

The Haar measure (3.6) reduces to $dL = \frac{1}{\pi} \sin^2\theta d\theta$, normalized so that the group volume is unity.

Since all traced Polyakov loops of $SU(2)$ are real, only one mean field α is needed in Eq. (3.5). Using the definition of the modified Bessel function of integer order,

$$I_n(x) = \frac{1}{\pi} \int_0^\pi d\theta e^{x \cos\theta} \cos n\theta, \quad (3.22)$$

and the recurrence relation $I_{n-1}(x) - I_{n+1}(x) = \frac{2n}{x} I_n(x)$, one derives the expectation value of the Polyakov loops [50],

$$\langle \ell_j \rangle_{\text{mf}} = \frac{I_{2j+1}(2\alpha)}{I_1(2\alpha)}. \quad (3.23)$$

The gauge part of the thermodynamic potential (3.9) in turn becomes

$$\frac{\Omega_g^{\text{W}}}{V} = bT \left[-24e^{-a/T} \langle \ell_{\text{F}} \rangle_{\text{mf}}^2 + 2\alpha \langle \ell_{\text{F}} \rangle_{\text{mf}} - \log \frac{I_1(2\alpha)}{\alpha} \right], \quad (3.24)$$

where $b = a_s^{-3}$ and can be compared with the ‘‘standard’’ PNJL model [26, 49]. The weights of the adjoint representation are $-2, 0, 2$ and the group average in the quark sector is also easily evaluated. The result is most conveniently written in terms of the expectation value of the adjoint Polyakov loop,

$$\begin{aligned} \frac{\Omega_q}{VN_f} = & \frac{\sigma^2 + \Delta^2}{4G} - \sum_e \int \frac{d^3\mathbf{k}}{(2\pi)^3} \left[3E_{\mathbf{k}}^e + 2T \log(1 + e^{-E_{\mathbf{k}}^e/T}) + \right. \\ & \left. + 2T \log(1 - e^{-E_{\mathbf{k}}^e/T} + e^{-2E_{\mathbf{k}}^e/T} + 3e^{-E_{\mathbf{k}}^e/T} \langle \ell_{\text{A}} \rangle_{\text{mf}}) \right]. \end{aligned} \quad (3.25)$$

This is the formula that is used for the analysis of the phase diagram.

3.2.1. Phase diagram

The first thing that needs to be done is to fix the parameters of the model. There are altogether five of them: the coupling, current quark mass, and cutoff in the quark sector, and a, b in the

gauge sector. The method to estimate the NJL input parameters was explained in Sec. 3.1.4, so I simply use the parameter set for QC₂D established in Ref. [49] and rescale the coupling according to Eq. (3.20). Also, we introduce an additional factor of two to account for the fact that there is only one quark flavor here. As to the gauge sector, I use the same *physical* input as in Ref. [49], that is, the critical temperature in the pure gauge theory $T_d^0 = 270$ MeV and the string tension $\sigma_s = (425 \text{ MeV})^2$. These values were obtained from the three-color pure gauge theory using their scaling properties in the limit of a large number of colors, so quantitatively they do not precisely agree with those one would obtain directly from the two-color lattice gauge theory. However, this does not matter since we do not fit the parameters in the quark sector to lattice data. I merely wish to demonstrate the general trends as the number of colors or the quark representation are varied.

Since I use a different potential for the Polyakov loop than in Ref. [49], the parameters a, b will actually take different values despite the same input for T_d^0 and σ_s . The deconfinement transition in the pure gauge theory is of second order with two colors, hence we can expand the thermodynamic potential (3.24) to second order in α ,

$$\frac{\Omega_g^W}{V} = bT\alpha^2 \left(\frac{1}{2} - 6e^{-a/T} \right) + O(\alpha^4). \quad (3.26)$$

From here one concludes that $a = T_d^0 \log 12$. The lattice spacing a_s , hence the parameter b , is then determined from the strong-coupling relation $a = \sigma_s a_s$. The numerical values of all parameters are summarized in Tab. 3.1.

a [MeV]	$b^{1/3}$ [MeV]	Λ [MeV]	G [GeV ⁻²]	m_0 [MeV]
670.9	269.2	657	25.71	5.4

Table 3.1.: Model parameters for two-color QCD with adjoint quarks.

The Weiss mean-field approximation employed here differs from the mean-field approximation used in Ref. [49], which I will henceforth refer to as “naive” for reasons explained in Appendix C. In the latter, the gauge sector potential can be expressed solely in terms of the fundamental Polyakov loop and it reads,

$$\frac{\Omega_g^{\text{naive}}}{V} = -bT[24e^{-a/T} \ell_F^2 + \log(1 - \ell_F^2)], \quad (3.27)$$

cf. Eq. (3.24). It is therefore mandatory to compare the results obtained with the two approaches. I do so within the pure gauge theory. The expectation values of the fundamental Polyakov loop and the mean field α are shown in Fig. 3.1.⁵ It is obvious that the results for the Polyakov loop are not sensitive to the particular implementation of the gauge sector as long as the parameters are adjusted to reproduce the same physical observables.

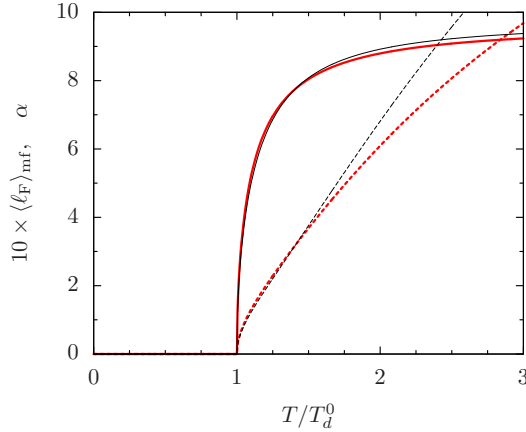


Figure 3.1.: Comparison of the expectation values of the mean field α (dashed) and the fundamental Polyakov loop (solid) in the naive (thin black lines) and Weiss (thick red lines) mean-field approximations to the pure gauge theory.

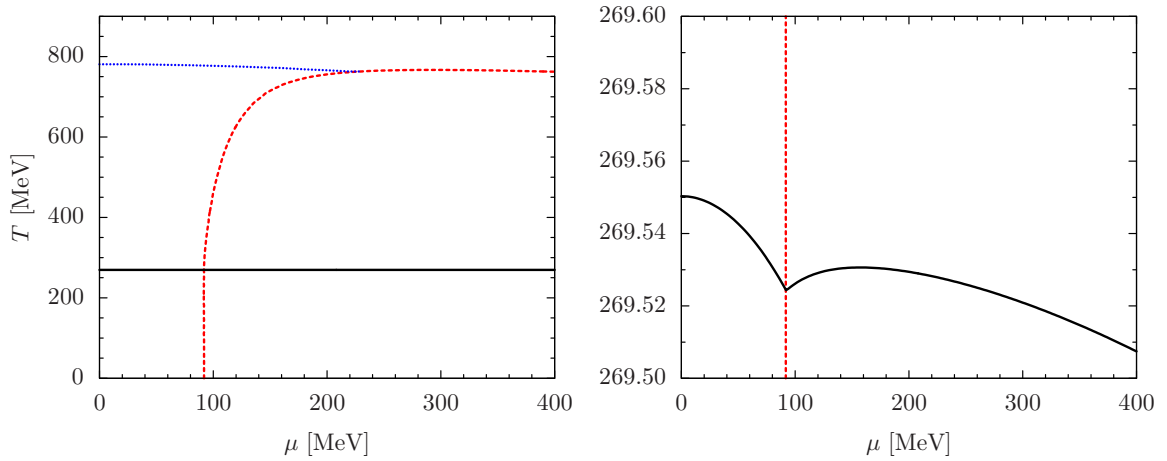


Figure 3.2.: Phase diagram of two-color QCD with one flavor of adjoint quarks. Black solid line: deconfinement transition. Red dashed line: BEC transition. Blue dotted line: chiral crossover. The right panel zooms in the temperature scale so that the cusp in the deconfinement critical line is visible.

Figure 3.2 shows the phase diagram of aQC_2D with one quark flavor in the plane of temperature and quark chemical potential. The deconfinement transition associated with the break-

⁵Note that there is no α in the naive mean-field approximation. The values plotted in Fig. 3.1 were obtained by inverting the relation (3.23).

ing of the center Z_2 is denoted by the black solid line, while the BEC transition at which the baryon number $U(1)_B$ is broken is indicated by the red dashed line. In addition to these two sharp phase transitions, there is a smooth crossover associated with the melting of the chiral condensate. Its position, shown in the left panel of Fig. 3.2 by the blue dotted line, is defined here by the maximum temperature gradient of σ . In the chiral limit, this also becomes a sharp second-order phase transition. As expected, it does appear at a temperature much higher than that of the deconfining transition ($T_d = 270$ MeV, while $T_\chi = 780$ MeV so that $T_\chi/T_d = 2.89$). However, the precise value of this temperature as determined by our model is strongly affected by the cutoff, as is discussed in more detail in Sec. 3.3.1.

The temperature of the deconfining transition depends on the chemical potential extremely weakly, even less than in QC_2D [49]. The reason apparently is that the adjoint quarks are neutral with respect to the center symmetry. The behavior of the transition lines in the vicinity of their “intersection” will be analyzed in detail in the following subsection. Finally, the BEC transition at zero temperature occurs at $\mu = 92$ MeV, which is in a good agreement with the fact that the mass of the pion/diquark multiplet in the vacuum is $m_\pi = 184$ MeV within our parameter set.

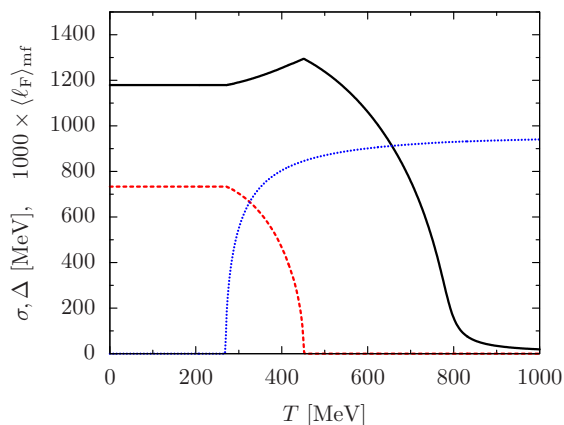


Figure 3.3.: Condensates in aQC₂D at $\mu = 100$ MeV as a function of temperature. The chiral condensate σ (black solid line), diquark condensate Δ (red dashed line), and the fundamental Polyakov loop (blue dotted line) are shown.

As an illustration of the solution of the gap equations, I plot in Fig. 3.3 the condensates at $\mu = 100$ MeV as a function of temperature. One can clearly see the effect of the suppression of thermal quark fluctuations in the confined phase: the condensates are nearly constant for $T < T_d$.

3.2.2. Tetracritical point

Since the BEC and deconfinement phase transitions are both well-defined, being associated with exact symmetries even in the presence of massive dynamical quarks, aQC₂D exhibits a rather unusual critical behavior in the vicinity of the tetracritical point where the two second-order transition lines cross each other [51]. This is unlike (three-color) aQCD in which the deconfinement transition is of first order. There, the second-order BEC critical line is interrupted around the deconfinement transition, meeting the deconfinement line at two tricritical points. This general expectation is confirmed by our explicit model calculation here and in the following sections.

Here I will analyze the details of the phase transitions in the vicinity of the tetracritical point using the GL theory. The thermodynamic potential depends on three mean fields, α , σ , Δ . Only two of them, α and Δ , comprise order parameters for spontaneous symmetry breaking of an exact symmetry (unless we consider the chiral limit). In order to construct the GL free energy, one therefore needs to eliminate σ in favor of α, Δ by means of its gap equation. Around the tetracritical point, we can then perform a double Taylor expansion of the total thermodynamic potential, $\Omega = \Omega_g^W + \Omega_q$. Thanks to the Z_2 and $U(1)_B$ symmetries, it depends just on the squares of the mean fields,

$$\frac{\Omega(\alpha^2, \Delta^2)}{V} = b_\alpha \alpha^2 + b_\Delta \Delta^2 + \frac{1}{2} \left[\lambda_{\alpha\alpha} (\alpha^2)^2 + 2\lambda_{\alpha\Delta} \alpha^2 \Delta^2 + \lambda_{\Delta\Delta} (\Delta^2)^2 \right]. \quad (3.28)$$

The effective quartic couplings are determined by the second *total* derivatives of the thermodynamic potential,

$$\lambda_{\alpha\alpha} = \frac{1}{V} \frac{d^2 \Omega}{d(\alpha^2)^2}, \quad \lambda_{\alpha\Delta} = \frac{1}{V} \frac{d^2 \Omega}{d\alpha^2 d\Delta^2}, \quad \lambda_{\Delta\Delta} = \frac{1}{V} \frac{d^2 \Omega}{d(\Delta^2)^2}, \quad (3.29)$$

evaluated at $\alpha = \Delta = 0$. These total derivatives are in turn given in terms of the partial derivatives of the thermodynamic potential as a function of all three mean fields,

$$\frac{d^2 \Omega}{d\chi_i d\chi_j} = \frac{\partial^2 \Omega}{\partial \chi_i \partial \chi_j} - \frac{\partial^2 \Omega}{\partial \chi_i \partial \sigma} \left(\frac{\partial^2 \Omega}{\partial \sigma^2} \right)^{-1} \frac{\partial^2 \Omega}{\partial \sigma \partial \chi_j}, \quad (3.30)$$

where χ_i stands for α^2, Δ^2 . In order to evaluate the GL quartic couplings, we need to know six second partial derivatives of the thermodynamic potential,

$$\begin{aligned}
\frac{\partial_{\alpha^2 \alpha^2} \Omega}{V} &= \frac{1}{4} b T (16e^{-a/T} - 1) + N_f T \sum_e \int \frac{d^3 \mathbf{k}}{(2\pi)^3} \frac{\cosh(\xi_{\mathbf{k}}^e/T)}{[2 \cosh(\xi_{\mathbf{k}}^e/T) - 1]^2}, \\
\frac{\partial_{\alpha^2 \Delta^2} \Omega}{V} &= N_f \sum_e \int \frac{d^3 \mathbf{k}}{(2\pi)^3} \frac{\sinh(\xi_{\mathbf{k}}^e/T)}{\xi_{\mathbf{k}}^e} \frac{1}{[2 \cosh(\xi_{\mathbf{k}}^e/T) - 1]^2}, \\
\frac{\partial_{\Delta^2 \Delta^2} \Omega}{V} &= \frac{3}{4} N_f \sum_e \int \frac{d^3 \mathbf{k}}{(2\pi)^3} \frac{1}{(\xi_{\mathbf{k}}^e)^3} \left[\tanh \frac{3\xi_{\mathbf{k}}^e}{2T} - \frac{3\xi_{\mathbf{k}}^e}{2T \cosh^2(3\xi_{\mathbf{k}}^e/2T)} \right], \\
\frac{\partial_{\sigma \alpha^2} \Omega}{V} &= 2MN_f \sum_e \int \frac{d^3 \mathbf{k}}{(2\pi)^3} \frac{1}{\epsilon_{\mathbf{k}}} \frac{\sinh(\xi_{\mathbf{k}}^e/T)}{[2 \cosh(\xi_{\mathbf{k}}^e/T) - 1]^2}, \\
\frac{\partial_{\sigma \Delta^2} \Omega}{V} &= \frac{3}{2} MN_f \sum_e \int \frac{d^3 \mathbf{k}}{(2\pi)^3} \frac{1}{\epsilon_{\mathbf{k}} (\xi_{\mathbf{k}}^e)^2} \left[\tanh \frac{3\xi_{\mathbf{k}}^e}{2T} - \frac{3\xi_{\mathbf{k}}^e}{2T \cosh^2(3\xi_{\mathbf{k}}^e/2T)} \right], \\
\frac{\partial_{\sigma \sigma} \Omega}{V} &= \frac{N_f m_0}{2G M} + 3M^2 N_f \sum_e \int \frac{d^3 \mathbf{k}}{(2\pi)^3} \frac{1}{\epsilon_{\mathbf{k}}^3} \left[\tanh \frac{3\xi_{\mathbf{k}}^e}{2T} - \frac{3\epsilon_{\mathbf{k}}}{2T \cosh^2(3\xi_{\mathbf{k}}^e/2T)} \right].
\end{aligned} \tag{3.31}$$

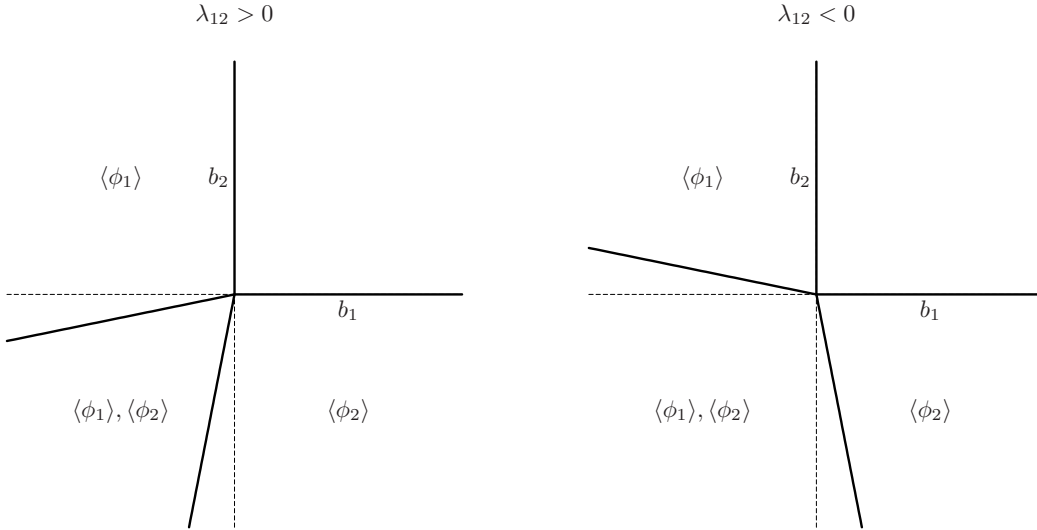


Figure 3.4.: Schematic phase diagram of the Ginzburg–Landau theory with two order parameters. Thick lines denote second-order phase transitions. The labels indicate which order parameters take nonzero values in a given phase.

In order to see how the two condensates affect each other close to the tetracritical point, consider the general GL functional with two order parameters $\phi_{1,2}$ and assume it is constrained

to have the form

$$\frac{\Omega(\phi_1, \phi_2)}{V} = b_1\phi_1^2 + b_2\phi_2^2 + \frac{1}{2}(\lambda_{11}\phi_1^4 + 2\lambda_{12}\phi_1^2\phi_2^2 + \lambda_{22}\phi_2^4). \quad (3.32)$$

[In our case, all other terms are prohibited by the Z_2 and $U(1)_B$ symmetries.] The phase diagram of such a model is depicted in Fig. 3.4. If only one condensate were present, the position of the phase transition would be determined by the point where the respective b coefficient changes sign. However, when both condensates are present, the transition lines shift. This is most easily seen from the expression for the nontrivial solution to the gap equations with both order parameters being nonzero,

$$\phi_1^2 = \frac{-\lambda_{22}b_1 + \lambda_{12}b_2}{\lambda_{11}\lambda_{22} - \lambda_{12}^2}, \quad \phi_2^2 = \frac{\lambda_{12}b_1 - \lambda_{11}b_2}{\lambda_{11}\lambda_{22} - \lambda_{12}^2}. \quad (3.33)$$

We can therefore see that the size of the region with both condensates depends on the sign and magnitude of the offdiagonal coupling λ_{12} .

The description of the phase transitions based on the GL theory is universal and model independent as long as it captures the correct degrees of freedom and symmetries. A non-trivial task in general is to find the mapping of the (b_1, b_2) plane displayed in Fig. 3.4 to the physical observables, in our case the temperature and chemical potential. Even though this is in principle possible with our PNJL model, here I performed just a basic compatibility check. Evaluating the GL coefficients for our parameter set using Eq. (3.31), one finds that $\lambda_{\alpha\alpha} \approx 2.3 \times 10^{-3}\Lambda^4$, $\lambda_{\alpha\Delta} \approx 5.7 \times 10^{-7}\Lambda^2$, and $\lambda_{\Delta\Delta} \approx 9.7 \times 10^{-6}$. The offdiagonal coupling is positive which means that the two condensates “repel” each other as in the left panel of Fig. 3.4. However, since the GL couplings are numerically very small, the angles between the critical lines hardly change at the tetracritical point. The slight deflection of the BEC transition line is visible in the left panel of Fig. 3.2. That the same happens to the deconfinement line is made manifest by the detail of the critical line shown in the right panel of Fig. 3.2.

3.2.3. Casimir scaling

The Casimir scaling hypothesis [50, 52] states that the color-singlet potential between a static quark and antiquark at intermediate distance is proportional to the quadratic Casimir invariant, $C_2(\mathcal{R})$, of the representation \mathcal{R} of the quarks. This statement is exact at two-loop order in perturbation theory [53] and receives corrections only at three-loop order [54]. At the same time, there is compelling evidence from lattice simulations that it holds to a high accuracy even

in the nonperturbative regime [40, 55, 56, 57]. It may thus provide a handle to understand the nonperturbative behavior of QCD-like theories, and as such should be a necessary ingredient in any model attempting to mimic QCD (thermo)dynamics [58].

In the PNJL model, one cannot directly access the confining potential feature of QCD. However, the scaling of the static potential implies an analogous property of the expectation values of the Polyakov loops [40, 59]: the quantity $\langle \ell_{\mathcal{R}} \rangle^{1/C_2(\mathcal{R})}$ should be independent of the representation \mathcal{R} . This can be easily obtained from the relationship between the quark-antiquark potential and the Polyakov loop in 2.1.3. Since we have the analytic formula (3.23) for the expectation values of all Polyakov loops in two-color QCD, where one has simply $C_2(j) = j(j+1)$, we can easily check to what extent Casimir scaling is satisfied by our model.

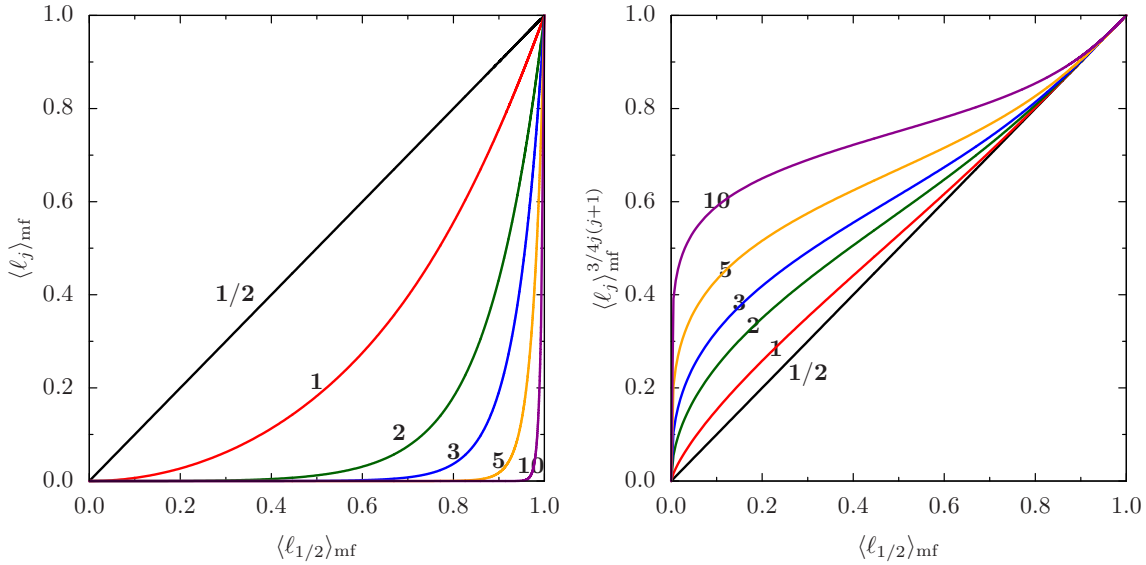


Figure 3.5.: Expectation values of the Polyakov loops in various representations as a function of the fundamental Polyakov loop in the case of two colors. Boldface numbers indicate the “spin” j of the representation. Left panel: unscaled Polyakov loops. Right panel: Casimir-scaled Polyakov loops. For convenience, we take the $C_2(F)/C_2(\mathcal{R})$ power of the expectation values of the Polyakov loops so that the fundamental loop is left intact.

Note that the expectation values of all Polyakov loops are expressed in terms of the mean field α , which can in turn be traded for the fundamental loop. In Fig. 3.5 I therefore plot the expectation values of the Polyakov loops in selected representations against that in the fundamental representation [40, 60]. Comparing the left and right panels that display the unscaled and scaled Polyakov loops, we can see that the Casimir scaling is very well reproduced as the value of the fundamental loop approaches one, which corresponds to high temperatures. It becomes worse at low temperatures where the nearest-neighbor interaction model (3.1) over-

simplifies the physics. Lattice data that hint at almost exact scaling even at low temperatures can be reproduced more satisfactorily once we add more terms including higher representation Polyakov loops in Eq. (3.1) [40].

Within our model, we can check even analytically how well Casimir scaling is satisfied at high temperatures, and hence, at high values of α . Carrying out the Taylor expansion of Eq. (3.23) around $\alpha = +\infty$, one finds

$$\langle \ell_j \rangle_{\text{mf}}^{1/j(j+1)} = 1 - \frac{1}{\alpha} + \frac{1}{4\alpha^2} + \frac{j^2 + j - \frac{1}{8}}{12\alpha^3} + \mathcal{O}\left(\frac{1}{\alpha^4}\right). \quad (3.34)$$

We can see that Casimir scaling is only violated at the fourth order of the expansion.

One important observation regarding the results in Fig. 3.5 is that they are based just on the group average (3.8) and do not make any reference to the quark sector of the model. Therefore, they apply equally well to two-color QCD with quarks in *any* representation as well as to the pure gauge theory. In particular, the same curves hold even for nonzero chemical potential, which provides us with a unique opportunity to study Casimir scaling at nonzero baryon density. The quark sector will just affect the dependence of the mean field α on the temperature and chemical potential, and therefore the speed at which the curves are traversed as T and μ vary.

3.3. Three colors

For three colors, the group integration is performed with the measure

$$dL = \frac{d\theta_1 d\theta_2}{6\pi^2} [\sin(\theta_1 - \theta_2) - \sin(2\theta_1 + \theta_2) + \sin(\theta_1 + 2\theta_2)]^2. \quad (3.35)$$

Three-color QCD with fundamental quarks has a charge conjugation invariance, which is implemented in the PNJL model by a simultaneous change $\theta_i \rightarrow -\theta_i$, $\mu \rightarrow -\mu$. Therefore, at any fixed nonzero chemical potential this charge conjugation invariance is explicitly broken. As a result, the expectation values $\langle \ell_F \rangle$ and $\langle \ell_F^* \rangle$ split. At the same time, the mean-field β becomes nonzero [26].

On the other hand, the situation in aQCD is different. Thanks to the reality of the gauge group representation, the nonzero weights appear in pairs with opposite sign. Consequently, the theory is invariant under *separate* charge conjugation in the quark and gluon sectors. The

charge conjugation invariance in the gauge sector guarantees that the Polyakov loop in a given (e.g. fundamental) representation and its complex conjugate always have the same expectation value. We may therefore dispense with the mean field β , which greatly simplifies the group integration. In the gauge sector one can still obtain an analytic expression for the thermodynamic potential, albeit in the form of an infinite series [39]. One defines a function

$$F(\alpha) = \sum_{m=-\infty}^{+\infty} \det I_{m+i-j}(\alpha), \quad (3.36)$$

where the determinant is taken with respect to the indices i, j . One then finds the following expression for the thermodynamic potential,

$$\frac{\Omega_g^W a_s^3}{TV} = -6e^{-a/T} \left[\frac{F'(\alpha)}{F(\alpha)} \right]^2 + \alpha \frac{F'(\alpha)}{F(\alpha)} - \log F(\alpha), \quad (3.37)$$

and the expectation value of the fundamental Polyakov loop,

$$\langle \ell_F \rangle_{\text{mf}} = \frac{1}{N_c} \frac{F'(\alpha)}{F(\alpha)}. \quad (3.38)$$

The derivation of this formula is deferred to Appendix D where it will be generalized and used to write analytic expressions for the expectation values of all Polyakov loops.

The eigenvalues of the Polyakov loop in the adjoint representation are 1 [$(N_c - 1)$ -times degenerate] and $e^{i(\theta_i - \theta_j)}$ for all pairs $i \neq j$. The logarithmic term in Eq. (3.18) becomes

$$2 \log \left\langle (1+x)^{N_c-1} \prod_{i < j}^{N_c} [1 + 2x \cos(\theta_i - \theta_j) + x^2] \right\rangle_{\text{mf}}, \quad (3.39)$$

where I abbreviated $x = e^{-E_k^e/T}$. Specifically for three colors this is equal to

$$2 \log \left\{ (1+x)^2 [1 + 2x\omega_1 + x^2(3 + 4\omega_2) + 4x^3(\omega_1 + 2\omega_3) + x^4(3 + 4\omega_2) + 2x^5\omega_1 + x^6] \right\}. \quad (3.40)$$

Group integration reduces to evaluation of three averages,

$$\begin{aligned}
\omega_1 &= \langle \cos(\theta_1 - \theta_2) + \cos(\theta_2 - \theta_3) + \cos(\theta_3 - \theta_1) \rangle_{\text{mf}}, \\
\omega_2 &= \langle \cos(\theta_1 - \theta_2) \cos(\theta_3 - \theta_1) + \cos(\theta_2 - \theta_3) \cos(\theta_1 - \theta_2) + \cos(\theta_3 - \theta_1) \cos(\theta_2 - \theta_3) \rangle_{\text{mf}}, \\
\omega_3 &= \langle \cos(\theta_1 - \theta_2) \cos(\theta_2 - \theta_3) \cos(\theta_3 - \theta_1) \rangle_{\text{mf}}.
\end{aligned}
\tag{3.41}$$

These can be performed independently of the value of x , so the evaluation of the quark thermodynamic potential factorizes into a one-dimensional momentum integral and a two-dimensional group integration. The latter can be performed either numerically or even analytically in a fashion similar to Eq. (3.36), as sketched in Appendix D.

3.3.1. Phase diagram

Again, we fix the parameters for the subsequent numerical computations first. The parameter a is determined by the deconfinement temperature T_d^0 in the pure gauge theory. With the thermodynamic potential (3.37), this corresponds to $e^{-a/T_d^0} = 0.13427$. Demanding $T_d^0 = 270$ MeV, this yields $a = 542.1$ MeV. The parameter b is in turn obtained from the physical string tension $\sigma_s = (425 \text{ MeV})^2$, as in the two-color case. In the NJL sector, we use the parameters of the two-flavor model with fundamental quarks, $\Lambda = 651$ MeV, $G = 5.04 \text{ GeV}^{-2}$, $m_0 = 5.5$ MeV, fitted to reproduce the pion mass and decay constant and the chiral condensate in the vacuum (see, for instance, Ref. [28]). The coupling is rescaled by the factor $27/32$ in accord with Eq. (3.20), and an additional factor of two to account for the fact that we have only one flavor here. The values of all parameters used in our calculations are summarized in Tab. 3.2.

a [MeV]	$b^{1/3}$ [MeV]	Λ [MeV]	G [GeV $^{-2}$]	m_0 [MeV]
542.1	333.2	651	8.51	5.5

Table 3.2.: Model parameters for three-color QCD with adjoint quarks.

As a basic cross-check I again evaluated first the deconfinement and chiral restoration temperatures (in the chiral limit) at zero chemical potential. The values $T_d = 270$ MeV and $T_\chi = 663$ MeV yield the ratio $T_\chi/T_d = 2.46$. This is quite far from the value ≈ 8 measured on the lattice [32, 33]. (Note that in Ref. [41] the lattice value of this ratio was achieved by tuning

the parameters of the model.) However, one should keep in mind that we made just a rough estimate of the NJL coupling G and cutoff Λ , on which the chiral restoration temperature depends very sensitively. In principle, one could use the lattice value for the ratio T_χ/T_d as an input in the model. Nevertheless, one cannot really hope to describe the chiral restoration in a quantitatively satisfactory manner within our model. The first reason is that at such high temperatures, the calculation of the thermodynamic potential is plagued by cutoff artifacts. (We regulate the whole quark contribution to the thermodynamic potential, including its finite thermal part.) The second reason is that the PNJL model ceases to be physically appropriate at temperatures about two to three times T_d [30], since it does not capture the correct gauge degrees of freedom, that is, the deconfined transversely polarized gluons. We are therefore just content with demonstrating that QCD with adjoint quarks indeed features a large splitting of the deconfinement and chiral restoration temperatures.

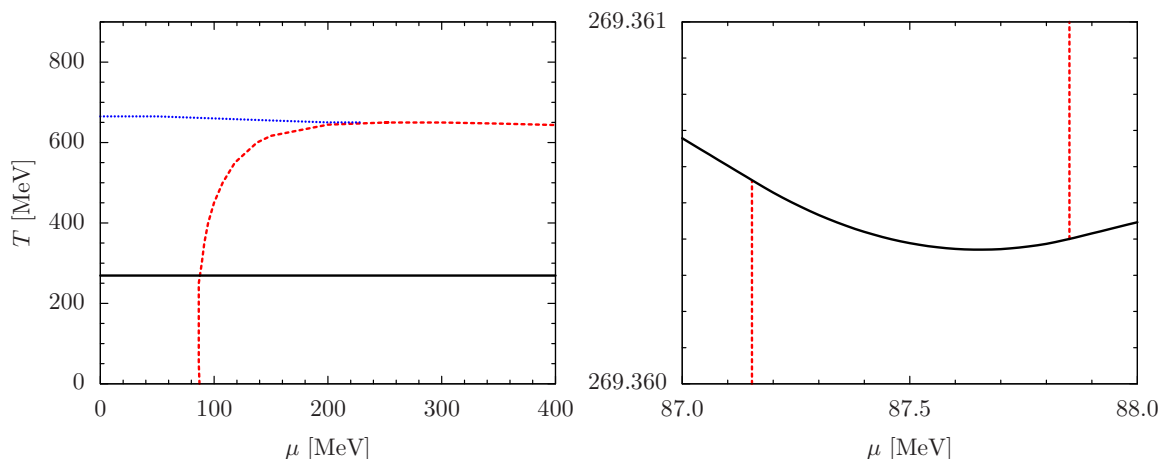


Figure 3.6.: Phase diagram of three-color QCD with one flavor of adjoint quarks. Black solid line: deconfinement transition. Red dashed line: BEC transition. Blue dotted line: chiral crossover. The right panel zooms in the chemical potential and temperature scales so that the two tricritical points are discernible.

The phase diagram of aQCD determined within our PNJL model is shown in Fig. 3.6. While on the large scale it looks the same as the phase diagram of aQC₂D in Fig. 3.2, there is a marked difference in the topology as one zooms in the neighborhood of the “intersection” of the deconfinement and BEC transition lines. Since the deconfinement transition is now first order, the BEC critical line is broken, meeting the deconfinement line at two tricritical points. Thus, there is a narrow range of chemical potentials in which, as the temperature is increased, the diquark condensate rather unusually disappears in a first-order phase transition.

3.3.2. Casimir scaling

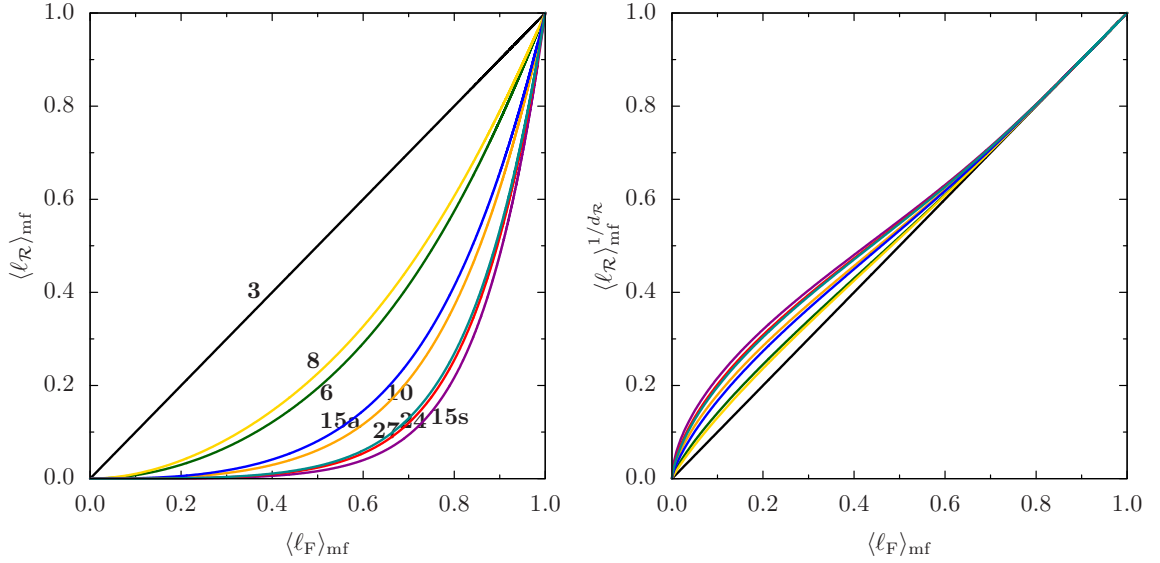


Figure 3.7.: Expectation values of the Polyakov loops in various representations as a function of the fundamental Polyakov loop in the case of three colors. Boldface numbers indicate the dimension (and possibly the symmetry) of the representation. Left panel: unscaled Polyakov loops. Right panel: Casimir-scaled Polyakov loops. For convenience, we take the $C_2(\mathcal{F})/C_2(\mathcal{R}) \equiv 1/d_{\mathcal{R}}$ power of the expectation values of the Polyakov loops so that the fundamental loop is left intact. For the sake of clarity, the labels are not shown in the right panel. The color assignment of the lines is the same as in the left panel.

Any irreducible representation of $SU(3)$ can be uniquely characterized by a pair of positive integers (p, q) that determine the highest weight of the representation in the basis of the fundamental weights. The triplet representation thus corresponds to $(1, 0)$ and its complex conjugate to $(0, 1)$. The dimension of a general irreducible representation is $\dim(p, q) = \frac{1}{2}(p+1)(q+1)(p+q+2)$ and the value of the quadratic Casimir invariant (up to a common prefactor) is $C_2(p, q) = \frac{1}{3}(p^2 + pq + q^2) + p + q$ [61]. Following Refs. [26, 56], the expectation values of the Polyakov loops in the lowest few representations, satisfying $p + q \leq 4$, are calculated and are shown in Fig. 3.7.

As before, these results are largely independent of the quark content of the theory. The only assumption made is that the mean field β is zero so that there is a one-to-one correspondence between the mean field α and the expectation value of the fundamental Polyakov loop. Thus, the plots in Fig. 3.7 apply to three-color QCD modeled by the action (3.1) with quarks in *any* representation at zero chemical potential. Once the quark representation is (pseudo)real, the same results are valid even at nonzero chemical potential. As compared to the two-color case shown in Fig. 3.5, the scaling violation seems to be significantly smaller for three colors.

However, this observation is somewhat misleading since even the unscaled Polyakov loops show smaller depletion compared to the fundamental loop in the three-color case.

Chapter 4.

Dimensional reduction for two-color QCD

EQCD, a dimensionally reduced effective theory for QCD, was introduced in Section 2.4.4. It contains the degrees of freedom at the soft scale, gT , which are the electrostatic and magnetostatic gluons. In order to be applicable, EQCD requires that there exists a clear scale hierarchy between T and gT . This means that the running coupling g should be small enough, or equivalently the temperature should be asymptotically high. EQCD can well reproduce the long distance dynamics of QCD at very high temperatures. However this requirement is not always fulfilled and there are evidences that EQCD fails to produce correct results down to temperatures about a few times T_c , where T_c is the critical temperature of the deconfinement transition [62, 63]. This failure has a reason, which is the fact that EQCD breaks the Z_3 center symmetry explicitly, even in the absence of quarks. Its leading-order Lagrangian can be obtained by expanding the one-loop effective potential of the Wilson line around one of its three degenerate minima, $A_0 = 0$ [64]. Since the center symmetry is so important to obtain the correct physics around T_c , its missing in EQCD invalidates its usage close to T_c .

To modify EQCD and build a new effective theory is a possible way to conquer this problem. The new one should be able to reproduce results of QCD or EQCD at asymptotically high temperatures and respect the center symmetry in order to be valid down to around T_c . In this chapter I will construct a dimensionally reduced effective theory with center symmetry, which is called ZQCD.

In order to simplify the consideration, the $SU(2)$ gauge group is used here instead of $SU(3)$, *i.e.*, a two-color QCD-like theory and the Z_2 center symmetry is considered. I will construct the theory directly with the quark effects which explicitly break the center symmetry. Therefore the Yang-Mills theory with vanishing Z_2 breaking coefficients can be studied as a special case throughout this chapter.

This chapter is organized as follows. In section 4.1, I will construct center-symmetric effective theories with Z_2 breaking operators that emerge upon inclusion of fundamental fermions in the case of two colors. In section 4.2, I will identify the degrees of freedom of the effective theory and explain how they are related to those of EQCD, while in section 4.3, the detailed matching of the ZQCD parameters to the full theory is carried out. Section 4.4 contains the first predictions of the new theory, *i.e.*, the solution of static field configurations for the domain wall and stable bubble.¹

4.1. Model setup of ZQCD

The first step to formulate the desired effective theory is to introduce the proper degrees of freedom. The minimal set of degrees of freedom for a Z_2 invariant theory should be the magnetostatic gluon $A_i^a(\mathbf{x})$ and the Polyakov loop $L(\mathbf{x})$. But because $L(\mathbf{x})$ is unitary, a theory with polynomial interactions will not be perturbatively renormalizable. This is in principle not a problem for an effective theory with a UV cutoff, but it brings complexity to the practical matching to the underlying theory and to lattice simulations. Therefore, we substitute a spatially coarse-grained Wilson line operator $\mathcal{Z}(\mathbf{x})$ for the Polyakov loop.² The coarse-grained matrix is defined via the block transformation as

$$\mathcal{Z}(\mathbf{x}) = \frac{T}{V_{\text{Block}}} \int_V d^3y U(\mathbf{x}, \mathbf{y}) L(\mathbf{y}) U(\mathbf{y}, \mathbf{x}), \quad (4.1)$$

where the integration goes over the arbitrary $\mathcal{O}(T^{-3})$ volume of a block and $U(\mathbf{y}, \mathbf{x})$ is a Wilson line from the point $(\mathbf{x}, \tau = 0)$ to $(\mathbf{y}, \tau = 0)$ with a path at constant time $\tau = 0$.

As discussed at length in Ref. [66], a unique feature of the gauge group $SU(2)$ is that the coarse graining procedure almost preserves the group property of the Wilson line, as an arbitrary sum of $SU(2)$ matrices is itself an $SU(2)$ matrix up to a multiplicative real factor. This implies that we may parameterize the field \mathcal{Z} in the form

$$\mathcal{Z} = \frac{1}{2} (\Sigma \mathbb{1} + i \vec{\Pi} \cdot \vec{\sigma}), \quad (4.2)$$

¹This chapter is based on the publication Ref. [65].

²Since there is no confusion in this chapter, I use the symbol \mathcal{Z} for the matrix field but not the partition function.

where $\vec{\Pi} \cdot \vec{\sigma} = \Pi^a \sigma^a$, Σ and Π_a with $a = 1, 2, 3$ are real scalar fields, and σ_a are the three Pauli matrices. Out of these four degrees of freedom we expect three to correspond to the light adjoint Higgs fields of EQCD, while one should be an unphysical auxiliary field that effectively decouples from the dynamics of the light fields and has a mass of the order of the cutoff scale of the effective theory ($\sim T$), corresponding to the inverse length scale introduced by the coarse graining. While the heavy auxiliary field decouples from the dynamics in the infrared, its fluctuations in the ultraviolet render the theory superrenormalizable, providing important technical simplifications.

ZQCD should inherit the gauge and center symmetry from the fundamental theory. The gauge transformation acts on the fields as

$$\mathcal{Z}(\mathbf{x}) \rightarrow s(\mathbf{x})\mathcal{Z}(\mathbf{x})s(\mathbf{x})^\dagger, \quad \mathbf{A}(\mathbf{x}) \rightarrow s(\mathbf{x})[\mathbf{A}(\mathbf{x}) + i\nabla]s(\mathbf{x})^\dagger, \quad (4.3)$$

where $s(\mathbf{x}) \in \text{SU}(2)$, while the Z_2 transformation acts on the \mathcal{Z} field as

$$\mathcal{Z}(\mathbf{x}) \rightarrow e^{i\pi n} \mathcal{Z}(\mathbf{x}) = \pm \mathcal{Z}(\mathbf{x}). \quad (4.4)$$

The relation of the latter transformation to the $\text{SU}(2)$ gauge invariance of the full theory is explained in detail in Appendix F.

To obtain the Lagrangian of the effective theory, we collect all superrenormalizable operators up to fourth order in the fields that respect three-dimensional gauge invariance.³ This leads to the expression

$$\mathcal{L} = \frac{1}{g_3^2} \left[\frac{1}{2} \text{Tr} F_{ij}^2 + \text{Tr}(D_i \mathcal{Z}^\dagger D_i \mathcal{Z}) + V(\mathcal{Z}) \right], \quad (4.5)$$

where g_3 is the effective theory gauge coupling, $D_i \equiv \partial_i - i[A_i, \cdot]$, $F_{ij} \equiv \partial_i A_j - \partial_j A_i - i[A_i, A_j]$, and the potential $V(\mathcal{Z})$ reads

$$V(\mathcal{Z}) = b_1 \Sigma^2 + b_2 \vec{\Pi}^2 + c_1 \Sigma^4 + c_2 (\vec{\Pi}^2)^2 + c_3 \Sigma^2 \vec{\Pi}^2 + d_1 \Sigma^3 + d_2 \Sigma \vec{\Pi}^2. \quad (4.6)$$

Here, all terms with the exception of the last two operators in the potential respect the Z_2 center symmetry, and were present in the model constructed for pure $\text{SU}(2)$ Yang-Mills theory

³While in a three-dimensional theory operators of order five in the fields are in principle still relevant and those of order six marginal, we exclude them from our consideration, as their contributions to physical quantities are less important compared to the leading terms. This is because the higher order terms are suppressed by (large) positive powers of the ratio of the effective and full theory energy scales.

in Ref. [66]; the Z_2 violating operators then clearly result from the presence of quarks. It is a straightforward exercise to verify that Eq. (4.5) really is the most general Lagrangian compatible with the required symmetries: simple redefinitions of the fields allow us to combine independent kinetic terms for Σ and $\vec{\Pi}$ and remove a Z_2 breaking term linear in Σ , while a term cubic in $\vec{\Pi}$ is forbidden by the vanishing of the symmetric structure constant d_{abc} in $SU(2)$.

Next, we can redefine the coefficients as

$$\begin{aligned} b_1 &= \frac{1}{2}h_1, & b_2 &= \frac{1}{2}(h_1 + g_3^2 s_1), \\ c_1 &= \frac{1}{4}h_2 + g_3^2 s_3, & c_2 &= \frac{1}{4}(h_2 + g_3^2 s_2), & c_3 &= \frac{1}{2}h_2, \\ d_1 &= \frac{1}{2}g_3^2 s_4, & d_2 &= \frac{1}{2}g_3^2 s_5, \end{aligned} \quad (4.7)$$

and split the effective theory potential into ‘hard’ and ‘soft’ parts, parametrized by the $O(g^0)$ constants h_i and s_i , respectively. This results in the alternative expression

$$V(\mathcal{Z}) = h_1 \text{Tr}(\mathcal{Z}^\dagger \mathcal{Z}) + h_2 (\text{Tr} \mathcal{Z}^\dagger \mathcal{Z})^2 + g_3^2 \left[\frac{s_1}{2} \vec{\Pi}^2 + \frac{s_2}{4} (\vec{\Pi}^2)^2 + s_3 \Sigma^4 + \frac{s_4}{2} \Sigma^3 + \frac{s_5}{2} \Sigma \vec{\Pi}^2 \right], \quad (4.8)$$

where we have assumed the Z_2 breaking couplings d_i to be of the soft type. The kinetic terms as well as the hard part of the potential possess an extended (global) $SU(2) \times SU(2)$ invariance,

$$\mathcal{Z} \rightarrow \Omega_1 \mathcal{Z} \Omega_2, \quad \Omega_i \in SU(2), \quad (4.9)$$

which will later be seen to translate to a shift invariance of the light physical fields of ZQCD upon integrating out the heavy one. As a consequence, the hard part of the potential is minimized by all matrices that are special unitary up to a common real factor. It is only the soft terms that provide the $O(g^2)$ structure inside this ‘valley’, necessary to match the effective theory potential to that of the full theory Wilson line, cf. Eq. (E.1).

4.2. Identification of the fields

It is well known that at high temperatures, where the renormalized gauge coupling becomes small, the Wilson line effectively freezes to the global minimum of its perturbative effective potential [64, 67, 68], and to correctly describe its long-distance dynamics it is sufficient to consider only its small fluctuations around it. It is thus natural to require that the predictions

of our effective theory reduce to those of EQCD in the same limit, as the Lagrangian of EQCD can be obtained from an expansion of the Wilson line potential in powers (and derivatives) of the temporal component of the gauge field, A_0 . This property can be most straightforwardly ensured by explicitly integrating out the heavy degree of freedom in the vicinity of one of the minima of the ZQCD effective potential, and by matching the resulting non-center-symmetric (even in the absence of fermions) theory to EQCD. Through this procedure, the light field of ZQCD becomes associated with the adjoint Higgs A_0 of EQCD, and we automatically obtain the values of several of the effective theory parameters.

In this and the following section, we will explicitly perform the high-temperature matching of ZQCD to EQCD, and find the values of the s_i , i.e. the soft parameters of ZQCD. We begin this by parameterizing the field \mathcal{Z} as in Eq. (26) of Ref. [66],

$$\mathcal{Z} = \frac{\nu}{2} \mathbb{1} + \frac{g_3}{2} (\phi \mathbb{1} + i \vec{\chi} \cdot \vec{\sigma}), \quad (4.10)$$

which amounts to the redefinition $\Sigma = \nu + g_3 \phi$ and $\vec{\Pi} = g_3 \vec{\chi}$, where ν is a real positive number, chosen so that $\langle \mathcal{Z} \rangle = (\nu/2) \mathbb{1}$. Clearly, the precise choice of the parametrization of \mathcal{Z} can have no effect on the physics, as long as it contains the correct degrees of freedom: once the effective theory is matched to the full theory properly, it will automatically reproduce the correct long-distance physics. One should nevertheless note that, had we chosen to use a non-linear field parametrization, we would have had to consider the Jacobian associated with the change of variables in the defining path integral of the theory.

Upon rewriting Eq. (4.10) as $\mathcal{Z} = \frac{\nu+g_3\phi}{2} [\mathbb{1} + i(g_3/\nu)\vec{\chi} \cdot \vec{\sigma}] + \mathcal{O}(g^2)$ and comparing with the full theory Polyakov loop,

$$\Omega(\mathbf{x}) \equiv \mathcal{P} \exp \left[ig \int_0^\beta d\tau A_0(\tau, \mathbf{x}) \right] = \mathbb{1} + ig \int_0^\beta d\tau A_0(\tau, \mathbf{x}) + \mathcal{O}(g^2), \quad (4.11)$$

we identify the real scalar field ϕ as the auxiliary heavy degree of freedom of the effective theory (to leading order). Subsequently, we associate the field χ_a with the light, physical field that corresponds to the adjoint scalar A_0 of EQCD, which, together with the identification of the effective theory gauge coupling, $g_3^2 = g^2 T + \mathcal{O}(g^4)$, fixes the leading order value of the parameter ν ,

$$\nu = 2T + \mathcal{O}(g^2). \quad (4.12)$$

Beyond the field identifications, the matching of ZQCD to the full theory is performed by demanding that the long-distance behavior of static gluonic correlators is correctly reproduced by the effective theory, order by order in a weak-coupling expansion. As the effects of the soft couplings s_i are suppressed by a factor g_3^2 in comparison with the hard ones h_i , one-loop graphs with only hard vertices enter the effective theory calculation with the same power of g_3 as tree graphs containing one soft vertex. This implies that to obtain the correlators in a consistent manner, we need to determine the one-loop effective potential of ZQCD. This function can be read off from Eq. (18) of Ref. [66] for the case of pure SU(2) Yang-Mills theory, and it has been generalized to include the effects of fermionic operators in Appendix G. Inspecting the result reveals the anticipated effect that the degeneracy of the two minima present in the center symmetric case is broken by the nonzero values of $s_{4,5}$. Without loss of generality, we may choose $s_4 < 0$ so that the ground state expectation value of Σ is positive. Solving for the minimum of the potential iteratively, we then find $v = v_0 + g_3^2 v_2 + \dots$, where

$$v_0 = \sqrt{-\frac{h_1}{h_2}}, \quad v_2 = -\frac{1}{2h_2} \left(4s_3 v_0 + \frac{3}{2}s_4 \right) + \frac{3}{8\pi} \sqrt{2h_2}. \quad (4.13)$$

Comparing this to the identification made in Eq. (4.12), we infer from here the first nontrivial relation among our effective theory parameters,

$$h_1 + 4T^2 h_2 = 0. \quad (4.14)$$

4.3. Matching of the soft parameters

In this section, I will perturbatively determine the values of the soft ZQCD parameters s_i . I begin this in section 4.3.1 by integrating out the heavy field ϕ from the effective theory, requiring that the resulting Lagrangian for $\vec{\chi}$ agrees with that of EQCD. After this, I will in section 4.3.2 match the remaining soft effective theory parameters by demanding that the global structure of the one-loop effective potential of ZQCD agrees with that of the full theory.

4.3.1. Perturbative matching of the Lagrangians

Our first goal will be to explicitly integrate out the heavy auxiliary field ϕ in order to obtain an effective potential for $\vec{\chi}$ only, to be compared with the effective potential of the A_0 field in

EQCD. At the level of the quantum (Wilsonian) effective action, integrating out a given field amounts to eliminating it using its equation of motion or, equivalently, adding to the action of the other fields all *tree-level* Feynman graphs containing this field in the internal lines and all other fields as external legs.

At this point, the $SU(2) \times SU(2)$ invariance of the hard part of the Lagrangian (4.5) proves its utility. The fields $\vec{\chi}$ can namely be identified as the Nambu-Goldstone bosons stemming from the spontaneous breaking of this extended symmetry by the nonzero expectation value $\langle \mathcal{Z} \rangle$. As a consequence, any contribution to the static correlators of $\vec{\chi}$ must come with at least one factor of s_i , and in particular, the one-loop part of the effective potential of ZQCD — the second line of Eq. (G.3) — need not be taken into account. In addition, the gauge-fixing dependent part of the effective potential matches automatically to EQCD.

Keeping only terms up to fourth order in $\vec{\chi}$ and rescaling the spatial gluon field to achieve canonical normalization of its kinetic term, we arrive at a Lagrangian for this field that has the exact same form as that of EQCD,

$$\mathcal{L}_{\text{light}} = \frac{1}{2} \text{Tr} F_{ij}^2 + \frac{1}{2} (D_i \vec{\chi})^2 + \frac{1}{2} m_\chi^2 \vec{\chi}^2 + \frac{\tilde{\lambda}}{8} (\vec{\chi}^2)^2 + \dots, \quad (4.15)$$

with the mass parameter and quartic coupling reading

$$\begin{aligned} m_\chi^2 &= g_3^2 \left(s_1 - 4s_3 v_0^2 - \frac{3}{2} s_4 v_0 + s_5 v_0 \right), \\ \tilde{\lambda} &= 2g_3^4 \left(s_2 + 4s_3 + \frac{3s_4}{4v_0} - \frac{s_5}{v_0} \right). \end{aligned} \quad (4.16)$$

When expressed in terms of Feynman diagrams, the quartic coupling $\tilde{\lambda}$ consists of two contributions, one from a soft operator of the $(\vec{\chi}^2)^2$ type, and another from a soft, $SU(2) \times SU(2)$ breaking mass correction to a ϕ propagator connecting two hard cubic $\phi \vec{\chi}^2$ vertices.⁴

⁴It should be noted that the same diagram with two cubic vertices leads to the generation of kinetic terms of the type $\vec{\chi}^2 (D_i \vec{\chi})^2$ and $(\vec{\chi} \cdot D_i \vec{\chi})^2$ with couplings of order $\mathcal{O}(g_3^2)$, which enter the EQCD Lagrangian only at order $\mathcal{O}(g_3^4)$. Such terms can in principle be cancelled by adding similar (non-renormalizable) operators to the effective theory Lagrangian of Eq. (4.5).

Finally, the expressions in Eq. (4.16) can be equated with their EQCD counterparts, given in Eq. (E.4). This gives us two new matching conditions,

$$\begin{aligned} s_1 - 4s_3v_0^2 - \frac{3}{2}s_4v_0 + s_5v_0 &= \frac{2T}{3} - \frac{T\kappa_0^-}{\pi^2}, \\ 2s_2 + 8s_3 + \frac{3s_4}{2v_0} - \frac{2s_5}{v_0} &= \frac{2}{3\pi^2T} + \frac{\kappa_2^-}{12\pi^2T}, \end{aligned} \quad (4.17)$$

where the constants κ_ℓ^\pm , parametrizing the effects of the quarks, are defined in Eq. (E.6).

4.3.2. The Z_2 breaking parameters

The matching conditions of Eq. (4.17) should be viewed as fixing the values of two linear combinations of $s_{1,2,3}$ — an interpretation that becomes trivial in the limit of unbroken center symmetry. In contrast, a third, independent linear combination of these parameters does not affect the physics of the soft scale at the leading order at all, and can thus take any value. This is because in the nonlinear version of our theory, where the heavy mode has been integrated out in a center-symmetric fashion, the three operators multiplying the coefficients $s_{1,2,3}$ are not independent, but there is a linear relation between Σ^4 , $\vec{\Pi}^2$, and $(\vec{\Pi}^2)^2$. As the linear and nonlinear models describe the same long-distance physics, there *must* be one combination of $s_{1,2,3}$ that is left undetermined by the leading-order matching of the linear theory, and can only be found through a higher-order computation. The insensitivity of the long-distance physics to this linear combination will be further demonstrated in section 4.4, where the domain-wall solution of the field equations of motion is discussed.

As EQCD violates the center symmetry explicitly, it is clear that the parameters $s_{4,5}$, which facilitate the soft breaking of this symmetry in the presence of fermions, cannot be found by matching to EQCD. To determine their values, we instead have to consider the global structure of the ZQCD effective potential, which we do by applying the Nielsen theorem [69] and concentrating on the second stationary point (local minimum) of the effective potential that provides additional gauge-invariant observables. A natural measure of the center symmetry breaking is the energy-density difference of the absolute and metastable minima, which on the full theory side is represented by the parameter δ , defined in Eq. (E.7). In the effective theory, the stable and metastable minima are to leading order located at $\Sigma = \pm v_0$ (and $\Pi_a = 0$). A comparison of the values of the potentials gives then the matching condition $s_4v_0^3T = -\delta T^4$

which, using Eq. (4.12), leads to the identification

$$s_4 = -\frac{\delta}{8} = \frac{1}{2\pi^2}(\kappa_{-2}^- - \kappa_{-2}^+). \quad (4.18)$$

The last parameter to be fixed, s_5 , does not contribute to the energy difference of the two vacua, but does affect the shape of the effective potential. One simple and gauge invariant (although by no means unique) quantity sensitive to s_5 is the difference of the squared mass parameters at the two minima, *i.e.*, m_χ^2 of Eq. (4.16) and the analogous parameter at the metastable minimum. The corresponding quantities are also straightforward to evaluate in the full theory, see Appendix E, yielding the last perturbative matching condition,

$$2s_5 - 3s_4 = \frac{1}{2\pi^2}(\kappa_0^+ - \kappa_0^-). \quad (4.19)$$

It is interesting to note that the right-hand side of this equation is proportional to the second derivative of the parameter δ with respect to the chemical potential(s), *i.e.*, the difference of the quark number susceptibilities in the stable and metastable vacua of the theory.

4.4. Extended field configurations

Having now finished the leading-order matching of ZQCD to the full theory, it is important to test its predictions in particular for quantities that are sensitive to the center symmetry. Perhaps the most straightforward such test is to study extended gauge-field configurations which probe the global structure of the effective potential. In the absence of fermions, and thus Z_2 breaking operators, we can construct a stable domain wall joining the two physically equivalent minima of the theory. With fermions, this is no longer possible, as the minima are not degenerate in energy, but one can still look for a rotationally invariant three-dimensional solution that represents a bubble of the stable vacuum in a metastable environment. Although this bubble evolves with time, its growth rate can be estimated using a semiclassical *static* solution, representing a stationary point of a three-dimensional effective action with suitable boundary conditions [70].

Consider first a bubble-wall configuration in the full theory, in which the (static) temporal gauge field A_0 depends only on the radial coordinate r and points in the same direction in color

space everywhere. It is described by a single scalar function $a(r)$, whose action has the form

$$S_{\text{eff}} = \beta \int_0^\infty dr 4\pi r^2 \left[\frac{1}{2} \left(\frac{da}{dr} \right)^2 + V_{\text{eff}}(a) \right], \quad (4.20)$$

where the potential V_{eff} is obtainable from Eq. (E.3). One may then solve the equation of motion stemming from this action with the boundary condition $a(\infty) = 2\pi T/g$, and use it to obtain the domain-wall energy density and tension as well as the bubble profile, as has indeed been done in Refs. [71, 72] (see also Ref. [73] for a recent similar calculation).

Within the effective theory, we first note that in order to minimize the energy cost of creating a bubble, it is clearly optimal to have the fields Σ , $\vec{\Pi}$ minimize the hard part of the potential (G.3) everywhere in space, *i.e.*, have them satisfy $\Sigma^2 + \vec{\Pi}^2 = v_0^2$. Recalling the identification of Eq. (4.12), we see that we can express the fields in terms of one dimensionless function α , ranging from 0 to 1, as $\Sigma = v_0 \cos(\pi\alpha)$, $|\vec{\Pi}| = v_0 \sin(\pi\alpha)$. Plugging these formulas into Eq. (G.3), we obtain upon a trivial shift the potential

$$V_{\text{eff}}(\alpha) = \frac{v_0^2}{2}(s_1 - 4s_3 v_0^2) \sin^2(\pi\alpha) + \frac{v_0^4}{4}(s_2 + 4s_3) \sin^4(\pi\alpha) - \frac{v_0^3}{3\pi} |\sin(\pi\alpha)|^3 + \frac{v_0^3}{2} s_4 [\cos^3(\pi\alpha) - 1] + \frac{v_0^3}{2} s_5 \cos(\pi\alpha) \sin^2(\pi\alpha), \quad (4.21)$$

using which the bubble profile can again be solved.

Specializing for the moment to the domain-wall calculation in the Z_2 invariant, pure Yang-Mills case, we observe that the potential of Eq. (4.21) depends exactly on the two linear combinations of $s_{1,2,3}$ that were determined in our perturbative matching, cf. Eq. (4.17). We conclude that the domain-wall tension and profile become genuine predictions of the effective theory. Indeed, from Eq. (4.17) we infer the results $s_1 - 4s_3 v_0^2 = 2T/3$ and $s_2 + 4s_3 = 1/(3\pi^2 T)$, using which we straightforwardly obtain for the domain-wall tension

$$\sigma \approx 4.899 \times \frac{T^3}{g} \approx 0.91 \sigma_{\text{YM}}, \quad (4.22)$$

where $\sigma_{\text{YM}} = \left(\frac{2}{3}\right)^{3/2} \frac{\pi^2 T^3}{g}$ denotes the full theory result [71]. In Figure 4.1, we plot the full and effective theory domain-wall profiles which we find to agree at a satisfactory level.

Let us finally return to the three-dimensional bubble solution, relevant when dynamical quarks are present. Its formation and profile are determined by a balance between a volume energy gain, scaling like δR^3 (with the energy-density difference δ introduced in Eq. (E.7)),

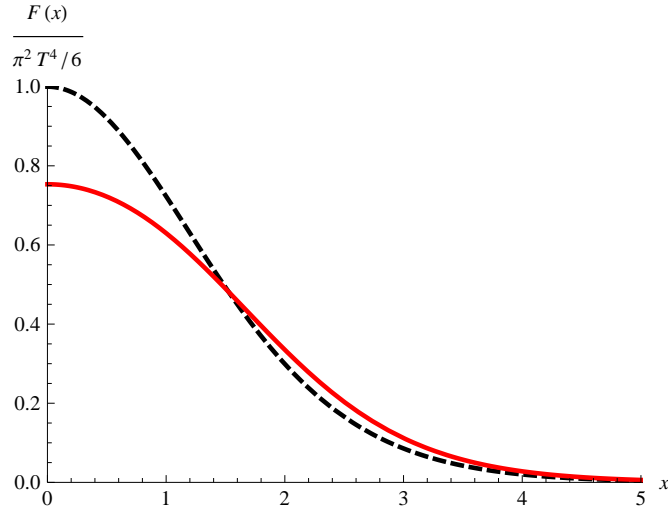


Figure 4.1.: Free energy profiles of the leading-order domain-wall solution in the center-symmetric limit as a function of the dimensionless length variable $x \equiv gTr$, with the wall residing at $x = 0$. The solid red curve is the prediction of the effective theory, while the dashed black one is the full Yang-Mills result. The boundary condition for this one-dimensional solution is $\alpha(-\infty) = 0$ and $\alpha(+\infty) = 1$.

and a surface energy cost, scaling like σR^2 , where R stands for the bubble radius in units of $1/(gT)$. We will not attempt a full numerical solution of the corresponding equation of motion, which is straightforward but not particularly illuminating, but instead provide an analytic approximation valid in the limit of parametrically small δ , corresponding to weak Z_2 breaking effects. As we expect R to scale like $1/\delta$, the explicit r -dependence of the action becomes then negligible and the bubble-profile calculation reduces to the type of domain-wall problem encountered above. This is usually called the thin-wall approximation [74].

In the thin-wall approximation, the bubble solution is universal in the sense that the bubble action (and therefore the radius) indeed only depend on the surface tension, obtained from the one-dimensional domain-wall problem, and the energy-density splitting of the two vacua. The critical radius of the bubble, obtained by *maximizing* the action with respect to R , and the value of the action become

$$R_c = \frac{2}{\delta} \times \frac{\sigma}{T^3/g}, \quad S_{\text{bubble}} = \frac{16\pi}{3g^3\delta^2} \times \left(\frac{\sigma}{T^3/g} \right)^3. \quad (4.23)$$

Quantitatively, the applicability of the thin-wall approximation is determined by the condition that the radius of the bubble is much larger than the width of the domain wall, a quantity of order one in dimensionless units. Using the full-theory value for the surface tension, this trans-

lates to $\delta \lesssim 1$, which is certainly satisfied for quarks with $m_j \gtrsim T, \mu_j$, as δ is then exponentially suppressed.

Chapter 5.

Conclusions

In this thesis I studied the thermodynamics of QCD-like theories at nonzero temperature and baryon chemical potential using the PNJL and ZQCD models.

In the PNJL model constructed in Chapter 3, the gauge sector is simulated by a lattice-spin model with nearest-neighbor interactions whose parameters are fixed with the help of the strong-coupling expansion of the full lattice gauge theory. The quark sector was modeled using the standard NJL model constructed for both type-I and type-II QCD-like theories.

We showed at hand of the example of QCD with adjoint quarks that the Weiss mean-field approximation to the lattice-spin model used here is superior to the naive mean-field approximation, commonly employed in literature, which leads to a thermodynamic instability. The Weiss mean-field approximation also allowed us to derive the expectation value of the Polyakov loop in an arbitrary representation. The results are given in an implicit form applicable at all temperatures and chemical potentials, which enables us to study Casimir scaling in hot and/or dense matter.

As a concrete example, we studied the phase diagram of QCD with adjoint quarks of two and three colors. We confirmed that in adjoint QCD the critical temperature for chiral restoration is much higher than that of deconfinement, both being well-defined phase transitions associated with spontaneous breaking/restoration of an exact symmetry (the former in the chiral limit). We checked the model-independent prediction that the phase diagram of aQC₂D features a tetracritical point. On the contrary, in the phase diagram of aQCD the second-order BEC transition line is interrupted and meets the first-order deconfinement line at two tricritical points.

It is worth emphasizing that while fine numerical details of our phase diagrams depend on our guess for the model parameters as well as on the particular way quarks are implemented, their qualitative features are largely based on symmetry and thus model-independent. Moreover, our results for Casimir scaling do not depend on the quark sector, in particular on the choice of the NJL parameters. They can therefore be understood as a direct test of the lattice spin model with nearest-neighbor interactions. Once a model for the quark sector is introduced, they give a prediction for Casimir scaling of Polyakov-loop expectation values in the whole phase diagram.

In Chapter 4 we constructed a dimensionally reduced effective theory for two-color Yang-Mills theory and generalized it by including in the consideration the effects of fundamental quarks of in principle arbitrary masses and chemical potentials on the dynamics of the Wilson line. The effective theory is formulated in terms of a coarse grained Wilson line \mathcal{Z} defined by Eq. (4.2), as well as the Lagrangian of Eqs. (4.5)–(4.8). The theory has by construction a notion of the center symmetry of the full theory, and is invariant under it in the absence of dynamical quarks. The matching of the effective theory to the full one was performed by requiring that the former reproduce the correct long-distance physics of the latter, a task most conveniently accomplished by demanding that the theory reduces to EQCD upon integrating out the momentum scale πT . This we carried out explicitly in section 4.3, where the s_i parameters appearing in the effective-theory Lagrangian were determined with the exception of one, for which a higher-order computation is needed.

Upon fixing its soft parameters, our effective theory becomes fully predictive, as the physics of the distance scales $1/(gT)$ and larger is to a very good accuracy independent of the values of the hard parameters h_i [66]. We reproduced the free-energy profiles of the leading-order domain-wall solution in the center-symmetric limit and predicted the three-dimensional bubble solution when dynamical quarks are present. Our theory is immediately amenable to nonperturbative lattice simulations, with which one may study two-color QCD over an extensive range of temperatures, quark chemical potentials, and masses. It should be recalled that the only reason we have chosen to study two-color QCD and not the physical case of three colors is notational and computational simplicity. If the predictions of the effective theory turn out to match two-color lattice data well, then the investigations can be generalized to full three-color QCD.

Finally, another interesting topic for future work would clearly be to consider the relation of our effective theory to the strong-coupling effective actions derived in Refs. [75, 76, 77, 78]. It appears that these two approaches are strongly complementary in the sense that they

approach the deconfinement transition from opposite directions; whether this can be used to gain more insight into the dynamics of the transition itself remains to be seen.

Appendix A.

Haar measure of unitary groups

Here I briefly summarize the definition and properties of the Haar measure [79] of Lie groups and give a method to calculate the distribution of eigenvalues of $U(N)$ and $SU(N)$ groups, which is used in the calculation of the matrix model in Chapter 3.

Let G be a locally compact topological group and let $C_0(G)$ and $C_0^+(G)$ denote the space of continuous and continuous and non-negative functions on G with a compact support, respectively. A linear form μ on $C_0(G)$ is called a *left Haar measure* or a *left Haar integral*, if

1. it is a positive linear form, *i.e.*, $\mu(f) \geq 0$, $\forall f \in C_0^+(G)$,
2. it is left-invariant, *i.e.*, $\mu(L_g f) = \mu(f)$, where $L_g f(x) = f(g^{-1}x)$, $x, g \in G$.

Similarly we can define the *right Haar measure*. It turns out that every locally compact group has a left Haar measure and any two nonzero left Haar measures must be the same up to a positive constant. This is also true for the right Haar measure, although the right one is not necessarily the same as the left one. Actually the existence of a left Haar measure implies the existence of a right one,¹ and *vice versa*.

By Riesz' theorem we can represent the Haar integral by a set function $\mu(x)$, for $x \in G$, as

$$\mu(f) = \int_G f(g) d\mu(g). \quad (\text{A.1})$$

The left-invariant feature implies

$$d\mu(gx) = d\mu(x), \quad (\text{A.2})$$

¹Let μ be the left Haar measure on G , the new measure defined by $\tilde{\mu}(f) = \mu(\tilde{f})$, where $\tilde{f}(x) = f(x^{-1})$, is in fact the right Haar measure on G .

for all $x, g \in G$. It is similar for the right Haar measure. Moreover it can be shown using the modular function² that every compact group has equal (thus unique up to a positive constant) left and right Haar measures. Such a Haar measure which is both left- and right-invariant is called an *invariant measure*. It can be shown that every invariant Haar measure is also invariant under the inversion, *i.e.*, $d\mu(g^{-1}) = d\mu(g)$ for $g \in G$. Unitary groups $U(N)$ and $SU(N)$ are compact, thus they have all the above properties.

After summarizing the definition and basic properties, we are confronted with the question how to calculate the Haar measure of a Lie group. A straightforward method is using the definition. We can first parameterize the Lie group G , thus the Haar measure $d\mu(x)$ can be written as

$$\mu(X)dX = \mu(x_1, \dots, x_n)dx_1 \cdots dx_n, \quad (\text{A.3})$$

where $X = (x_1, \dots, x_n)$ is the coordinate of $x \in G$, $\mu(X)$ is a function of the coordinate, and $dx_1 \cdots dx_n$ is the natural measure on \mathbb{R}^n . The left-invariance $d\mu(gx) = d\mu(x)$ tells us that for X' of $x' = gx$

$$\mu(X)dX = \mu(X')dX' = \mu(X') \left| \frac{\partial X'}{\partial X} \right| dX, \quad (\text{A.4})$$

with an explicit Jacobian determinant inside. Thus we have

$$\mu(X) = \mu(X') \left| \frac{\partial X'}{\partial X} \right|, \quad \forall x, g \in G. \quad (\text{A.5})$$

Making use of the fact that the left-hand side is independent of any $g \in G$, the function $\mu(X)$ can be finally determined, up to a positive constant. Since g can be an arbitrary element of the group, it can be chosen as $g = x^{-1}$, which results in the relation to the Haar measure at the unit element of the group

$$\mu(X) = \mu_0 \left| \frac{\partial X'}{\partial X} \right|_{g=x^{-1}}, \quad (\text{A.6})$$

where μ_0 is the measure evaluated at unity.

²The modular function is a group homomorphism into the multiplicative group of nonzero real numbers. A group is unimodular if and only if the modular function is identically 1, or, equivalently, if the Haar measure is both left and right invariant. Examples of unimodular groups are abelian groups, compact groups, discrete groups (e.g. finite groups), semisimple Lie groups, and connected nilpotent Lie groups.

As an example, let us now calculate the Haar measure of $SU(2)$. It is a compact Lie group, thus has an invariant measure. An $SU(2)$ matrix can be parametrized as

$$U = w\mathbb{1} + i(x\sigma_x + y\sigma_y + z\sigma_z),$$

where $\sigma_{x,y,z}$ are Pauli matrices, $w, x, y,$ and z are four real numbers. Since $SU(2)$ requires $w^2 + x^2 + y^2 + z^2 = 1$, there only exist three degrees of freedom, which can be chosen as any three out of the four. Here we choose x, y, z . Now consider a left transformation under $g \in SU(2)$ with $g = a\mathbb{1} + i(b\sigma_x + c\sigma_y + d\sigma_z)$ and again $a^2 + b^2 + c^2 + d^2 = 1$. The transformed one is

$$gU = U' = w'\mathbb{1} + i(x'\sigma_x + y'\sigma_y + z'\sigma_z)$$

with

$$w' = aw - bx - cy - dz,$$

$$x' = bw + ax + dy - cz,$$

$$y' = cw - dx + ay + bz,$$

$$z' = dw + cx - by + az.$$

Using

$$\frac{\partial w}{\partial x} = -\frac{x}{w}$$

and similar for y and z , the Jacobian reads

$$\left| \frac{\partial(x', y', z')}{\partial(x, y, z)} \right| = \begin{vmatrix} b\frac{\partial w}{\partial x} + a & b\frac{\partial w}{\partial y} + d & b\frac{\partial w}{\partial z} - c \\ c\frac{\partial w}{\partial x} - d & c\frac{\partial w}{\partial y} + a & c\frac{\partial w}{\partial z} + b \\ d\frac{\partial w}{\partial x} + c & d\frac{\partial w}{\partial y} - b & d\frac{\partial w}{\partial z} + a \end{vmatrix} = \frac{(a^2 + b^2 + c^2 + d^2)(aw - bx - cy - dz)}{w} = \frac{w'}{w}. \quad (\text{A.7})$$

Thus the Haar measure should satisfy

$$\mu(x, y, z) = \mu(x', y', z') \left| \frac{\partial(x', y', z')}{\partial(x, y, z)} \right| = \mu(x', y', z') \frac{w'}{w}.$$

The most convenient (and also unique) choice is

$$\mu(x, y, z) = \frac{1}{w} = \frac{1}{\sqrt{1 - (x^2 + y^2 + z^2)}}, \quad (\text{A.8})$$

where we choose the positive square root as required by the definition of the Haar measure.

The above parametrization explicitly shows that $SU(2)$ is isomorphic to S^3 . This suggests to choose the three phases as the degrees of freedom,

$$\begin{aligned} w &= \cos \theta_1, \\ x &= \sin \theta_1 \cos \theta_2, \\ y &= \sin \theta_1 \sin \theta_2 \cos \theta_3, \\ z &= \sin \theta_1 \sin \theta_2 \sin \theta_3. \end{aligned} \tag{A.9}$$

It is not difficult to express the Haar measure as

$$d\mu(U) = \frac{dx dy dz}{w} = \sin^2 \theta_1 \sin \theta_2 d\theta_1 d\theta_2 d\theta_3, \tag{A.10}$$

which is in fact the product of a part with eigenvalues and one with angles only appearing in the eigenvectors

$$\left(|\lambda_1 - \lambda_2|^2 d\theta_1 \right) (\sin \theta_2 d\theta_2 d\theta_3)$$

when realizing that the eigenvalues of U are $\lambda_{1,2} = e^{\pm i\theta_1}$ and the eigenvectors³ only depend on $\theta_{2,3}$.

As we will see later, the statement that the Haar measure is the product of two parts can be generalized to unitary groups, with the first one containing only eigenvalues as $\prod |\lambda_i - \lambda_j|^2 d\theta_i$, and the second containing all other ‘‘angles’’. By integrating out all angles which are not the eigenvalues, we can get the distribution of eigenvalues needed in Chapter 3. Formally this idea can be expressed as

$$d\mu(U) = \mu_1(\lambda) \mu_2(\omega) d\lambda d\omega, \tag{A.11}$$

where $U \in U(N)$, λ is the collection of eigenvalues of U , and ω is for all other angles. For all functions $f \in C_0(G)$ which depend only on the eigenvalues λ , namely, $f(U) = f(\lambda)$, the

³The eigenvectors corresponding to $\lambda_{1,2} = e^{\pm i\theta_1}$ are

$$\sqrt{\frac{1 \mp \sin \theta_2 \sin \theta_3}{2}} \left(\frac{\sin \theta_2 \sin \theta_3 \pm 1}{\cos \theta_2 + i \sin \theta_2 \cos \theta_3}, 1 \right)^T.$$

following integral

$$\mu(f) = \int_G f(\lambda) \mu_1(\lambda) d\lambda \quad (\text{A.12})$$

is invariant under any left or right transformation

$$f(U) \rightarrow f(g^{-1}U) \quad \text{or} \quad f(Ug^{-1}) \quad (\text{A.13})$$

for any $g \in U(N)$. This is simply because the the integral can be rewritten with the explicit invariant measure (A.11) as

$$\mu(f) = \frac{1}{c} \left(\int_\lambda f(\lambda) \mu_1(\lambda) d\lambda \right) \left(\int_\omega \mu_2(\omega) d\omega \right), \quad (\text{A.14})$$

where we just put back the integration over ω as a constant c . This c must be positive otherwise the Haar measure (A.11) would vanish.

Now let us calculate the desired distribution of eigenvalues of unitary groups, $U(N)$. Instead of the method demonstrated above, the Haar measure can be obtained from the invariant metric tensor.⁴ First we can define an inner product of complex matrices as $\langle A|B \rangle = \text{Tr}(A^\dagger B)$, which induces the norm $\|A\|^2 = \langle A|A \rangle$, which then induces the distance of two matrices

$$s(A, B) = \|A - B\| = \sqrt{\text{Tr}[(A - B)^\dagger (A - B)]}. \quad (\text{A.15})$$

This distance is invariant under any left and right unitary transformation, namely,

$$s(UA, UB) = s(AU, BU) = s(A, B).$$

It therefore defines an invariant metric when restricted to unitary groups. Thus we can calculate the metric tensor from the infinitesimal squared distance

$$ds^2 = g_{\alpha\beta}(x) dx^\alpha dx^\beta, \quad (\text{A.16})$$

and then obtain the invariant volume element in $U(N)$ as

$$d\mu(x) = \sqrt{\det g(x)} \prod_\alpha dx^\alpha. \quad (\text{A.17})$$

⁴I thank Tomáš Brauner for providing his notes on this method.

As mentioned above, we diagonalize any unitary matrix U as $U = W\Lambda W^\dagger$ with diagonal Λ and unitary W . There are N eigenvalues in Λ , $\lambda_i = e^{i\theta_i}$, and $(N^2 - N)$ other “angles” in W , denoted as ω_a , provided that all eigenvalues λ_i are different. They together give all N^2 real degrees of freedom of the $U(N)$ group.⁵ An infinitesimal shift dU inside the group gives the infinitesimal squared distance

$$ds^2 = \text{Tr}(dU^\dagger dU). \quad (\text{A.18})$$

The shift of U can be expressed by

$$\begin{aligned} dU &= Wd\Lambda W^\dagger + dW\Lambda W^\dagger + W\Lambda dW^\dagger \\ &= Wd\Lambda W^\dagger + WW^\dagger dW\Lambda W^\dagger - W\Lambda W^\dagger dW W^\dagger \\ &= W(d\Lambda + [W^\dagger dW, \Lambda])W^\dagger, \end{aligned} \quad (\text{A.19})$$

where we used the unitarity of W and its constraint

$$WdW^\dagger + dW W^\dagger = 0. \quad (\text{A.20})$$

Denoting $W^\dagger dW$ as $d\Omega$, Eq. (A.18) becomes

$$ds^2 = \text{Tr}(d\Lambda^\dagger d\Lambda) + \text{Tr}([d\Omega, \Lambda]^\dagger [d\Omega, \Lambda]) + 2 \text{Re} \text{Tr}(d\Lambda^\dagger [d\Omega, \Lambda]). \quad (\text{A.21})$$

The last term vanishes since $\text{Tr}(d\Lambda^\dagger [d\Omega, \Lambda]) = \text{Tr}(d\Omega[\Lambda, d\Lambda^\dagger])$, and $[\Lambda, d\Lambda^\dagger] = 0$ because both are diagonal. Noting that $[d\Omega, \Lambda]_{ij} = (\lambda_j - \lambda_i)d\Omega_{ij}$, finally we obtain

$$ds^2 = \sum_i d\theta_i d\theta_i + 2 \sum_{i>j} |\lambda_i - \lambda_j|^2 |d\Omega_{ij}|^2. \quad (\text{A.22})$$

The last step before identifying the coefficients of the above equation with $g_{\mu\nu}$ in Eq. (A.16) is to find the relationship between the well-defined coordinates $d\omega_a$ and the antihermitian shift $d\Omega = W^\dagger(\omega_a)dW$. It can be calculated straightforwardly when the matrix entries of W are given in the explicit form of $W_{ij}(\omega_a)$, for example ω_a are chosen as the real and imaginary parts of the entries in W . It may also be a nontrivial task when another parameterization is

⁵ W always contains one additional overall phase factor for each of the N eigenvectors of U . However, these phases can be factored out in the form of a diagonal unitary matrix multiplied to the right of W , which commutes with Λ and cancels with the one from W^\dagger . Thus they are not degrees of freedom of U .

chosen, such as the exponential mapping between the Lie group and its Lie algebra.⁶ In any case we can express it as $d\Omega_a = Q_{ab}(\omega)d\omega_a$, where $d\Omega_a$ stands collectively for the real and imaginary parts of $d\Omega_{ij}$. It is still good enough to see that $\det g$ can be formally written as a product of two factors with λ_i and ω_a separately as

$$\det g \propto (\det Q)^2 \prod_{i>j} |\lambda_i - \lambda_j|^4. \quad (\text{A.23})$$

up to a numerical prefactor. Finally after integrating out the angles ω_a , we obtain the distribution of the eigenvalues on the unitary group

$$d\mu(\theta) = \prod_{i>j} |e^{i\theta_i} - e^{i\theta_j}|^2 \prod_i d\theta_i. \quad (\text{A.24})$$

This result is valid for $U(N)$. For $SU(N)$ we have to add a constrain

$$\sum_i \theta_i = 0 \pmod{2\pi},$$

which can be easily implemented using a δ -function.

I use the explicit example of $SU(2)$ to end this appendix. Again using $(\theta_1, \theta_2, \theta_3)$ as parameters, the $SU(2)$ matrix $U = W\Lambda W^\dagger$ has

$$\Lambda = \begin{pmatrix} e^{i\theta_1} & \\ & e^{-i\theta_1} \end{pmatrix}, \quad W = \begin{pmatrix} \frac{\cos \theta_2 - i \sin \theta_2 \cos \theta_3}{\sqrt{2(1 - \sin \theta_2 \sin \theta_3)}} & -\frac{\cos \theta_2 - i \sin \theta_2 \cos \theta_3}{\sqrt{2(1 + \sin \theta_2 \sin \theta_3)}} \\ \sqrt{\frac{1 - \sin \theta_2 \sin \theta_3}{2}} & \sqrt{\frac{1 + \sin \theta_2 \sin \theta_3}{2}} \end{pmatrix}. \quad (\text{A.25})$$

It is straightforward to get $|d\Omega_{12}|^2 = \frac{1}{4}(d\theta_2 d\theta_2 + \sin^2 \theta_2 d\theta_3 d\theta_3)$, thus

$$ds^2 = d\theta_1 d\theta_1 + \frac{2}{4} |e^{i\theta_1} - e^{-i\theta_1}|^2 (d\theta_2 d\theta_2 + \sin^2 \theta_2 d\theta_3 d\theta_3), \quad (\text{A.26})$$

which recovers the Haar measure we already obtained previously in this appendix.

⁶It is proved that every compact Lie group has such an exponential mapping, namely, every element represented as a matrix can be expressed as an exponential function of a matrix which is a vector in the Lie algebra. Obviously such mapping cannot be bijective because we know that many Lie groups can be locally isomorphic and share the same Lie algebra.

Appendix B.

Fierz transformation of the current–current interaction

Consider a fermionic field ψ transforming in a representation \mathcal{R} of the symmetry group. In NJL-like models, one deals with contact four-fermion interactions of the type $\sum_a (\bar{\psi} \Gamma_a^{\mathcal{A}} \psi)^2$, where $\Gamma_a^{\mathcal{A}}$ is a set of matrices that project out a particular irreducible component \mathcal{A} of the product representation $\bar{\mathcal{R}} \otimes \mathcal{R}$. The Fierz rearrangement of the four-fermion interaction is equivalent to the group-theoretical identity

$$\sum_a (\Gamma_a^{\mathcal{A}})_{ij} (\Gamma_a^{\mathcal{A}})_{kl} = \sum_{\mathcal{B}} C_{\mathcal{A}\mathcal{B}} \sum_b (\Gamma_b^{\mathcal{B}})_{il} (\Gamma_b^{\mathcal{B}})_{kj}, \quad (\text{B.1})$$

where the coefficients $C_{\mathcal{A}\mathcal{B}}$ depend only on the representations \mathcal{A}, \mathcal{B} . In order to fix the effective coupling in the meson channel, we do not need to evaluate the Fierz coefficients for all \mathcal{B} . All we need to know is the coefficient for the one-dimensional representation $\mathcal{B} = \mathcal{I}$, which is always contained in the product $\bar{\mathcal{R}} \otimes \mathcal{R}$.

Setting $\Gamma^{\mathcal{I}} = \mathbb{1}$, the coefficient $C_{\mathcal{A}\mathcal{I}}$ is projected out by multiplying Eq. (B.1) by $\delta_{li} \delta_{jk}$, which yields

$$C_{\mathcal{A}\mathcal{I}} = \frac{\sum_a \text{Tr}(\Gamma_a^{\mathcal{A}} \Gamma_a^{\mathcal{A}})}{(\dim \mathcal{R})^2}. \quad (\text{B.2})$$

In particular for $\mathcal{A} = \mathcal{I}$ this leads to $C_{\mathcal{I}\mathcal{I}} = 1/\dim \mathcal{R}$. This explains the $1/N_f$ factor in the effective NJL couplings derived from the current–current interaction (3.19): both the original interaction as well as the term $(\bar{\psi}\psi)^2$ whose coefficient we calculate are in the flavor-singlet

channel. Likewise, the Fierz transformation from the Lorentz-vector channel to the Lorentz-scalar channel has the Fierz coefficient one.

The color structure of the current–current interaction (3.19) is such that \mathcal{A} corresponds to the adjoint representation, that is, $\Gamma_a^{\mathcal{A}} = T_{a\mathcal{R}}$ are the generators of the color group in the representation \mathcal{R} of the quark fields. The Fierz coefficient (B.2) then reduces to $C_{\mathcal{AI}} = C_2(\mathcal{R})/\dim \mathcal{R}$. Specifically for the $SU(N)$ group, once the generators in the fundamental representation are normalized as $\text{Tr}(T_{aF}T_{bF}) = \frac{1}{2}\delta_{ab}$, one finds $C_2(F) = (N^2 - 1)/(2N)$ for the fundamental and $C_2(A) = N$ for the adjoint representation [7]. This concludes the derivation of the effective NJL couplings G_F and G_A given below Eq. (3.19).

Appendix C.

Gauge group averaging with continuum quarks

In this appendix we justify our prescription (3.18) for adding quarks to the lattice model of the gauge sector. In contrast to Eq. (3.18), the authors of Ref. [26] calculated the quark thermodynamic potential Ω_q in the mean-field NJL model with a constant background gauge field and set $\langle \Omega_q \rangle_{\text{mf}}$ as the quark contribution to the thermodynamic potential.

To start, let us emphasize that any attempt at adding *continuum* quarks to a lattice gauge model is at best heuristic. For a proper treatment one would need to discretize the quark action as well, thereby losing the computational simplicity of the mean-field NJL model. With this in mind, below we provide a qualitative argument why Eq. (3.18) is a reasonable approximation.

Imagine adding quarks to the lattice model (3.1); the full action then formally reads $\mathcal{S} = \mathcal{S}_g + \bar{\psi} \mathcal{D} \psi$, where \mathcal{D} is the Dirac operator including the background gauge field the quarks interact with. The full partition function of the system is obtained as

$$\mathcal{Z} = \int dL d\psi d\bar{\psi} e^{-\mathcal{S}} = \int dL e^{-\mathcal{S}_g} \det \mathcal{D}. \quad (\text{C.1})$$

Using the same trick of introducing the Weiss mean-field action as in Sec. 3.1, this leads to

$$\mathcal{Z} = \left\langle e^{-(\mathcal{S}_g - \mathcal{S}_{\text{mf}})} \det \mathcal{D} \right\rangle_{\text{mf}} \int dL e^{-\mathcal{S}_{\text{mf}}}. \quad (\text{C.2})$$

This expression is still exact and includes all correlations between the gauge and the quark sectors. However, to evaluate it numerically would be very demanding. We therefore perform

a mean-field approximation by setting

$$\left\langle e^{-(S_g - S_{\text{mf}})} \det \mathcal{D} \right\rangle_{\text{mf}} \approx e^{-\langle S_g - S_{\text{mf}} \rangle_{\text{mf}}} \langle \det \mathcal{D} \rangle_{\text{mf}}. \quad (\text{C.3})$$

This is equivalent to the Weiss mean-field approximation introduced in Sec. 3.1 plus neglecting the correlations between the gauge and quark sectors.¹ The full thermodynamic potential is then given by the gauge part (3.9) augmented with $-T \log \langle \det \mathcal{D} \rangle_{\text{mf}}$. One can therefore see that averaging the determinant of the Dirac operator is more natural than averaging its logarithm. However, Eq. (3.18) commits one more approximation: it neglects correlations between modes of different momentum and spin. While the former is naturally incorporated in Eq. (3.18) by the momentum integral, the latter has to be imposed by hand (by adding the power 1/2 to the argument of the logarithm) in presence of a diquark condensate, since this ties together quarks of opposite spin. Somewhat ambiguous as this procedure is, it does reproduce the prescription of Abuki and Fukushima [26] when $\Delta = 0$, and, unlike other prescriptions, it leads to a thermodynamically consistent potential Ω_q as will now be discussed.

Let us start rather generally by addressing the following question: why have we used the complicated-looking Weiss mean-field approximation instead of the simple “naive” one?² To find the answer it is useful to understand the relation between the two approximations. Let us write the Haar measure (3.6) as

$$dL = H(\theta) \prod_{i=1}^{N_c-1} d\theta_i. \quad (\text{C.4})$$

The group integral of a given function $f(\theta)$, weighted by the mean-field action, can then be expressed as

$$\int dL f(\theta) e^{-S_{\text{mf}}} = \int \prod_{i=1}^{N_c-1} d\theta_i f(\theta) e^{-S_{\text{mf}} + \log H(\theta)}. \quad (\text{C.5})$$

While in the Weiss mean-field approximation this group integral is evaluated exactly, the naive mean-field approximation can be obtained by picking the contribution of the saddle point of the “action” $S_{\text{mf}} - \log H(\theta)$. Indeed, let the saddle point, depending on α, β , be θ_{mf} . Then the above integral is approximated by $f(\theta_{\text{mf}}) e^{-S_{\text{mf}}(\theta_{\text{mf}}) + \log H(\theta_{\text{mf}})}$. The average of any function of the

¹The lack of correlations, in particular the feedback from the dense quark matter into the gauge sector, makes the usual PNJL model rather trivial in the region of cold dense matter. It would be interesting to see to what extent these correlations can be taken into account within the present model.

²We are indebted to Kenji Fukushima for clarifying this point at the initial stage of the project.

Polyakov loop is thus simply

$$\langle f(\theta) \rangle_{\text{mf}} = f(\theta_{\text{mf}}). \quad (\text{C.6})$$

Then, in the gauge thermodynamic potential (3.9), the Weiss mean fields α, β drop out and the result depends only on θ_{mf} ,

$$\frac{\Omega_g^{\text{naive}} a_s^3}{TV} = -2(d-1)N_c^2 e^{-a/T} \ell_{\text{F}}(\theta_{\text{mf}}) \ell_{\text{F}}^*(\theta_{\text{mf}}) - \log H(\theta_{\text{mf}}). \quad (\text{C.7})$$

In some particular cases, it can even be expressed solely in terms of the traced Polyakov loop.

Let us now for simplicity assume that the chemical potential is zero so that there is no pairing and the Polyakov loop and its complex conjugate give rise to the same expectation values. The quasiparticle contribution to the quark thermodynamic potential (3.18) with quarks in the representation \mathcal{R} of the gauge group then reads

$$-2 \int \frac{d^3 \mathbf{k}}{(2\pi)^3} \left[\epsilon_{\mathbf{k}} \dim \mathcal{R} + T \text{Tr} \log(\mathbb{1} + L_{\mathcal{R}} e^{-\epsilon_{\mathbf{k}}/T}) \right]. \quad (\text{C.8})$$

The fundamental and adjoint Polyakov loops are related by $\text{Tr} L_{\Lambda} = |\text{Tr} L_{\text{F}}|^2 - 1$, hence the same relation holds for their expectation values in the naive mean-field approximation. This means that at low temperature when the fundamental Polyakov loop goes to zero, the adjoint loop should become negative. Disregarding the obvious disagreement of this conclusion with lattice simulations, it would moreover be a disaster for the mean-field PNJL model. Indeed, at low temperatures,

$$\text{Tr} \log(\mathbb{1} + L_{\mathcal{R}} e^{-\epsilon_{\mathbf{k}}/T}) \approx e^{-\epsilon_{\mathbf{k}}/T} \text{Tr} L_{\mathcal{R}}. \quad (\text{C.9})$$

A negative value of the Polyakov loop would thus imply that the quasiquarks would give a negative contribution to the pressure, leading to a thermodynamic instability. We conclude that the naive mean-field approximation cannot be applied to QCD with adjoint quarks.

We will now show that a similar, albeit milder, instability occurs when one defines the quark contribution to the thermodynamic potential by taking $\langle \Omega_q \rangle_{\text{mf}}$. For the sake of simplicity we focus on aQC₂D at low temperature. The mean field α is then strictly zero (deconfinement is a sharp phase transition for adjoint quarks) and the average of the quark thermodynamic potential is easily evaluated using the integrals (14) of Ref. [39]. In accord with the general

expression (3.18) (with swapped logarithm and averaging operations), one finds

$$2 \left\langle \log[(1+x)(1+2x \cos 2\theta + x^2)] \right\rangle_{\text{mf}} = 2[\log(1+x) - x], \quad (\text{C.10})$$

where $x = e^{-E_k^e/T}$. Even though the leading term, linear in x and proportional to $\langle \text{Tr } L_A \rangle_{\text{mf}}$, now vanishes, the total quasiquark pressure is still negative. This negative contribution is numerically small, yet it makes the thermodynamics in principle ill-defined.

It is easy to see that this problem does not arise when the group average is taken inside the logarithm as in Eq. (3.18). Then at low temperature when $\alpha = 0$, one gets instead of Eq. (C.10)

$$2 \log \langle (1+x)(1+2x \cos 2\theta + x^2) \rangle_{\text{mf}} = 2 \log[(1+x)(1-x+x^2)] = 2 \log(1+x^3). \quad (\text{C.11})$$

The pressure is now strictly positive and even looks like a pressure of noninteracting fermionic quasiparticles with energy $3E_k^e$.

One comment is appropriate regarding the last claim. In the PNJL model for physical, three-color QCD with fundamental quarks, one observes the same behavior at low temperature. More precisely, the mean field α is never strictly zero at any nonzero temperature, so the quark contribution to the pressure is proportional to $\log(1 + 3x\ell_F + 3x^2\ell_F^* + x^3)$. At low temperature when the Polyakov loop is suppressed this reduces to $\log(1+x^3)$, which is usually interpreted as a manifestation of the fact that one needs three quarks to create a color-singlet state. This observation suggests that the PNJL model is a natural framework for a description of the quarkyonic phase in cold dense quark matter [80, 81, 82]. However, as Eq. (C.11) clearly shows, this is somewhat misleading: the same low-temperature behavior of the pressure arises in *two-color* QCD with adjoint quarks, so it does not directly reflect the number of quarks needed to construct a color singlet.

A second attempt at interpreting $\log(1+x^3)$ might be that both examples of three-color fundamental and two-color adjoint quarks are governed by the dimension of the representation. However, in two-color QCD it is easy to calculate the same quantity with quarks in higher representations, showing that there is no simple general relation between the representation and the form of the low-temperature pressure. For instance, in aQCD below the deconfinement temperature, the coefficients $\omega_{1,2,3}$ take on the values $\omega_1 = -1$, $\omega_2 = 0$, $\omega_3 = 1/8$. Consequently, the quark pressure is proportional to $2 \log(1 + x^3 + x^5 + x^8)$.

Appendix D.

Group integration for $SU(N)$

In this appendix we show that some of the group integrals can be performed for arbitrary N [83, 84]. (For the sake of legibility, we abbreviate N_c as N .) Let us define the generating function

$$\mathcal{G}(z, \bar{z}) = \left\langle \prod_{i=1}^N e^{z e^{i\theta_i}} e^{\bar{z} e^{-i\theta_i}} \right\rangle_{\text{mf}} . \quad (\text{D.1})$$

In order to calculate it, we write the mean-field action (3.5) for one lattice site as

$$\mathcal{S}_{\text{mf}} = - \sum_{i=1}^N (\alpha \cos \theta_i + i\beta \sin \theta_i) . \quad (\text{D.2})$$

Furthermore, we use the fact that the Haar measure (3.6) may be written as a square of a Vandermonde determinant,

$$dL = \prod_{i=1}^N d\theta_i \delta(\theta_1 + \dots + \theta_N) \varepsilon_{i_1 \dots i_N} \varepsilon_{j_1 \dots j_N} e^{i\theta_1(i_1 - j_1)} \dots e^{i\theta_N(i_N - j_N)} . \quad (\text{D.3})$$

The last trick is to express the (periodic) δ -function in terms of its Fourier series,

$$\delta(\theta_1 + \dots + \theta_N) = \frac{1}{2\pi} \sum_{m=-\infty}^{+\infty} e^{im(\theta_1 + \dots + \theta_N)} . \quad (\text{D.4})$$

The integration over the angles θ_i now completely factorizes in terms of a single master integral,

$$\mathcal{T}_n(u, v) = \frac{1}{2\pi} \int_0^{2\pi} d\theta e^{in\theta} e^{u \cos \theta + iv \sin \theta}, \quad (\text{D.5})$$

For real u and pure imaginary v , $v = iw$, which is the case if $\beta = 0$, the master integral can again be expressed with the help of the modified Bessel function,

$$\mathcal{T}_n(u, iw) = \left(\frac{u - iw}{\sqrt{u^2 + w^2}} \right)^n I_n(\sqrt{u^2 + w^2}). \quad (\text{D.6})$$

The final formula for the generating function (D.1) reads

$$\mathcal{G}(z, \bar{z}) = \frac{\sum_{m=-\infty}^{+\infty} \det \mathcal{T}_{m+i-j}(\alpha + z + \bar{z}, \beta + z - \bar{z})}{\sum_{m=-\infty}^{+\infty} \det \mathcal{T}_{m+i-j}(\alpha, \beta)}. \quad (\text{D.7})$$

Looking back at Eq. (D.1) one sees that expanding the exponentials, the Taylor coefficient of the $z^m \bar{z}^n$ term resums all eigenvalues of the Polyakov loop in the $F^m \otimes \bar{F}^n$ representation, F being the fundamental one. That is, one has

$$\langle \text{Tr} L_{F^m \otimes \bar{F}^n} \rangle_{\text{mf}} = \left. \frac{\partial^{m+n}}{\partial z^m \partial \bar{z}^n} \mathcal{G}(z, \bar{z}) \right|_{\substack{z=0 \\ \bar{z}=0}}. \quad (\text{D.8})$$

The expectation values of Polyakov loops in all *irreducible* representations can be obtained from this formula by simply observing that the (traced) Polyakov loop in a direct sum of two representations is equal to the sum of the loops in these representations.

Let us remark here that the thermodynamic potential of the three-color pure gauge theory (3.37) can be derived using the same argument, and the group integrals involved are special cases of those considered above. Indeed, the function $F(\alpha)$ (3.36) equals the denominator in Eq. (D.7) at $\beta = 0$ up to a trivial numerical prefactor. Changing this prefactor just shifts the thermodynamic potential by a constant, and noting that $F(0) = 1$, it can be fixed by demanding that $\Omega_g = 0$ for $\alpha = 0$.

A more compact formula can again be obtained for the special case of two colors. Then, we can set $\beta = 0$ and $\bar{z} = 0$. Also, $\prod_{i=1}^2 e^{ze^{i\theta}} = e^{2z \cos \theta}$. The one-dimensional group integration

can be performed directly and one finds

$$\mathcal{G}(z) = \frac{I_0(2\alpha + 2z) - I_2(2\alpha + 2z)}{I_0(2\alpha) - I_2(2\alpha)} = \frac{\alpha}{\alpha + z} \frac{I_1(2\alpha + 2z)}{I_1(2\alpha)}. \quad (\text{D.9})$$

While the latter expression is more compact, the former is more convenient for taking the derivatives in order to extract the expectation values of the Polyakov loops.

Finally, let us show that even the averages (3.41) can be expressed analytically in terms of a series of modified Bessel functions [85], and thus speed up the numerical evaluation of the thermodynamic potential. Using trigonometric identities, these averages can be written as a linear combination of terms of the type

$$K_{abc}(\alpha) = \langle e^{i(a\theta_1 + b\theta_2 + c\theta_3)} \rangle_{\text{mf}}, \quad (\text{D.10})$$

where a, b, c are integers. Using the same trick of rewriting the Haar measure as a Vandermonde determinant and introducing the periodic δ -function as in Eqs. (D.3) and (D.4), this becomes

$$K_{abc}(\alpha) = \frac{1}{6F(\alpha)} \sum_{m=-\infty}^{+\infty} \sum_{i,j,k=1}^3 \varepsilon_{ijk} \begin{vmatrix} I_{m+i-1+a}(\alpha) & I_{m+i-2+a}(\alpha) & I_{m+i-3+a}(\alpha) \\ I_{m+j-1+b}(\alpha) & I_{m+j-2+b}(\alpha) & I_{m+j-3+b}(\alpha) \\ I_{m+k-1+c}(\alpha) & I_{m+k-2+c}(\alpha) & I_{m+k-3+c}(\alpha) \end{vmatrix}. \quad (\text{D.11})$$

Appendix E.

EQCD parameters in the presence of massive fermions

The one-loop QCD effective potential evaluated in a static background A_0 field was first determined in Refs. [64, 67, 68]. Rewriting it in a form invariant under *global* SU(2) symmetry and parametrizing the gauge field as $A_0 = \vec{a} \cdot \vec{\sigma}/2$, the result becomes

$$V_{\text{eff}}(\vec{a}) = \frac{4}{3}\pi^2 T^4 \left\langle \frac{g|\vec{a}|}{2\pi T} \right\rangle^2 \left(1 - \left\langle \frac{g|\vec{a}|}{2\pi T} \right\rangle \right)^2 - 2T \sum_{j=1}^{N_f} \sum_{\pm} \int \frac{d^3\mathbf{k}}{(2\pi)^3} \log \left[1 + 2e^{-\beta(\epsilon_{j\mathbf{k}} \pm \mu_j)} \cos \frac{g|\vec{a}|}{2T} + e^{-2\beta(\epsilon_{j\mathbf{k}} \pm \mu_j)} \right], \quad (\text{E.1})$$

where $\langle \cdot \rangle$ denotes the fractional part of a real number ($\langle x \rangle = x - [x]$), μ_j the set of (flavor) quark number chemical potentials, and $\epsilon_{j\mathbf{k}} = \sqrt{\mathbf{k}^2 + m_j^2}$ the dispersion relation of the j th quark flavor. Also, we used the shorthand notation $|\vec{a}| = \sqrt{\vec{a} \cdot \vec{a}}$. Expanding this expression in powers of \vec{a} around zero and subtracting the contribution of the static modes (amounting to the term cubic in \vec{a}), one may readily identify the EQCD parameters

$$m_\chi^2 = \frac{2g^2 T^2}{3} - 2g^2 \sum_{j=1}^{N_f} \int \frac{d^3\mathbf{k}}{(2\pi)^3} \bar{f}'(\epsilon_{j\mathbf{k}}, \mu_j), \quad (\text{E.2})$$

$$\tilde{\lambda} = \frac{2g^4 T}{3\pi^2} + \frac{g^4}{6} \sum_{j=1}^{N_f} \int \frac{d^3\mathbf{k}}{(2\pi)^3} \bar{f}'''(\epsilon_{j\mathbf{k}}, \mu_j),$$

where $\bar{f}(x, \mu) = [f(x + \mu) + f(x - \mu)]/2$, the prime denotes differentiation with respect to x , and $f(x) = 1/(e^{\beta x} + 1)$ is the Fermi–Dirac distribution function.

Compact as the above expressions (E.1) and (E.2) are, one can further evaluate the integrals over the quark momentum analytically in terms of the modified Bessel function of the second kind, K_n . Expanding the logarithm in powers of fugacity and using some identities for the Bessel functions, one obtains the result

$$V_{\text{eff}}(\vec{d}) = \frac{4}{3}\pi^2 T^4 \left\langle \frac{g|\vec{d}|}{2\pi T} \right\rangle^2 \left(1 - \left\langle \frac{g|\vec{d}|}{2\pi T} \right\rangle \right)^2 + \frac{4T^2}{\pi^2} \sum_{j=1}^{N_f} m_j^2 \sum_{n=1}^{\infty} \frac{(-1)^n}{n^2} K_2(n\beta m_j) \cosh(n\beta\mu_j) \cos \frac{ng|\vec{d}|}{2T}, \quad (\text{E.3})$$

where the sum converges as long as $\mu_j < m_j$ for all quark flavors. Analogously, one derives by differentiation analytic expressions for the EQCD mass parameter and quartic coupling,

$$m_\chi^2 = \frac{2g^2 T^2}{3} - \frac{g^2}{\pi^2} \sum_{j=1}^{N_f} m_j^2 \sum_{n=1}^{\infty} (-1)^n K_2(n\beta m_j) \cosh(n\beta\mu_j), \quad (\text{E.4})$$

$$\tilde{\lambda} = \frac{2g^4 T}{3\pi^2} + \frac{g^4}{12\pi^2 T} \sum_{j=1}^{N_f} m_j^2 \sum_{n=1}^{\infty} (-1)^n n^2 K_2(n\beta m_j) \cosh(n\beta\mu_j).$$

When the quark mass is parametrically larger than both the temperature and the respective chemical potential, the infinite series in Eq. (E.4) can be replaced by its asymptotic form,

$$m_\chi^2 \approx \frac{2g^2 T^2}{3} + 2g^2 T^2 \sum_{j=1}^{N_f} \left(\frac{m_j}{2\pi T} \right)^{3/2} e^{-m_j/T} \cosh(\beta\mu_j), \quad (\text{E.5})$$

$$\tilde{\lambda} \approx \frac{2g^4 T}{3\pi^2} - \frac{g^4 T}{6} \sum_{j=1}^{N_f} \left(\frac{m_j}{2\pi T} \right)^{3/2} e^{-m_j/T} \cosh(\beta\mu_j).$$

On the other hand, for massless quarks at vanishing chemical potentials, the integrals in eq. (E.2) are readily evaluated analytically and one finds $m_\chi^2 = (2g^2 T^2/3)[1 + (N_f/4)]$ and $\tilde{\lambda} = (2g^4 T/3\pi^2)[1 - (N_f/8)]$, in agreement with Ref. [86].

As the above infinite series containing Bessel and hyperbolic functions will appear frequently in our results, it is convenient to introduce a shorthand notation,

$$\kappa_\ell^\pm = \sum_{j=1}^{N_f} (\beta m_j)^2 \sum_{n=1}^{\infty} (\pm 1)^n n^\ell K_2(n\beta m_j) \cosh(n\beta\mu_j), \quad (\text{E.6})$$

in terms of which the EQCD parameters (E.4) take the simple forms $m_\chi^2 = (2g^2T^2/3)[1 - (3\kappa_0^-/2\pi^2)]$ and $\tilde{\lambda} = (2g^4T/3\pi^2)[1 + (\kappa_2^-/8)]$.¹ To introduce one final piece of notation, observe that in the presence of dynamical quarks, the potential of Eq. (E.3) has only one global minimum (up to periodicity) at $|\vec{a}| = 0$, while the point $|\vec{a}| = 2\pi T/g$ corresponds to a mere local minimum. The most important quantity carrying information on the explicit $Z(2)$ breaking due to dynamical quarks is thus the energy-density difference between the two minima. It can be encoded in a single dimensionless parameter

$$\delta \equiv \frac{V_{\text{eff}}(g|\vec{a}| = 2\pi T) - V_{\text{eff}}(g|\vec{a}| = 0)}{T^4} = \frac{4}{\pi^2}(\kappa_{-2}^+ - \kappa_{-2}^-). \quad (\text{E.7})$$

¹Note that at any given time, the infinite sum can be replaced by the corresponding integral expression. This is in particular necessary for reasons of convergence, if $m_j < \mu_j$ for some quark flavor.

Appendix F.

Center symmetry for the SU(2) gauge group

The zeroth component of the gauge field $A_0(\tau)$ (the dependence on the spatial coordinates does not play any role in what follows and is thus suppressed) transforms under the local transformation $s(\tau) \in \text{SU}(2)$ as $\tilde{A}_0(\tau) = s(\tau)A_0(\tau)s(\tau)^\dagger + \frac{i}{g}s(\tau)\partial_\tau s(\tau)^\dagger$. Under the same transformation, the (untraced) Wilson line operator defined in Eq. (4.11) transforms as $\tilde{\Omega} = s(\beta)\Omega s(0)^\dagger$. Let us now write the gauge field as $A_0(\tau) = \vec{a}(\tau) \cdot \vec{\sigma}/2$, and the most general SU(2) gauge transformation as $s(\tau) = \exp[i\varphi(\tau)\vec{n}(\tau) \cdot \vec{\sigma}]$, where $\vec{n}(\tau)$ is a unit vector. In this representation, the gauge field transforms as

$$\begin{aligned} \vec{a} = & \vec{n}(\vec{n} \cdot \vec{a}) + [\vec{a} - \vec{n}(\vec{n} \cdot \vec{a})] \cos 2\varphi - (\vec{n} \times \vec{a}) \sin 2\varphi + \\ & + \frac{1}{g} [2\vec{n}\varphi' + \vec{n}' \sin 2\varphi - 2(\vec{n} \times \vec{n}') \sin^2 \varphi], \end{aligned} \quad (\text{F.1})$$

where the prime denotes a derivative with respect to τ . Demanding that the gauge transformation preserves the periodicity of the gauge field, $\vec{a}(\beta) = \vec{a}(0)$, leads to the conditions

$$\varphi(\beta) = \varphi(0) + N\pi, \quad \varphi'(\beta) = \varphi'(0), \quad \vec{n}(\beta) = \vec{n}(0), \quad \vec{n}'(\beta) = \vec{n}'(0), \quad (\text{F.2})$$

up to an overall minus sign, which only matters if we require the parameters φ, \vec{n} to change continuously with τ . In either case, the unitary matrix $s(\tau)$ satisfies $s(\beta) = (-1)^N s(0)$ for some integer N , which is precisely a transformation of the Z(2) center of the gauge group.

Let us now specialize to the Polyakov gauge, in which A_0 is diagonal and independent of τ . Which gauge transformations from the local SU(2) group preserve this structure? Obviously,

\vec{n} must point in the third direction at all times. Preservation of time independence of \vec{a} then results in the condition $\varphi' = \text{const}$, and the admissible gauge transformations take the form $\vec{n} = (0, 0, 1)$ and $\varphi(\tau) = \varphi(0) + N\pi\tau/\beta$. As a consequence, the gauge field transforms by a mere overall shift, $a_3 \rightarrow a_3 + 2N\pi T/g$. It is worth emphasizing, though, that this conclusion only holds in the Polyakov gauge, as otherwise the *vector function* $\vec{a}(\tau)$ transforms in a rather complicated manner. In any case, since the nontrivial center transformations correspond to time-dependent $s(\tau)$, while there is no time in the three-dimensional effective theory, this effective theory must be augmented with a suitable *definition* of the center symmetry.

Appendix G.

One-loop effective potential of ZQCD

The derivation of the one-loop effective potential of the theory defined by Eq. (4.5) follows closely Appendix A of Ref. [66], and we will therefore merely write down the result here. In practice, we choose $\vec{\Pi}$ to point in the third color direction, $\Pi_a = |\vec{\Pi}|\delta_{a3}$, relying on the SU(2) invariance of the theory. The effective potential in a general R_ξ renormalizable gauge then consists of the tree-level contribution, the gluon and ghost loops, the loop in the mixed $\Sigma\Pi_3$ sector, as well as a separate contribution from the $\Pi_{1,2}$ loops,

$$\begin{aligned}
V_{\text{eff}} &= \frac{1}{g_3^2} V_{\text{tree}} + V_{\text{A+gh}} + V_{\Sigma\Pi_3} + V_{\Pi_{1,2}}, \\
V_{\text{tree}} &= b_1 \Sigma^2 + b_2 \vec{\Pi}^2 + c_1 \Sigma^4 + c_2 (\vec{\Pi}^2)^2 + c_3 \Sigma^2 \vec{\Pi}^2 + d_1 \Sigma^3 + d_2 \Sigma \vec{\Pi}^2, \\
V_{\text{A+gh}} &= -\frac{|\vec{\Pi}|^3}{6\pi} (2 - \xi^{3/2}), \quad V_{\Sigma\Pi_3} = -\frac{1}{12\pi} \left[(m_+^2)^{3/2} + (m_-^2)^{3/2} \right], \\
V_{\Pi_{1,2}} &= -\frac{1}{6\pi} (2b_2 + 4c_2 \vec{\Pi}^2 + 2c_3 \Sigma^2 + 2d_2 \Sigma + \xi \vec{\Pi}^2)^{3/2},
\end{aligned} \tag{G.1}$$

where

$$\begin{aligned}
m_\pm^2 &= b_1 + b_2 + 6c_1 \Sigma^2 + 6c_2 \vec{\Pi}^2 + c_3 (\Sigma^2 + \vec{\Pi}^2) + (3d_1 + d_2) \Sigma \pm \\
&\pm \sqrt{\left[b_1 - b_2 + 6c_1 \Sigma^2 - 6c_2 \vec{\Pi}^2 + c_3 (\vec{\Pi}^2 - \Sigma^2) + (3d_1 - d_2) \Sigma \right]^2 + 4\vec{\Pi}^2 (2c_3 \Sigma + d_2)^2}.
\end{aligned} \tag{G.2}$$

Using the parametrization of the couplings (4.7) and assuming that the background fields $\Sigma, \vec{\Pi}$ are of order $O(g_3^0)$ or smaller, we immediately obtain an expansion for the effective potential

to next-to-leading order in the coupling,

$$\begin{aligned}
V_{\text{eff}} \approx & \frac{1}{g_3^2} \left[\frac{h_1}{2} (\Sigma^2 + \vec{\Pi}^2) + \frac{h_2}{4} (\Sigma^2 + \vec{\Pi}^2)^2 \right] + \frac{s_1}{2} \vec{\Pi}^2 + \frac{s_2}{4} (\vec{\Pi}^2)^2 + s_3 \Sigma^4 + \frac{s_4}{2} \Sigma^3 + \frac{s_5}{2} \Sigma \vec{\Pi}^2 - \\
& - \frac{|\vec{\Pi}|^3}{6\pi} (2 - \xi^{3/2}) - \frac{1}{6\pi} (\tilde{m}_-^2 + \xi \vec{\Pi}^2)^{3/2} - \frac{1}{12\pi} (\tilde{m}_+^3 + \tilde{m}_-^3),
\end{aligned} \tag{G.3}$$

where $\tilde{m}_+^2 = h_1 + 3h_2(\Sigma^2 + \vec{\Pi}^2)$ and $\tilde{m}_-^2 = h_1 + h_2(\Sigma^2 + \vec{\Pi}^2)$.

Colophon

This thesis was made in $\text{\LaTeX} 2_{\mathcal{E}}$ using the “hepthesis” class [87].

Bibliography

- [1] S. Bethke, *The 2009 World Average of $\alpha_s(M_Z)$* , *Eur.Phys.J.* **C64** (2009) 689–703, [arXiv:0908.1135].
- [2] A. M. Polyakov, *Thermal Properties of Gauge Fields and Quark Liberation*, *Phys. Lett.* **B72** (1978) 477–480.
- [3] L. Susskind, *Lattice Models of Quark Confinement at High Temperature*, *Phys. Rev.* **D20** (1979) 2610–2618.
- [4] B. Svetitsky, *Symmetry Aspects of Finite Temperature Confinement Transitions*, *Phys. Rept.* **132** (1986) 1–53.
- [5] G. Boyd *et. al.*, *Thermodynamics of SU(3) Lattice Gauge Theory*, *Nucl. Phys.* **B469** (1996) 419–444, [hep-lat/9602007].
- [6] F. Karsch, E. Laermann, and A. Peikert, *The pressure in 2, 2+1 and 3 flavour QCD*, *Phys. Lett.* **B478** (2000) 447–455, [hep-lat/0002003].
- [7] M. E. Peskin and D. V. Schroeder, *An Introduction to quantum field theory*. Addison-Wesley Publishing Company, 1995. Reading, USA: Addison-Wesley (1995) 842 p.
- [8] S. Hands *et. al.*, *Numerical study of dense adjoint matter in two color QCD*, *Eur. Phys. J.* **C17** (2000) 285–302, [hep-lat/0006018].
- [9] M. G. Alford, A. Kapustin, and F. Wilczek, *Imaginary chemical potential and finite fermion density on the lattice*, *Phys. Rev.* **D59** (1999) 054502, [hep-lat/9807039].
- [10] M. Creutz, *Anomalies and discrete chiral symmetries*, arXiv:0909.5101.
- [11] J. B. Kogut, M. A. Stephanov, D. Toublan, J. J. M. Verbaarschot, and A. Zhitnitsky, *QCD-like theories at finite baryon density*, *Nucl. Phys.* **B582** (2000) 477–513, [hep-ph/0001171].

-
- [12] D. T. Son and M. A. Stephanov, *QCD at finite isospin density*, *Phys. Rev. Lett.* **86** (2001) 592–595, [hep-ph/0005225].
- [13] S. D. H. Hsu and D. Reeb, *On the sign problem in dense QCD*, *Int. J. Mod. Phys.* **A25** (2010) 53–67, [arXiv:0808.2987].
- [14] K. Fukushima and Y. Hidaka, *A model study of the sign problem in the mean-field approximation*, *Phys. Rev.* **D75** (2007) 036002, [hep-ph/0610323].
- [15] Z. Fodor and S. D. Katz, *The phase diagram of quantum chromodynamics*, arXiv:0908.3341.
- [16] A. Mocsy, F. Sannino, and K. Tuominen, *Confinement versus Chiral Symmetry*, *Phys. Rev. Lett.* **92** (2004) 182302, [hep-ph/0308135].
- [17] G. P. Lepage, *What is Renormalization?*, hep-ph/0506330.
- [18] A. V. Manohar, *Effective field theories*, hep-ph/9606222.
- [19] D. B. Kaplan, *Five lectures on effective field theory*, nucl-th/0510023.
- [20] A. Pich, *Effective field theory: Course*, hep-ph/9806303.
- [21] T. Appelquist and J. Carazzone, *Infrared Singularities and Massive Fields*, *Phys.Rev.* **D11** (1975) 2856.
- [22] Y. Nambu and G. Jona-Lasinio, *Dynamical Model of Elementary Particles Based on an Analogy with Superconductivity. I.*, *Phys.Rev.* **122** (1961) 345–358.
- [23] S. P. Klevansky, *The Nambu-Jona-Lasinio model of quantum chromodynamics*, *Rev. Mod. Phys.* **64** (1992) 649–708.
- [24] T. Hatsuda and T. Kunihiro, *QCD phenomenology based on a chiral effective Lagrangian*, *Phys.Rept.* **247** (1994) 221–367, [hep-ph/9401310].
- [25] M. Buballa, *NJL model analysis of quark matter at large density*, *Phys.Rept.* **407** (2005) 205–376, [hep-ph/0402234].
- [26] H. Abuki and K. Fukushima, *Gauge dynamics in the PNJL model: Color neutrality and Casimir scaling*, *Phys. Lett.* **B676** (2009) 57–62, [arXiv:0901.4821].
- [27] K. Fukushima, *Chiral effective model with the Polyakov loop*, *Phys. Lett.* **B591** (2004) 277–284, [hep-ph/0310121].

- [28] C. Ratti, M. A. Thaler, and W. Weise, *Phases of QCD: Lattice thermodynamics and a field theoretical model*, *Phys. Rev.* **D73** (2006) 014019, [hep-ph/0506234].
- [29] S. Roessner, C. Ratti, and W. Weise, *Polyakov loop, diquarks and the two-flavour phase diagram*, *Phys. Rev.* **D75** (2007) 034007, [hep-ph/0609281].
- [30] K. Fukushima, *Phase diagrams in the three-flavor Nambu–Jona-Lasinio model with the Polyakov loop*, *Phys. Rev.* **D77** (2008) 114028, [arXiv:0803.3318].
- [31] J. B. Kogut, J. Polonyi, H. W. Wyld, and D. K. Sinclair, *Hierarchical mass scales in lattice gauge theories with dynamical light fermions*, *Phys. Rev. Lett.* **54** (1985) 1980.
- [32] F. Karsch and M. Lutgemeier, *Deconfinement and chiral symmetry restoration in an $SU(3)$ gauge theory with adjoint fermions*, *Nucl. Phys.* **B550** (1999) 449–464, [hep-lat/9812023].
- [33] J. Engels, S. Holtmann, and T. Schulze, *Scaling and Goldstone effects in a QCD with two flavours of adjoint quarks*, *Nucl. Phys.* **B724** (2005) 357–379, [hep-lat/0505008].
- [34] T. Appelquist and R. D. Pisarski, *High-Temperature Yang-Mills Theories and Three-Dimensional Quantum Chromodynamics*, *Phys. Rev.* **D23** (1981) 2305.
- [35] A. D. Linde, *Infrared Problem in Thermodynamics of the Yang-Mills Gas*, *Phys. Lett.* **B96** (1980) 289.
- [36] E. Braaten and A. Nieto, *Free Energy of QCD at High Temperature*, *Phys. Rev.* **D53** (1996) 3421–3437, [hep-ph/9510408].
- [37] A. Gocksch and M. Ogilvie, *An effective strong coupling lattice model for finite temperature QCD*, *Phys. Lett.* **B141** (1984) 407.
- [38] A. Dumitru, Y. Hatta, J. Lenaghan, K. Orginos, and R. D. Pisarski, *Deconfining phase transition as a matrix model of renormalized Polyakov loops*, *Phys. Rev.* **D70** (2004) 034511, [hep-th/0311223].
- [39] K. Fukushima, *Relation between the Polyakov loop and the chiral order parameter at strong coupling*, *Phys. Rev.* **D68** (2003) 045004, [hep-ph/0303225].
- [40] S. Gupta, K. Huebner, and O. Kaczmarek, *Renormalized Polyakov loops in many representations*, *Phys. Rev.* **D77** (2008) 034503, [arXiv:0711.2251].

- [41] H. Nishimura and M. C. Ogilvie, *A PNJL Model for Adjoint Fermions with Periodic Boundary Conditions*, arXiv:0911.2696.
- [42] M. Unsal, *Abelian duality, confinement, and chiral symmetry breaking in QCD(adj)*, *Phys. Rev. Lett.* **100** (2008) 032005, [arXiv:0708.1772].
- [43] T. Zhang, T. Brauner, and D. H. Rischke, *QCD-like theories at nonzero temperature and density*, *JHEP* **06** (2010) 064, [arXiv:1005.2928].
- [44] H. Georgi, *Lie algebras in particle physics. From isospin to unified theories*, vol. 54. *Frontiers in Physics*. Perseus Books, Reading, Massachusetts, 1982.
- [45] J. O. Andersen and T. Brauner, *Phase diagram of two-color quark matter at nonzero baryon and isospin density*, arXiv:1001.5168.
- [46] K. Fukushima and K. Iida, *Larkin-Ovchinnikov-Fulde-Ferrell state in two-color quark matter*, *Phys. Rev.* **D76** (2007) 054004, [arXiv:0705.0792].
- [47] K. Splittorff, D. T. Son, and M. A. Stephanov, *QCD-like Theories at Finite Baryon and Isospin Density*, *Phys. Rev.* **D64** (2001) 016003, [hep-ph/0012274].
- [48] C. Vafa and E. Witten, *Parity Conservation in QCD*, *Phys. Rev. Lett.* **53** (1984) 535.
- [49] T. Brauner, K. Fukushima, and Y. Hidaka, *Two-color quark matter: $U(1)_A$ restoration, superfluidity, and quarkyonic phase*, arXiv:0907.4905.
- [50] J. Ambjorn, P. Olesen, and C. Peterson, *Stochastic Confinement and Dimensional Reduction. I. Four- Dimensional $SU(2)$ Lattice Gauge Theory*, *Nucl. Phys.* **B240** (1984) 189.
- [51] F. Sannino and K. Tuominen, *Tetracritical behavior in strongly interacting theories*, *Phys. Rev.* **D70** (2004) 034019, [hep-ph/0403175].
- [52] L. Del Debbio, M. Faber, J. Greensite, and S. Olejnik, *Casimir Scaling vs. Abelian Dominance in QCD String Formation*, *Phys. Rev.* **D53** (1996) 5891–5897, [hep-lat/9510028].
- [53] Y. Schroder, *The static potential in QCD to two loops*, *Phys. Lett.* **B447** (1999) 321–326, [hep-ph/9812205].
- [54] C. Anzai, Y. Kiyo, and Y. Sumino, *Violation of Casimir Scaling for Static QCD Potential at Three-loop Order*, *Nucl. Phys.* **B838** (2010) 28–46, [arXiv:1004.1562].

- [55] S. Deldar, *Static $SU(3)$ potentials for sources in various representations*, *Phys. Rev.* **D62** (2000) 034509, [hep-lat/9911008].
- [56] G. S. Bali, *Casimir scaling of $SU(3)$ static potentials*, *Phys. Rev.* **D62** (2000) 114503, [hep-lat/0006022].
- [57] C. Piccioni, *Casimir scaling in $SU(2)$ lattice gauge theory*, *Phys. Rev.* **D73** (2006) 114509, [hep-lat/0503021].
- [58] V. I. Shevchenko and Y. A. Simonov, *Casimir scaling as a test of QCD vacuum*, *Phys. Rev. Lett.* **85** (2000) 1811–1814, [hep-ph/0001299].
- [59] P. N. Meisinger, T. R. Miller, and M. C. Ogilvie, *Phenomenological equations of state for the quark-gluon plasma*, *Phys. Rev.* **D65** (2002) 034009, [hep-ph/0108009].
- [60] H.-M. Tsai and B. Muller, *Phenomenology of the three-flavour PNJL model and thermal strange quark production*, *J. Phys.* **G36** (2009) 075101, [arXiv:0811.2216].
- [61] R. N. Cahn, *Semisimple Lie algebras and their representations*. Dover Publications, New York, 2006. Menlo Park, Usa: Benjamin/cummings (1984) 158 P. (Frontiers In Physics, 59).
- [62] K. Kajantie, M. Laine, A. Rajantie, K. Rummukainen, and M. Tsypin, *The phase diagram of three-dimensional $SU(3)$ + adjoint Higgs theory*, *JHEP* **11** (1998) 011, [hep-lat/9811004].
- [63] K. Kajantie, M. Laine, K. Rummukainen, and Y. Schroder, *Four loop logarithms in 3-d gauge + Higgs theory*, *Nucl.Phys.Proc.Suppl.* **119** (2003) 577–579, [hep-lat/0209072].
- [64] D. J. Gross, R. D. Pisarski, and L. G. Yaffe, *QCD and Instantons at Finite Temperature*, *Rev. Mod. Phys.* **53** (1981) 43.
- [65] T. Zhang, T. Brauner, A. Kurkela, and A. Vuorinen, *Two-color QCD via dimensional reduction*, *JHEP* **1202** (2012) 139, [arXiv:1112.2983].
- [66] P. de Forcrand, A. Kurkela, and A. Vuorinen, *Center-Symmetric Effective Theory for High-Temperature $SU(2)$ Yang-Mills Theory*, *Phys. Rev.* **D77** (2008) 125014, [arXiv:0801.1566].
- [67] N. Weiss, *The Effective Potential for the Order Parameter of Gauge Theories at Finite*

- Temperature*, *Phys. Rev.* **D24** (1981) 475.
- [68] N. Weiss, *The Wilson Line in Finite Temperature Gauge Theories*, *Phys. Rev.* **D25** (1982) 2667.
- [69] N. K. Nielsen, *On the Gauge Dependence of Spontaneous Symmetry Breaking in Gauge Theories*, *Nucl. Phys.* **B101** (1975) 173.
- [70] S. R. Coleman, *The Fate of the False Vacuum. I. Semiclassical Theory*, *Phys. Rev.* **D15** (1977) 2929–2936.
- [71] T. Bhattacharya, A. Gocksch, C. Korthals Altes, and R. D. Pisarski, *Interface tension in an $SU(N)$ gauge theory at high temperature*, *Phys. Rev. Lett.* **66** (1991) 998–1000.
- [72] J. Ignatius, K. Kajantie, and K. Rummukainen, *Cosmological QCD $Z(3)$ phase transition in the 10-TeV temperature range?*, *Phys. Rev. Lett.* **68** (1992) 737–740.
- [73] A. Armoni, C. P. Korthals Altes, and A. Patella, *Domain Walls and Metastable Vacua in Hot Orientifold Field Theories*, *JHEP* **12** (2010) 004, [arXiv:1009.5486].
- [74] J. I. Kapusta and C. Gale, *Finite-temperature field theory: Principles and applications*. Cambridge University Press, Cambridge U.K., 2006. Cambridge, UK: Univ. Pr. (2006) 428 p.
- [75] J. Langelage, G. Munster, and O. Philipsen, *Strong coupling expansion for finite temperature Yang-Mills theory in the confined phase*, *JHEP* **07** (2008) 036, [arXiv:0805.1163].
- [76] J. Langelage, S. Lottini, and O. Philipsen, *Centre symmetric 3d effective actions for thermal $SU(N)$ Yang-Mills from strong coupling series*, *JHEP* **02** (2011) 057, [arXiv:1010.0951].
- [77] S. Lottini, O. Philipsen, J. Langelage, and J. Langelage, *Strong-coupling effective action(s) for $SU(3)$ Yang-Mills*, *Acta Phys. Polon. Suppl.* **4** (2011) 721–726, [arXiv:1105.5284].
- [78] M. Fromm, J. Langelage, S. Lottini, and O. Philipsen, *The QCD deconfinement transition for heavy quarks and all baryon chemical potentials*, arXiv:1111.4953.
- [79] A. O. Barut and R. Raczka, *Theory of group representations and applications*. Singapore: World Scientific, Singapore, 1986. Singapore, Singapore: World Scientific (

1986) 717p.

- [80] L. McLerran and R. D. Pisarski, *Phases of cold, dense quarks at large n_c* , *Nucl. Phys.* **A796** (2007) 83–100, [arXiv:0706.2191].
- [81] B.-J. Schaefer, J. M. Pawłowski, and J. Wambach, *The Phase Structure of the Polyakov–Quark-Meson Model*, *Phys. Rev.* **D76** (2007) 074023, [arXiv:0704.3234].
- [82] H. Abuki, R. Anglani, R. Gatto, G. Nardulli, and M. Ruggieri, *Chiral crossover, deconfinement and quarkyonic matter within a Nambu-Jona Lasinio model with the Polyakov loop*, *Phys. Rev.* **D78** (2008) 034034, [arXiv:0805.1509].
- [83] M. Creutz, *On invariant integration over $SU(N)$* , *J. Math. Phys.* **19** (1978) 2043.
- [84] J. B. Kogut, M. Snow, and M. Stone, *Mean field and Monte Carlo studies of $SU(N)$ chiral models in three-dimensions*, *Nucl. Phys.* **B200** (1982) 211.
- [85] P. H. Damgaard, *The free energy of higher representation sources in lattice gauge theories*, *Phys. Lett.* **B194** (1987) 107.
- [86] K. Kajantie, M. Laine, K. Rummukainen, and M. E. Shaposhnikov, *3d $SU(N)$ + adjoint Higgs theory and finite-temperature QCD*, *Nucl. Phys.* **B503** (1997) 357–384, [hep-ph/9704416].
- [87] A. Buckley, “The heptthesis L^AT_EX class.”

List of figures

1.1.	The measurements of α_s as a function of the energy scale Q . The curves are QCD predictions given the value of $\alpha_s(M_{Z^0})$ as shown in the figure. The empty, full and crossed symbols are extracted values from experiments and lattice calculations. Plot is taken from Ref. [1].	4
2.1.	The $T - \mu_B$ phase diagram of QCD.	14
2.2.	Four-fermion interaction in the NJL model.	21
2.3.	The Feynman diagrams for the gap equation using the MFA in the NJL model. A single line is the propagator of a free quark and a double line is that of a quasi-fermion with effective mass m^*	22
3.1.	Comparison of the expectation values of the mean field α (dashed) and the fundamental Polyakov loop (solid) in the naive (thin black lines) and Weiss (thick red lines) mean-field approximations to the pure gauge theory.	39
3.2.	Phase diagram of two-color QCD with one flavor of adjoint quarks. Black solid line: deconfinement transition. Red dashed line: BEC transition. Blue dotted line: chiral crossover. The right panel zooms in the temperature scale so that the cusp in the deconfinement critical line is visible.	39
3.3.	Condensates in aQC ₂ D at $\mu = 100$ MeV as a function of temperature. The chiral condensate σ (black solid line), diquark condensate Δ (red dashed line), and the fundamental Polyakov loop (blue dotted line) are shown.	40
3.4.	Schematic phase diagram of the Ginzburg–Landau theory with two order parameters. Thick lines denote second-order phase transitions. The labels indicate which order parameters take nonzero values in a given phase.	42

-
- 3.5. Expectation values of the Polyakov loops in various representations as a function of the fundamental Polyakov loop in the case of two colors. Boldface numbers indicate the “spin” j of the representation. Left panel: unscaled Polyakov loops. Right panel: Casimir-scaled Polyakov loops. For convenience, we take the $C_2(\mathcal{F})/C_2(\mathcal{R})$ power of the expectation values of the Polyakov loops so that the fundamental loop is left intact. 44
- 3.6. Phase diagram of three-color QCD with one flavor of adjoint quarks. Black solid line: deconfinement transition. Red dashed line: BEC transition. Blue dotted line: chiral crossover. The right panel zooms in the chemical potential and temperature scales so that the two tricritical points are discernible. 48
- 3.7. Expectation values of the Polyakov loops in various representations as a function of the fundamental Polyakov loop in the case of three colors. Boldface numbers indicate the dimension (and possibly the symmetry) of the representation. Left panel: unscaled Polyakov loops. Right panel: Casimir-scaled Polyakov loops. For convenience, we take the $C_2(\mathcal{F})/C_2(\mathcal{R}) \equiv 1/d_{\mathcal{R}}$ power of the expectation values of the Polyakov loops so that the fundamental loop is left intact. For the sake of clarity, the labels are not shown in the right panel. The color assignment of the lines is the same as in the left panel. 49
- 4.1. Free energy profiles of the leading-order domain-wall solution in the center-symmetric limit as a function of the dimensionless length variable $x \equiv gTr$, with the wall residing at $x = 0$. The solid red curve is the prediction of the effective theory, while the dashed black one is the full Yang-Mills result. The boundary condition for this one-dimensional solution is $\alpha(-\infty) = 0$ and $\alpha(+\infty) = 1$ 61

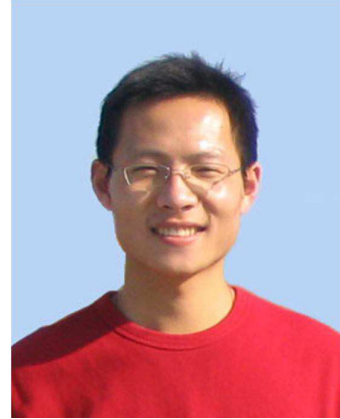
List of tables

3.1. Model parameters for two-color QCD with adjoint quarks.	38
3.2. Model parameters for three-color QCD with adjoint quarks.	47

Curriculum Vitae

Personal information

Name: Tian Zhang
Date of Birth: July 25, 1983
Place of Birth: Hubei, P. R. China
Gender: Male
Nationality: Chinese
Marital Status: Single
Email: tzhang@th.physik.uni-frankfurt.de



Education

04/2009 - 04/2012

Institut für Theoretische Physik, Goethe Universität, Frankfurt am Main, Germany
Dissertation: Study of QCD-like theories at nonzero temperatures and densities
Degree: Doctor of Philosophy
Supervisor: Prof. Dr. Dirk H. Rischke

09/2005 - 07/2008

Department of Physics, Tsinghua University, Beijing, China
Thesis: Bound states in chiral-restored phase
Degree: Master of Science
Supervisor: Prof. Dr. Pengfei Zhuang

09/2001 - 07/2005

Department of Physics, Tsinghua University, Beijing, China
Thesis: Quantum mechanics in non-commutative spacetime
Degree: Bachelor of Science
Supervisor: Prof. Dr. Pengfei Zhuang

Publications

2012

Tian Zhang, Tomáš Brauner, Aleksi Kurkela, Aleksi Vuorinen

Two-color QCD via dimensional reduction

JHEP 02(2012)139

arXiv: 1112.2983 (hep-ph)

2010

Tian Zhang, Tomáš Brauner, Dirk H. Rischke

QCD-like theories at nonzero temperature and density

JHEP 06(2010)064

arXiv: 1005.2928 (hep-ph)

Academic tutors

Physics of strongly interacting matter

Prof. Dr. Igor Mishustin

Aspects of chiral symmetry

Prof. Dr. Volker Koch

Lie algebras

Dr. Tomáš Brauner